Since January 2020 Elsevier has created a COVID-19 resource centre with free information in English and Mandarin on the novel coronavirus COVID-19. The COVID-19 resource centre is hosted on Elsevier Connect, the company's public news and information website.

Computers in Biology and Medicine 142 (2022) 105181

Contents lists available at ScienceDirect

Computers in Biology and Medicine

journal homepage: www.elsevier.com/locate/compbiomed

Horizontal and vertical search artificial bee colony for image segmentation of COVID-19 X-ray images

Hang Su [a], Dong Zhao [a,*], Fanhua Yu [a], Ali Asghar Heidari [b,1], Yu Zhang [a], Huiling Chen [c,**], Chengye Li [d], Jingye Pan [e,f,g], Shichao Quan [h,i,j,***]

[a] College of Computer Science and Technology, Changchun Normal University, Changchun, Jilin, 130032, China
[b] School of Surveying and Geospatial Engineering, College of Engineering, University of Tehran, Tehran, Iran
[c] College of Computer Science and Artificial Intelligence, Wenzhou University, Wenzhou, Zhejiang, 325035, China
[d] Department of Pulmonary and Critical Care Medicine, The First Affiliated Hospital of Wenzhou Medical University, Wenzhou, 325000, China
[e] Department of Intensive Care Unit, The First Affiliated Hospital of Wenzhou Medical University, Wenzhou, Zhejiang, 325000, China
[f] Key Laboratory of Intelligent Treatment and Life Support for Critical Diseases of Zhejiang Provincial, Wenzhou, Zhejiang, 325000, China
[g] Wenzhou Key Laboratory of Critical Care and Artificial Intelligence, Wenzhou, Zhejiang, 325000, China
[h] Department of General Medicine, The First Affiliated Hospital of Wenzhou Medical University, Wenzhou, Zhejiang, 325000, China
[i] Department of Big Data in Health Science, The First Affiliated Hospital of Wenzhou Medical University, Wenzhou, Zhejiang, 325000, China
[j] Zhejiang Engineering Research Center for Hospital Emergency and Process Digitization, Wenzhou, Zhejiang, 325000, China

ARTICLE INFO

Keywords:
Disease diagnosis
Multi-threshold image segmentation
Meta-heuristic
COVID-19
Swarm-intelligence

ABSTRACT

The artificial bee colony algorithm (ABC) has been successfully applied to various optimization problems, but the algorithm still suffers from slow convergence and poor quality of optimal solutions in the optimization process. Therefore, in this paper, an improved ABC (CCABC) based on a horizontal search mechanism and a vertical search mechanism is proposed to improve the algorithm's performance. In addition, this paper also presents a multilevel thresholding image segmentation (MTIS) method based on CCABC to enhance the effectiveness of the multilevel thresholding image segmentation method. To verify the performance of the proposed CCABC algorithm and the performance of the improved image segmentation method. First, this paper demonstrates the performance of the CCABC algorithm itself by comparing CCABC with 15 algorithms of the same type using 30 benchmark functions. Then, this paper uses the improved multi-threshold segmentation method for the segmentation of COVID-19 X-ray images and compares it with other similar plans in detail. Finally, this paper confirms that the incorporation of CCABC in MTIS is very effective by analyzing appropriate evaluation criteria and affirms that the new MTIS method has a strong segmentation performance.

1. Introduction

Image segmentation (IS) is an important research direction in the field of computer vision, which is an important part of image semantic understanding and one of the most difficult problems in image processing [1]. In recent years, more and more image segmentation methods have been proposed [2–5]. For example, multi-level threshold image segmentation (MTIS) [6], wavelet transform-based IS [7], hybrid threshold-based IS [8], multi-atlas-based IS [9], spatial patterns-based IS [10], deep learning-based IS [11], hierarchical clustering-based IS [12], etc. The multi-threshold segmentation method (MTIS) has become a hot technique to study and apply because of its simple implementation, small computational effort, and more stable performance. Peng et al. [13] designed a cell-like P system with the nested structure of three layers to improve MTIS. Zhao et al. [14] proposed an improved ant colony optimizer (RCACO) with a random spare strategy and chaotic intensification strategy to improve the processing efficiency of MTIS. Zhang et al. [15] presented a novel population-based bee foraging

* Corresponding author.
** Corresponding author.
*** Corresponding author. Department of General Medicine, The First Affiliated Hospital of Wenzhou Medical University, Wenzhou, Zhejiang, 325000, China.
E-mail addresses: suhang_v@163.com (H. Su), zd-hy@163.com (D. Zhao), yufanhua@163.com (F. Yu), as_heidari@ut.ac.ir (A.A. Heidari), zhangyu@ccsfu.edu.cn (Y. Zhang), chenhuiling.jlu@gmail.com (H. Chen), lichengye41@126.com (C. Li), panjingye@wzhospital.cn (J. Pan), generalpractice@qq.com (S. Quan).
[1] https://aliasgharheidari.com

https://doi.org/10.1016/j.compbiomed.2021.105181
Received 4 September 2021; Received in revised form 20 December 2021; Accepted 24 December 2021
Available online 3 January 2022

Table 1
Comparison of work related to image segmentation.

Authors	Method	Dataset	Performance and Contribution
The method proposed in this paper	CCABC + non-local means + 2D histogram+ 2D Kapur's entropy	COVID-19 X-ray images	The method has a high threshold search accuracy and image segmentation effect among the same type of segmentation methods tested with real datasets.
Peng et al. [13]	Membrane computing + fuzzy entropy	standard images	Membrane computing enhances the accuracy and efficiency of the fuzzy entropy-based segmentation method.
Zhao et al. [14]	RCACO + Kapur's entropy	standard images	This method improves the classic Kapur's entropy thresholding segmentation method's segmentation consistency and accuracy.
Zhang et al. [15]	improved BFA + Otsu	benchmark images	This method effectively uses image processing, and the target area segmentation is more complete.
Xing et al. [16]	TEO + gray-level co-occurrence matrix	satellite images	This method improves the accuracy and robustness of traditional image segmentation methods.
Wu et al. [17]	DI-TLBO + Otsu + Kapur's entropy	X-ray images	This method improves the stability of the threshold segmentation method using SIOA and has a better performance among similar methods.
Ewees et al. [18]	ABCSCA + Otsu	benchmark images	This method has a stronger threshold search capability and significantly improves the speed and accuracy of image segmentation.
Alwerfali et al. [19]	SSOSCA + fuzzy entropy	Berkeley dataset	This method uses SIOA combined with fuzzy entropy to significantly improve the image segmentation method.
Abd Elaziz et al. [20]	HHOSSA + Kapur's entropy	natural gray-scale images	This method shows the performance and accuracy of the algorithm by testing on natural datasets.

algorithm (BFA) to enhance the search efficiency of MTIS. Xing et al. [16] proposed a multi-threshold image segmentation method based on a thermal exchange optimization (TEO) algorithm, used to reduce the algorithm complexity of MTIS.

The application of multilevel thresholds to classify image pixels will inevitably improve the segmentation effect of the image. Still, the determination of multilevel thresholds will expand the search space as the number of thresholds itself increases, making the computational complexity much higher. The traditional multi-threshold segmentation method obtains the optimal threshold by exhaustive enumeration, and the computational complexity increases exponentially with the increasing number of thresholds, and the computational efficiency is low. For this reason, scholars have introduced the population intelligence algorithm to find the optimal combination of thresholds, which alleviates the problem of low computational efficiency to a certain extent. Wu et al. [17] presented an improved teaching-learning-based optimization (DI-TLBO) algorithm that increased the stability and accuracy of MTIS. Ewees et al. [18] integrated both the artificial bee colony algorithm and the sine-cosine algorithm (ABCSCA) to enhance the performance of MTIS. Alwerfali et al. [19] proposed a modified spherical search optimizer (SSOSCA) to find the appropriate threshold in MTIS. Abd Elaziz et al. [20] presented an enhanced Harris Hawks Optimizer (HHOSSA) to determine the best threshold of MTIS. Table 1 illustrates the image segmentation method proposed in this paper and compares recent related image segmentation techniques. As we can see, more and more scholars in the field of image processing have paid attention to MTIS in recent years, and many researchers have proposed the use of swarm intelligence optimization algorithm (SIOA) instead of the traditional exhaustive method to find the optimal threshold in order to reduce the computational effort and complexity of traditional multi-threshold image segmentation methods.

The swarm intelligence optimization algorithm is a random search evolutionary algorithm based on probability [21–24]. These optimizers have found an increasing momentum in the current big data world because they can help decision-makers understand the aspects of their decisions in a more resource-aware way [25,26]. It is an algorithm abstracted by simulating the intelligent collaborative behavior of groups such as insects, herds of animals, and fish [27–31]. Moreover, SIOA is simple and efficient in terms of optimization. And these SIOAs have found its application in many fields such as feature selection [32–36], wind speed prediction [37], engineering design problems [38,39], image segmentation [40], social support domains [41–44], industrial domain [45], the hard maximum satisfiability problem [46,47], disaster prediction [48], renewable energy prediction [49], medical data classification [50–54], complex network [55], bankruptcy prediction [56–58], parameter optimization [59–61], PID optimization control [62–64], fault diagnosis of rolling bearings [65,66], design of power electronic circuit [67,68], detection of foreign fiber in cotton [69,70], and prediction problems in educational field [71–75]. For example, there are particle swarm optimization (PSO) [76], moth search algorithm (MSA) [77], monarch butterfly optimization (MBO) [78], hunger games search (HGS)[2] [79], Harris hawks optimization (HHO)[3] [80],

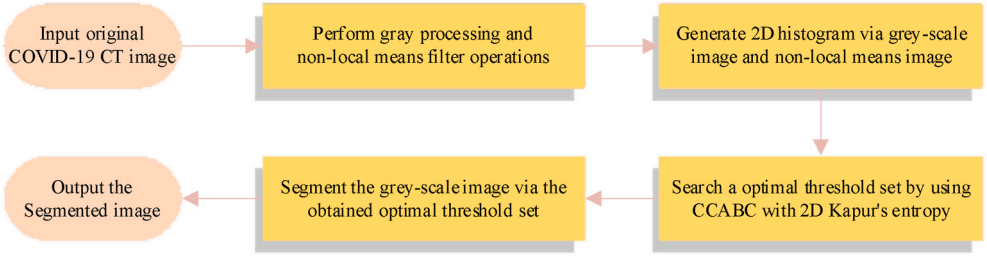

Fig. 1. Flowchart of MTIS

[2] https://aliasgharheidari.com/HGS.html.
[3] https://aliasgharheidari.com/HHO.html.

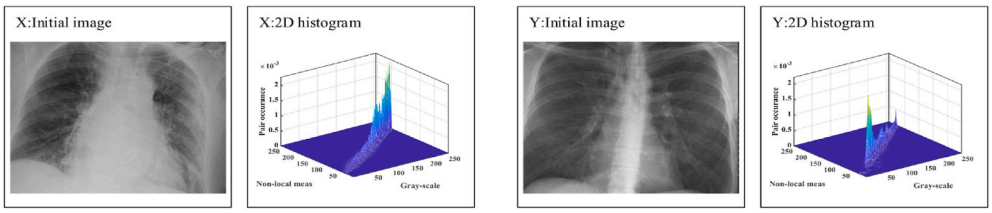

Fig. 2. Three-dimension view about 2D histograms of X and Y.

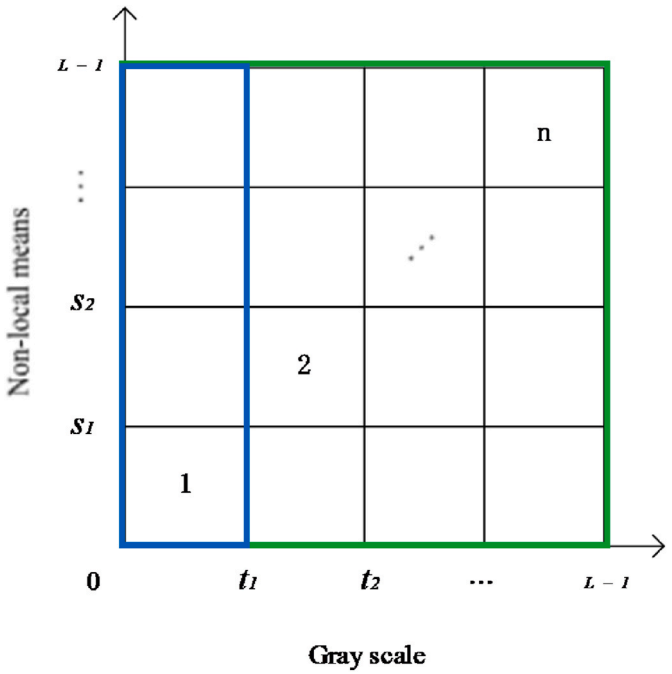

Fig. 3. Two-dimension view about the 2D histogram.

slime mould algorithm (SMA)[4] [81], Runge Kutta optimizer (RUN)[5] [82], colony predation algorithm (CPA) [83] and so on.

In 2005, Karaboga et al. proposed an SIOA called the artificial bee colony (ABC) [84] algorithm, which has a strong ability to solve the optimal solution. The standard ABC algorithm still suffers from the deficiencies of low optimality finding accuracy and slow convergence speed, especially in solving high-dimensional complex problems. There is still much room for improvement in the algorithm's optimality finding stability and adaptability to jump away from local optimum ability. Therefore, researchers have developed many improved versions of ABC and applied them to various fields. Zou et al. [85] presented a discrete ABC algorithm to address a new multiple automatic guided vehicle dispatching problem. Zhou et al. [86] proposed a dynamic ABC algorithm for a cloud service optimization method. Zhao et al. [87] proposed an improved ABC optimization algorithm to solve the problem of classifying hyperspectral images. Lin et al. [88] proposed a hybrid binary ABC algorithm to solve the maximum set k-covering problem. Ding et al. [89] presented a modified ABC algorithm to improve structural damage identification. Chu et al. [90] proposed a binary superior tracking ABC with dynamic Cauchy mutation to improve the feature selection algorithm. Chen et al. [91] proposed a fireworks explosion-based ABC framework to solve the problem of slow convergence of the ABC algorithm. Boudardara et al. [92] proposed a shrinking ABC to solve a sub-problem of robotic path planning. Yue et al. [93] proposed an improved ABC algorithm to enhance wireless sensor network coverage and connectivity.

This paper proposes a new and improved version of ABC by introducing a vertical and horizontal crossover strategy in ABC to improve ABC's efficiency in searching for optimal solutions and the ability to jump out of locally optimal solutions. Further, CCABC is applied to the field of multi-threshold image segmentation to improve image segmentation accuracy while ensuring segmentation efficiency. To demonstrate that CCABC has a better ability to jump out of local optimum and can obtain higher quality solutions more efficiently, this paper conducts comparative experiments on CCABC using 30 test functions of CEC2014. In the algorithm performance experiments, CCABC, original ABC, 5 well-known algorithms, 4 improved algorithms based on original ABC, and 6 other improved algorithms are compared. Furthermore, the comparison results are also analyzed in this paper using Wilcoxon signed-rank test [94] and the Freidman test [95], proving that CCABC outperforms ABC and other similar algorithms. Then, CCABC is likewise compared with multiple similar algorithms in the image segmentation experiments. This paper also utilizes Feature Similarity Index (FSIM) [96], Peak Signal to Noise Ratio (PSNR) [97], and Structural Similarity Index (SSIM) [98] to image segmentation results carefully evaluated. The evaluation results fully demonstrate that the MTIS method based on CCABC does not easily fall into the local optimum trap and thus obtains higher quality segmentation results. The main contributions of this study can be summarized as:

- This paper proposes an improved ABC algorithm (CCABC).
- CCABC is applied to COVID-19 multi-threshold image segmentation based on the 2D histogram.
- CCABC has a significant improvement in searching for the optimal solution.
- The segmentation performance of CCABC is verified by comparison with well-known algorithms.

The rest of this paper is organized as follows. In Section 2, the work related to image segmentation is described. In Section 3, the original ABC algorithm is described in this paper. In Section 4, this paper mainly describes the proposed CCABC and the improved MTIS (CCABC-MTIS) based on CCABC. In Section 5, comparative experiments on benchmark functions and image segmentation problems are conducted to verify the performance of CCABC. Finally, Section 6 concludes the whole paper and shows the direction of future work.

2. The related works of image segmentation

2.1. Multi-thresholding image segmentation

MTIS is a vital image segmentation method, which essentially marks targets with different features in an image with multiple thresholds. Therefore, the most crucial aspect of MTIS is setting the thresholds, which directly determines the effect of the image after segmentation. Among the many MTIS methods, the histogram-based segmentation method is one of the most widely used methods by researchers. The histogram-based segmentation methods can be divided into one-dimensional histogram segmentation and two-dimensional histogram

[4] https://aliasgharheidari.com/SMA.html.
[5] https://aliasgharheidari.com/RUN.html.

Initialize the parameters $x_{min}, x_{max}, N, D, T, limit, trail$

Initialize the positions of the food source $x_i (i = 1, 2, \ldots, F), F = N/2$

While $(t \le T)$ // T denotes the total number of iterations

For $i = 1 : F$

Form v_i by Eq. (9);

Calculate the fitness f_v and its weight fit_v by Eq. (8);

If $fit_v > fit_i$

Update x_i , fit_i and f_i;

Else

$trail = trail + 1$; // $trail$ is used to records has not been updated

End If

End For

Calculate the probability of each food source being selected p_i by Eq. (8) and Eq. (10);

While $(f \le F)$

If $rand(0,1) < p_i$

$f = f + 1$;

Form v_i by Eq. (9);

Calculate the fitness f_v and its weight fit_v by Eq. (8);

If $fit_v > fit_i$

Update x_i , fit_i and f_i;

Else

$trail = trail + 1$;

End If

End If

End While

If $(trail > limit)$

Update x_i by Eq. (7);

Calculate the new fitness f_v;

If $f_v < f_i$

Save x_i and f_v;

End If

End If

End While

segmentation. In contrast, the one-dimensional histogram-based segmentation methods do not make full use of the spatial information of the image, and the segmentation results are easily disturbed by noise. Abutaleb [99] proposed a two-dimensional histogram-based segmentation method by making full use of the spatial information of the image to combine grayscale images with local mean images. The 2D histogram formed based on grayscale image and local mean image ignores the details of some points and edges, and the traditional 2D histogram uses the exhaustive method to find the optimal threshold, which is very computationally intensive. Therefore, this paper generates a two-dimensional histogram using grayscale images and nonlocal mean images and then introduces SIOA based on Kapur's entropy to help MTIS find the optimal threshold. In the method proposed in this paper, Kapur's entropy is used as the objective function of CCABC, and the efficiency of the swarm intelligence optimization algorithm is used to find the optimal threshold, which greatly reduces the complexity. The detailed flowchart of the method is given in Fig. 1.

2.2. Nonlocal means 2D histogram

A new image denoising technique called Nonlocal means 2D histogram was proposed by Buades et al. [100]. It uses redundant information in the image for denoising while maintaining the maximum detailed features of the image. And Nonlocal mean value of pixels is obtained from pixels with similar neighborhood structures in the image, weighted by averaging. Assuming that the grayscale values of pixels p and q of image I are $I(p)$ and $I(q)$, respectively, the nonlocal mean value of image I can be calculated by Eqs. (1)–(4).

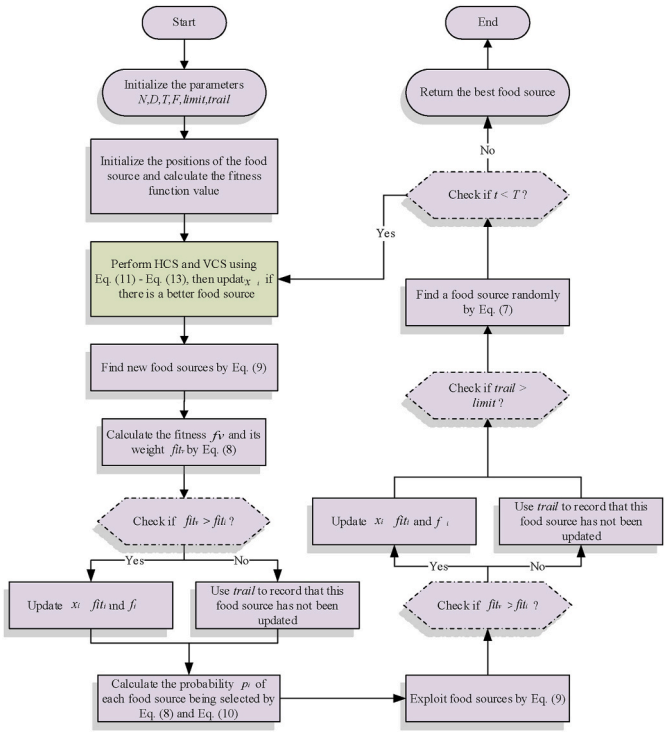

Fig. 4. Flowchart of CCABC

$$O(p)=\frac{\sum_{q\in I} I(q)\omega(p,q)}{\sum_{q\in I}\omega(p,q)} \tag{1}$$

$$\omega(p,q)=exp^{-\frac{|\mu(p)-\mu(q)|^2}{\sigma^2}} \tag{2}$$

$$\mu(p)=\frac{1}{m\times m}\sum_{i\in L(p)} I(i) \tag{3}$$

$$\mu(q)=\frac{1}{m\times m}\sum_{i\in L(q)} I(i) \tag{4}$$

where $O(p)$ is the filtered value of the nonlocal mean, $\omega(p,q)$ is used to calculate the weights of pixel p and pixel q, σ is the standard deviation, $\mu(p)$ and $\mu(q)$ are the local means, and also $L(p)$ and $L(q)$ are local images of size $m\times m$ centered on pixel p and pixel q, respectively.

The two-dimensional histogram is formed by combining the grayscale image based on the above method to form the nonlocal mean image. Therefore, the size and magnitude taking range $[0,L-1]$ of the grayscale image $G(x,y)$ must be the same as the size and magnitude taking range $[0,L-1]$ of the nonlocal mean image $D(x,y)$. Then, the final two-dimensional histogram can be obtained after normalizing Eq. (5), which is given in Fig. 2 to generate a two-dimensional histogram based on grayscale images and nonlocal mean images, where images X and Y are from the COVID-19 dataset.

$$P_{ij}=\frac{h(i,j)}{M\times N} \tag{5}$$

where i represents the value of $G(x,y)$ pixels, j represents the value of $D(x,y)$ pixels, and $h(i,j)$ denotes the number of times the point (i,j) appears on the gray value vector (s,t).

2.3. Kapur's entropy for 2D histogram

A two-dimensional planar histogram based on the above two-dimensional histogram is given in Fig. 3, where $\{t_1,t_2\ldots,L-1\}$ denotes the value of the grayscale image and $\{s_1s_2\ldots,L-1\}$ denotes the value of the nonlocal average image. Because the main diagonal of the two-dimensional histogram contains enough image information and to simplify the calculation, Kapur's entropy of the subregion on the main diagonal is calculated using Eq. (6). Since CCABC takes Kapur's entropy as the objective function, the optimal solution found by CCABC in $\{t_1, t_2\ldots,t_{n-1}\}$ is the optimal threshold.

$$\begin{aligned}\varphi(s,t)=&-\sum_{i=0}^{s_1}\sum_{j=0}^{t_1}\frac{P_{ij}}{P_1}ln\frac{P_{ij}}{P_1}-\sum_{i=t_1+1}^{s_2}\sum_{j=t_1+1}^{t_2}\frac{P_{ij}}{P_2}ln\frac{P_{ij}}{P_2}\\&-\ldots\sum_{i=s_{L-2}}^{s_{L-1}}\sum_{t_L-2}^{t_{L-1}}\frac{P_{ij}}{P_{L-1}}ln\frac{P_{ij}}{P_{L-1}}\end{aligned} \tag{6}$$

where $P_1=\sum_{i=0}^{S_1}\sum_{j=0}^{t_1}P_{ij}, P_2=\sum_{i=t_1+1}^{S_2}\sum_{j=t_1+1}^{t_2}P_{ij}, P_{L-1}=\sum_{i=s_{L-2}+1}^{S_{L-1}}\sum_{j=t_{L-2}+1}^{t_{L-1}}P_{ij}$.

3. An overview of ABC

Karaboga et al. [84] proposed the artificial bee colony algorithm (ABC) to solve the multivariate function optimization problem, which simulates the honey harvesting behavior of a bee colony. Like other SIOA, the optimization execution process of ABC is divided into two phases, namely the exploration phase and the exploitation phase. The bees are divided into employed bees, onlooker bees, and scout bees according to the division of labor, where employed bees and scout bees correspond to the exploration phase of the algorithm and onlooker bees correspond to the exploitation phase.

In ABC, the bees are divided into three categories: employed bees, onlooker bees, and scout bees, whose main behavior is finding a good food source and exploiting a certain food source. The employed bees are equal to the onlooker bees in terms of number. In addition, the location of each food source represents a candidate solution, which is a vector of dimension D in the algorithm. In contrast, the amount of honey each food source has corresponds to the quality of the problem solution. The process of the ABC algorithm can be divided into four phases: initialization phase, employed bee phase, onlooker bee phase, and scout bee phase.

The algorithm model generates N food sources randomly in the initialization phase, as shown in Eq. (7).

$$x_{i,j}=x_{min,j}+rand(0,1)\left(x_{max,j}-x_{min,j}\right) \tag{7}$$

Where $k\in\{1,2,\cdots,N\}, j\in\{1,2,\cdots,D\}$, $x_{min,j}$ and $x_{max,j}$ denote the minimum and maximum values of the randomly generated food source dimensions, and $rand(0,1)$ denotes a random number uniformly distributed between $[0,1]$. In this stage and initializing the food sources, the adaptation value is calculated for each food source, and the formula is shown in Eq. (8).

$$fit_i=\begin{cases}\dfrac{1}{1+f_i} & f_i\geq 0\\ 1+|f_i| & otherwise\end{cases} \tag{8}$$

where fit_i denotes the weight of food source x_i and f_i denotes the value of the objective function of the corresponding problem with the food source x_i as a parameter.

In the employed bee phase, each employed bee will be responsible for searching a food source and then generating a new candidate solution by searching around that food source by Eq. (9).

$$v_{i,j}=x_{i,j}+\varphi_{i,j}\left(x_{i,j}-x_{k,j}\right) \tag{9}$$

Initialize the parameters $x_{min}, x_{max}, N, D, T, limit, trail$

Initialize the positions of the food source $x_i\,(i = 1, 2, \ldots, F), F = N/2$

While $(t \le T)$ // T denotes the total number of iterations

While $(t \le T/4)$

Perform HCS and VCS using Eq. (11) - Eq. (13) after population initialization,

then update x_i if there is a better search agent;

continue;

End While

For $i = 1 : F$

Form v_i by Eq. (9);

Calculate the fitness f_v and its weight fit_v by Eq. (8);

If $fit_v > fit_i$

Update x_i , fit_i and f_i;

Else

$trail = trail + 1$; // $trail$ is used to records has not been updated

End If

End For

Calculate the probability of each food source being selected p_i by Eq. (8) and Eq. (10);

While $(f \le F)$

If $rand(0,1) < p_i$

$f = f + 1$;

Form v_i by Eq. (9);

Calculate the fitness f_v and its weight fit_v by Eq. (8);

If $fit_v > fit_i$

Update x_i , fit_i and f_i;

Else

$trail = trail + 1$;

End If

End If

End While

If $(trail > limit)$

Update x_i by Eq. (7);

Calculate the new fitness f_v;

If $f_v < f_i$

Save x_i and f_v;

End If

End If

End While

where $k \in \{1, 2, \cdots, N\}, j \in \{1, 2, \cdots, D\}$, x_i denotes the selected food source to be updated, x_k denotes the food source different from x_i, j denotes the dimension of random selection, and $\varphi_{i,j}$ denotes the random number generated from $[-1, 1]$. After updating the food source, the newly generated candidate solution v_i is greedily selected with x_i for iterating the optimal food source.

In the onlooker bee phase, the onlooker bee informs the employed bee of the information of the food source nectar source by dancing and then calculates the selection probability of the relevant food source based on the information obtained formula shown in Eq. (10).

$$p_i = \frac{fit_i}{\sum_{j=1}^{N} fit_i} \tag{10}$$

Table 2
Description of the 30 benchmark functions.

Class	No.	Functions	$F_i^* = F_i(x^*)$
Unimodal Functions	1	Rotated High Conditioned Elliptic Function	100
	2	Rotated Bent Cigar Function	200
	3	Rotated Discus Function	300
Simple Multimodal Functions	4	Shifted and Rotated Rosenbrock's Function	400
	5	Shifted and Rotated Ackley's Function	500
	6	Shifted and Rotated Weierstrass Function	600
	7	Shifted and Rotated Griewank's Function	700
	8	Shifted Rastrigin's Function	800
	9	Shifted and Rotated Rastrigin's Function	900
	10	Shifted Schwefel's Function	1000
	11	Shifted and Rotated Schwefel's Function	1100
	12	Shifted and Rotated Katsuura Function	1200
	13	Shifted and Rotated HappyCat Function	1300
	14	Shifted and Rotated HGBat Function	1400
	15	Shifted and Rotated Expanded Griewank's plus Rosenbrock's Function	1500
	16	Shifted and Rotated Expanded Scaffer's F6 Function	1600
Hybrid Functions	17	Hybrid Function 1 ($N = 3$)	1700
	18	Hybrid Function 2 ($N = 3$)	1800
	19	Hybrid Function 3 ($N = 4$)	1900
	20	Hybrid Function 4 ($N = 4$)	2000
	21	Hybrid Function 5 ($N = 5$)	2100
	22	Hybrid Function 6 ($N = 5$)	2200
Composition Functions	23	Composition Function 1 ($N = 5$)	2300
	24	Composition Function 2 ($N = 3$)	2400
	25	Composition Function 3 ($N = 3$)	2500
	26	Composition Function 4 ($N = 5$)	2600
	27	Composition Function 5 ($N = 5$)	2700
	28	Composition Function 6 ($N = 5$)	2800
	29	Composition Function 7 ($N = 3$)	2900
	30	Composition Function 8 ($N = 3$)	3000

Table 3
Parameter settings for benchmark function experiments.

Parameter name	Value
Population size	30
Maximum number of function evaluations	300,000
Number of tests per algorithm	50

where p_i denotes the probability of being selected for a food source x_i and fit_i denotes the adaptation value of the food source. It can be seen that the larger the fit value is, the higher the probability that the corresponding food source is selected. Based on this, the food source is selected by roulette, and the same Eq. (9) is used to generate a new candidate solution v_i for the selected individuals. v_i is replaced if its fitness value is better than x_i; otherwise, it remains unchanged.

In the scout bee phase, the algorithm model will select the food source i that has not been updated for the longest time, and if its number of not being updated is greater than the predefined *limit* value, the corresponding employed bee will be converted into a scout bee, and a new food source will be randomly generated to replace food source i by Eq. (7).

The pseudocode of ABC is shown in Algorithm 1.

Algorithm 1. Pseudo-code of ABC

4. The proposed CCABC-MTIS method

This section describes the vertical crossover optimizer Crisscross optimizer (CSO) and the proposed CCABC in detail. Among them, this paper uses CSO's horizontal crossover search (HCS) and vertical crossover search (VCS) to improve the early search efficiency of the ABC algorithm and the ability to jump out of the local optimum. After that, this paper introduces the improved ABC algorithm into the multi-threshold image segmentation technique to propose the CCABC-MTIS method.

4.1. Crisscross optimizer

In 2014, Meng et al. [101] proposed CSO, which mainly used HCS and VCS to complete the whole search process, and experimentally proved that this not only made the algorithm less prone to fall into the local optimum problem but also significantly improved the convergence speed and solution accuracy of the algorithm. After that, Patwal et al. [102] proposed an improved PSO algorithm based on HCS and VCS to improve the ability of PSO search and exploitation. Zhao et al. [103] proposed to use HCS and VCS to solve a variant of ant colony optimization (ACOR) which is prone to fall into local optimum and The problem of low convergence accuracy. Inspired by this, this paper introduces HCS and VCS into ABC to be able to improve its search and exploitation capabilities.

4.1.1. Horizontal crossover search (HCS)

HCS mainly acts between two different individuals and crosses the corresponding two individual dimensions arithmetically. Therefore, adding HCS to the ABC algorithm enables the bees to learn from each other and exchange information, thus enabling them to find the optimal solution quickly, thereby improving the convergence speed of the algorithm. Assuming that the n th column dimension of the parent bees x_i and x_j performs HCS, then the lateral crossover update formula can be expressed as Eq. (11) and Eq. (12).

$$MS_i^n = \varepsilon_1 \times x_{in} + (1-\varepsilon_1) \times x_{jn} + c_1 \times \left(x_{in} - x_{jn}\right) \tag{11}$$

$$MS_j^n = \varepsilon_2 \times x_{jn} + (1-\varepsilon_2) \times x_{in} + c_2 \times \left(x_{jn} - x_{in}\right) \tag{12}$$

where ε_1 and ε_2 are random numbers between $(0,1)$, c_1 and c_2 are random numbers between $(-1,1)$, x_{in} is the n th dimension of the i th bee, x_{jn} is the n th dimension of the j th bee, and MS_i^n and MS_j^n are the offspring generated by the parent bees x_i and x_j based on HCS.

4.1.2. Vertical crossover search (VCS)

The VCS mainly acts between two different dimensions, arithmetically crossing the corresponding individuals. This may allow some individuals who fall into a local optimum to continue participating in the search, and the individuals who perform the search normally remain as unchanged as possible. VCS is reflected in the ABC algorithm by swapping the dimensions of the bee's positions so that the ABC algorithm does not easily fall into a local optimum. Assuming that the dimension of the nth position of the bee performs VCS, the vertical cross update formula can be expressed as Eq. (13).

$$MS_i^m = \varepsilon \times x_{im} + (1-\varepsilon) \times x_{in} \tag{13}$$

where ε is a random number between $(0,1)$, x_{im} and x_{in} are the m th and n th dimensions of the i th bee, and MS_i^m is the offspring of bee x_i based on VCS.

4.2. The proposed CCABC

The CCABC proposed in this paper is mainly to improve the ability of the original ABC to jump out of the local optimum and the search ability in the early stage, and finally to achieve the purpose of improving the algorithm's ability to find the best. Therefore, this paper proposes a new CCABC algorithm based on the HCS and VCS. In CCABC, after the algorithm performs population initialization, HCS and VCS start to

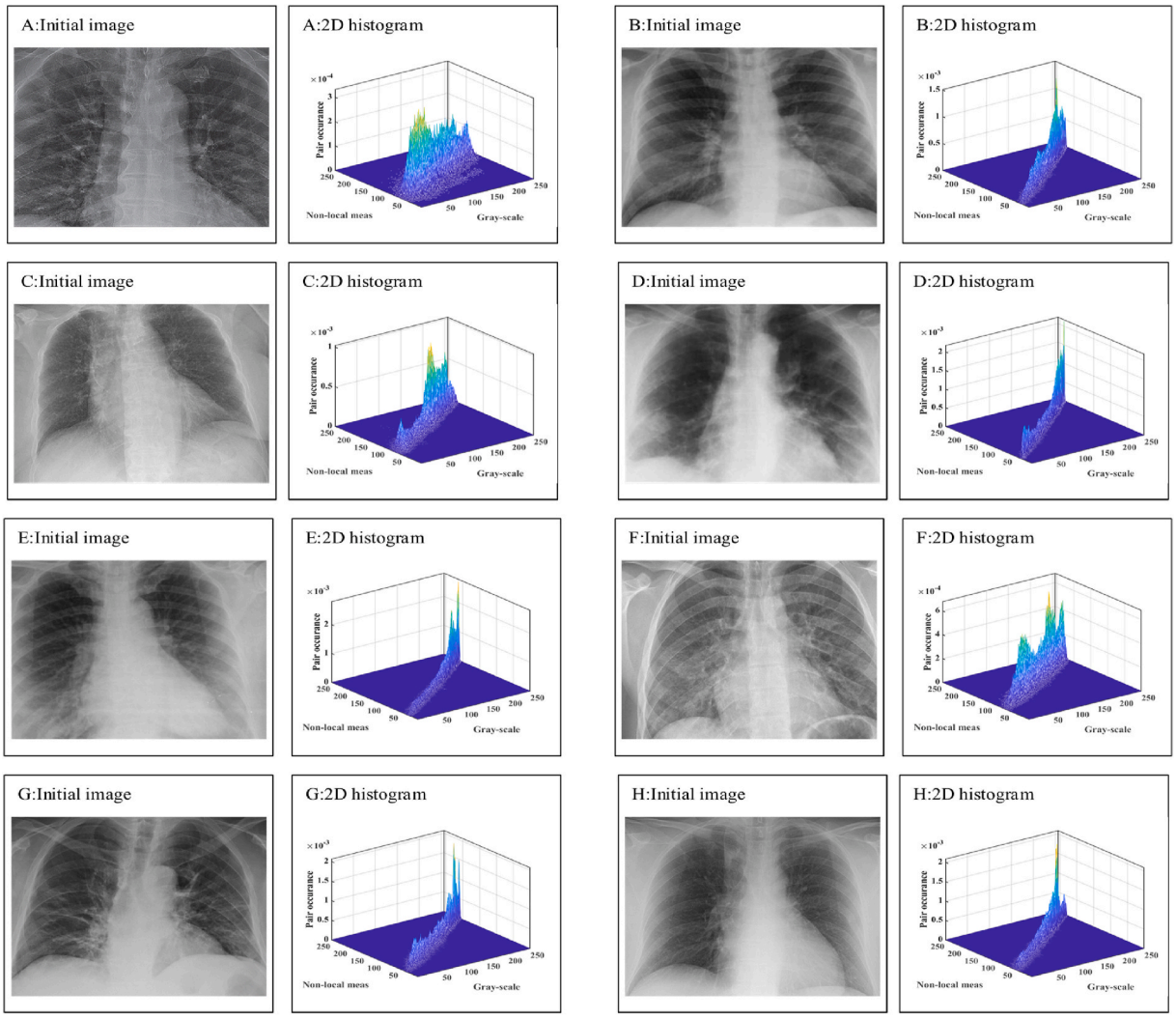

Fig. 5. Samples of the segmented images.

Table 4
Comparison results of CCABC and excellent algorithms.

Item	CCABC	ABC	SCA	MFO	PSO	SSA	HHO
+/−/ =	~	17/8/5	28/1/1	29/1/0	25/3/2	23/6/1	23/5/2
Mean	2.6	3.0	10.7	9.6	6.5	4.2	5.5
Rank	1	2	12	11	6	3	5
Item	**~**	**NCHHO**	**CBA**	**SCADE**	**IGWO**	**ACWOA**	**ASCA_PSO**
+/−/ =	~	22/7/1	26/2/2	26/3/1	27/3/0	27/2/1	28/2/0
Mean	~	6.6	7.9	10.7	5.3	9.5	8.3
Rank	~	7	8	13	4	10	9

participate in the population iteration to help individuals perform a fast search in the early stage and jump out of local optimum in the middle stage while giving full play to the strong exploitation capability of the ABC algorithm itself in the late iteration to improve the overall performance of the original algorithm. The flow chart of CCABC is shown in Fig. 4.

The pseudocode of CCABC is shown in Algorithm 2.

Algorithm 2. Pseudo-code of CCABC

The complexity of CCABC mainly includes introducing HCS and VCS, employing bees to search for food sources, onlooker bees to develop food sources, and calculating fitness values. First, the complexity level of HCS and VCS is $O(\mathrm{T} * \mathrm{N} * D + T * N^2)$. Then, the complexity level of employed bees searching for food sources is $O(T * N)$. The complexity level of the onlooker bee to exploit the food source is $O(T * N + T * F)$, which can be abbreviated as $O(T * N)$. Finally, the complexity level for both the search and the exploitation of food source fitness values calculation is $O(N * logN)$. Therefore, the overall complexity level of the CCABC algorithm is $O(CCABC) = O((D + N) * T * N^2 * logN)$.

5. Experiments and results

This section focuses on verifying the algorithm performance of CCABC and evaluating the image quality after segmentation using CCABC-MTIS. To show that CCABC has a better ability to jump out of local optimum and upfront search capability, this paper compares CCABC with six well-known optimization algorithms and six improved

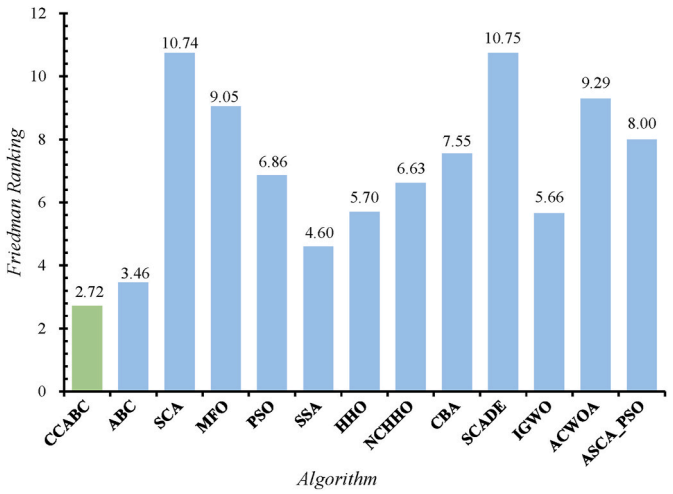

Fig. 6. Friedman test results of CCABC and excellent algorithms.

algorithms using 30 benchmark functions. Immediately after, to demonstrate the better segmentation performance of CCABC-MTIS in multilevel image segmentation, this paper compares CCABC-MTIS with nine peer methods and evaluates the segmentation results in detail using PSNR, SSIM, and FSIM.

5.1. Experiment setup

In the experimental part of the benchmark functions, 30 benchmark functions from CEC2014 are used in this paper to demonstrate the algorithmic performance of CCABC, and Table 2 represents the details of benchmark functions F1–F30. The test value of the benchmark function is the default value.

In addition, to ensure that the experiments are as fair as possible based on optimization and machine learning works [104–107], all the algorithm comparison experiments in this paper are done under the same conditions as below, with the settings in Table 3. The paper was analyzed using the mean, variance, Wilcoxon signed-rank test, and Freidman test for the experimental results.

In the experimental part of MTIS, segmented images A, B, C, D, E, F, G, and H are from the COVID-19 dataset. The COVID-19 disease is in the center of attention in recent years [108–110]. This dataset is from a publicly developed GitHub dataset containing chest X-rays and CT images of patients positive or suspected of having COVID-19 or other viral and bacterial pneumonia (MERS, SARS, and ARDS.). All images and data were collected through specialized physicians at each hospital and are under specified licenses. The dataset is publicly available at https://github.com/ieee8023/covid-chestxray-dataset. It has been studied in

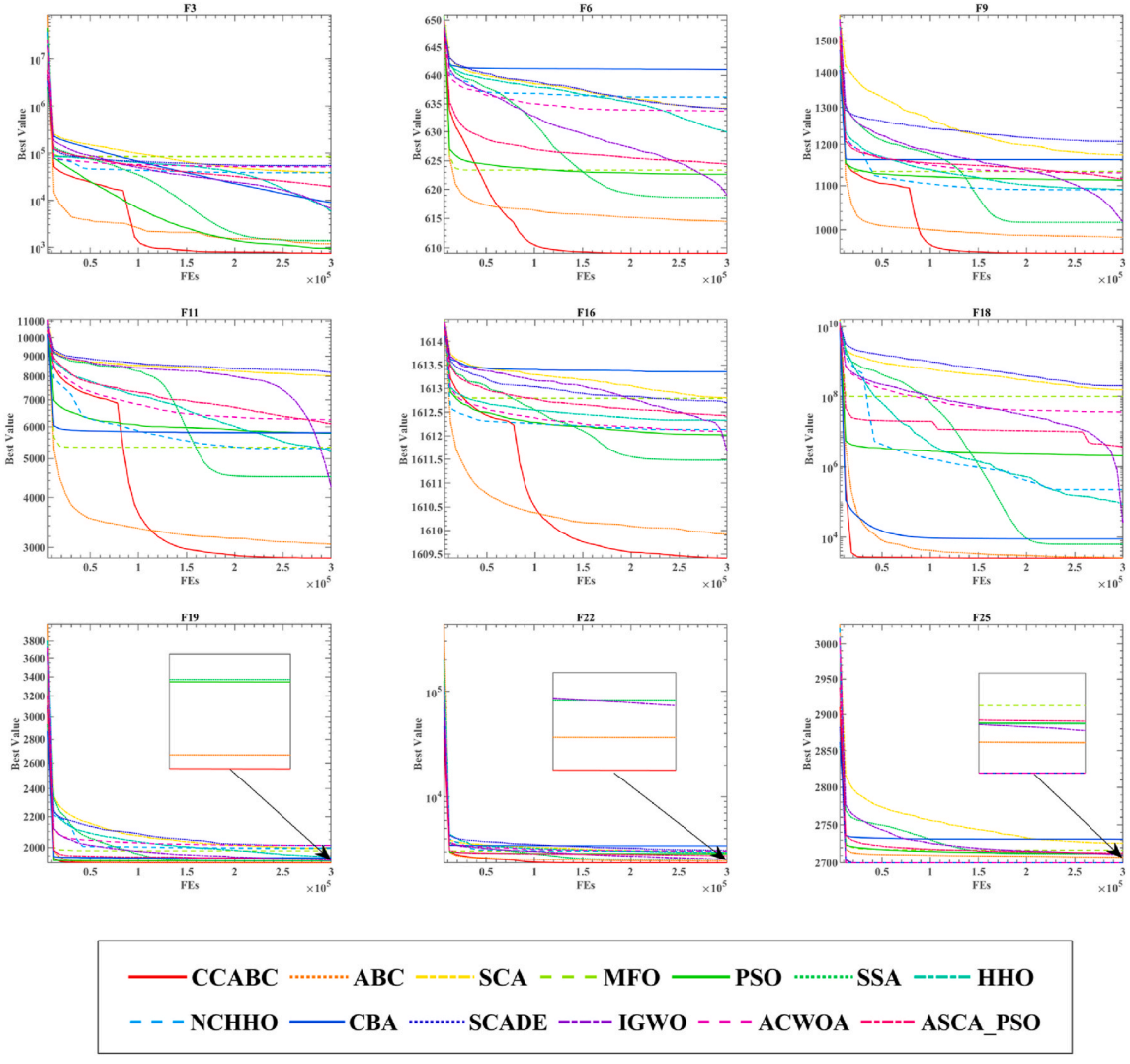

Fig. 7. Convergence curves of CCABC and excellent algorithms.

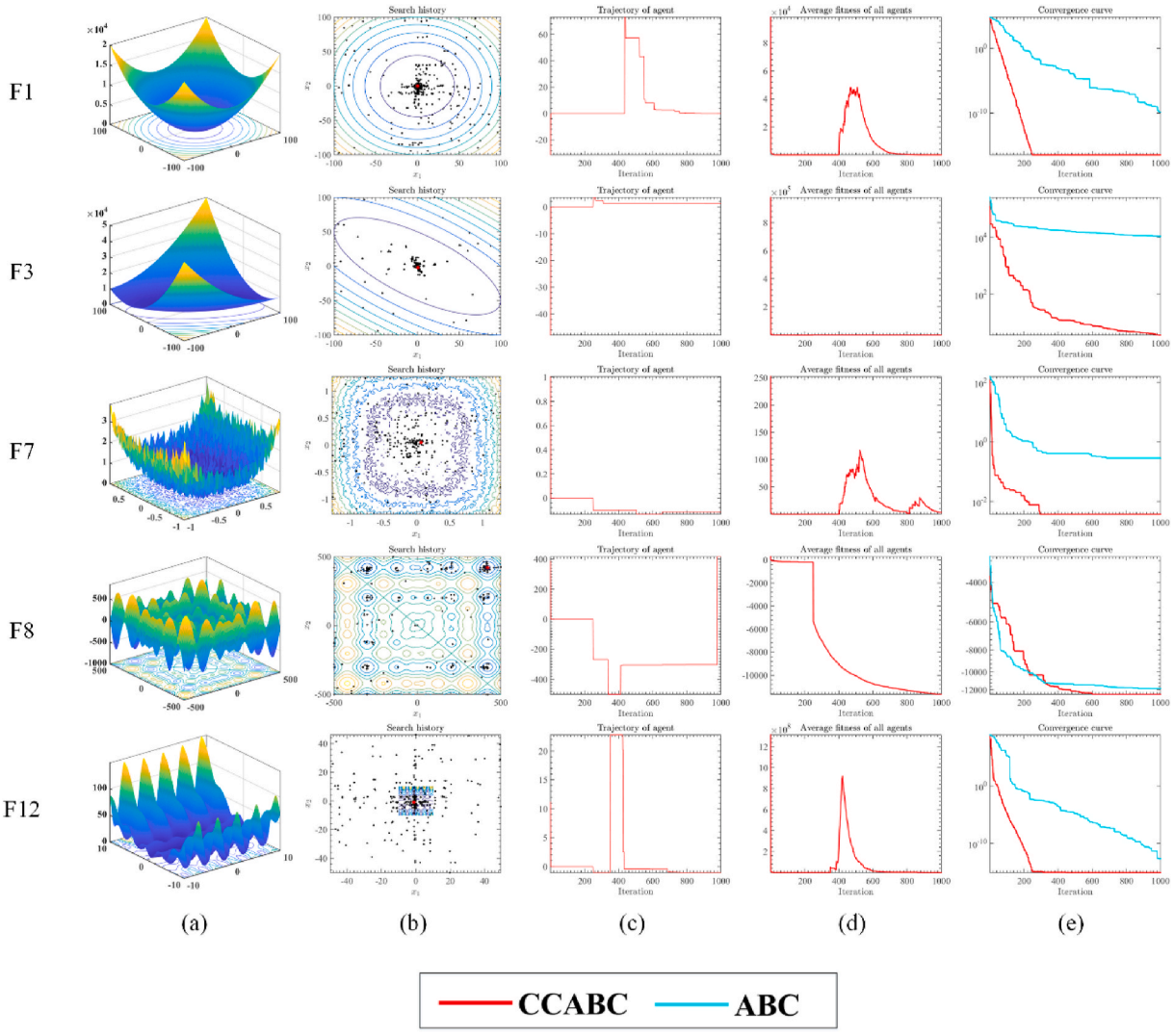

Fig. 8. (a) 3D location distribution of CCABC, (b) 2D location distribution of CCABC, (c) Trajectory of CCABC in the first dimension, (d) Average fitness of CCABC, (e) Convergence curves of CCABC and ABC.

several works [111,112].

In Fig. 5 shows their original images and the nonlocal average 2D histogram, respectively. To ensure the fairness of the experiment, all the algorithms involved in the comparison were tested under the same conditions. In addition, to accurately reflect each algorithm's performance at different threshold levels, this paper covers both low and high threshold levels as much as possible when setting the threshold levels. In the experiments, the 3, 5, and 7 thresholds represent the low threshold levels, and these 12, 15, and 18 thresholds represent the high threshold levels.

Finally, the experimental parameter settings for all algorithms in this paper are default values, and detailed parameter information is given in Table A1 in Appendix A. The experiments were conducted uniformly on the Windows Server 2008R2 operating system to ensure the same environment for all experiments. The main hardware of the device is an Intel(R) Xeon(R) CPUE5-2660v3 (2.60 GHz) and 16 GB of RAM, and the code running software is Matlab2017b.

5.2. CCABC benchmark function validation

5.2.1. Comparison of CCABC and excellent algorithms

In this section, CCABC is compared with six basic algorithms and six improved algorithms based on 30 benchmark functions, where the basic algorithms include sine cosine algorithm (SCA) [113], whale optimizer (WOA) [113], salp swarm algorithm (SSA) [113], moth-flame optimization (MFO) [113], multi-verse optimizer (MVO) [113], shortly shown by ABC, SCA, MFO, PSO, SSA, and HHO. Also, the improved algorithms include Nonlinear based chaotic HHO (NCHHO) [114], chaotic BA (CBA) [115], SCA with differential evolution [116], enhanced GWO with a new hierarchical structure (IGWO) [58], improved WOA (IWOA) [117], A-C parametric WOA (ACWOA) [118], adaptive SCA integrated with PSO (ASCA_PSO) [119], shortly all of them shown by NCHHO, CBA, SCADE, IGWO, ACWOA, and ASCA_PSO. The experimental results of comparing CCABC with other peer algorithms are given in Table A2, where AVG denotes the mean value of the algorithm after 50 independent runs and STD denotes its variance. We can initially see that CCABC has the smallest mean and variance in most benchmark function tests by observing the mean and variance. When using CCABC and similar algorithms for benchmark functions, CCABC obtains high-quality solutions and has a high degree of generalizability in optimizing the benchmark function.

In Table 4, this paper further analyzes the benchmark function optimization effect between CCABC and other classes of algorithms using Wilcoxon signed-rank test, where '+' indicates that CCABC outperforms other algorithms, '-' indicates that CCABC underperforms other algorithms, ' = ' indicates that CCABC's performance is equal to

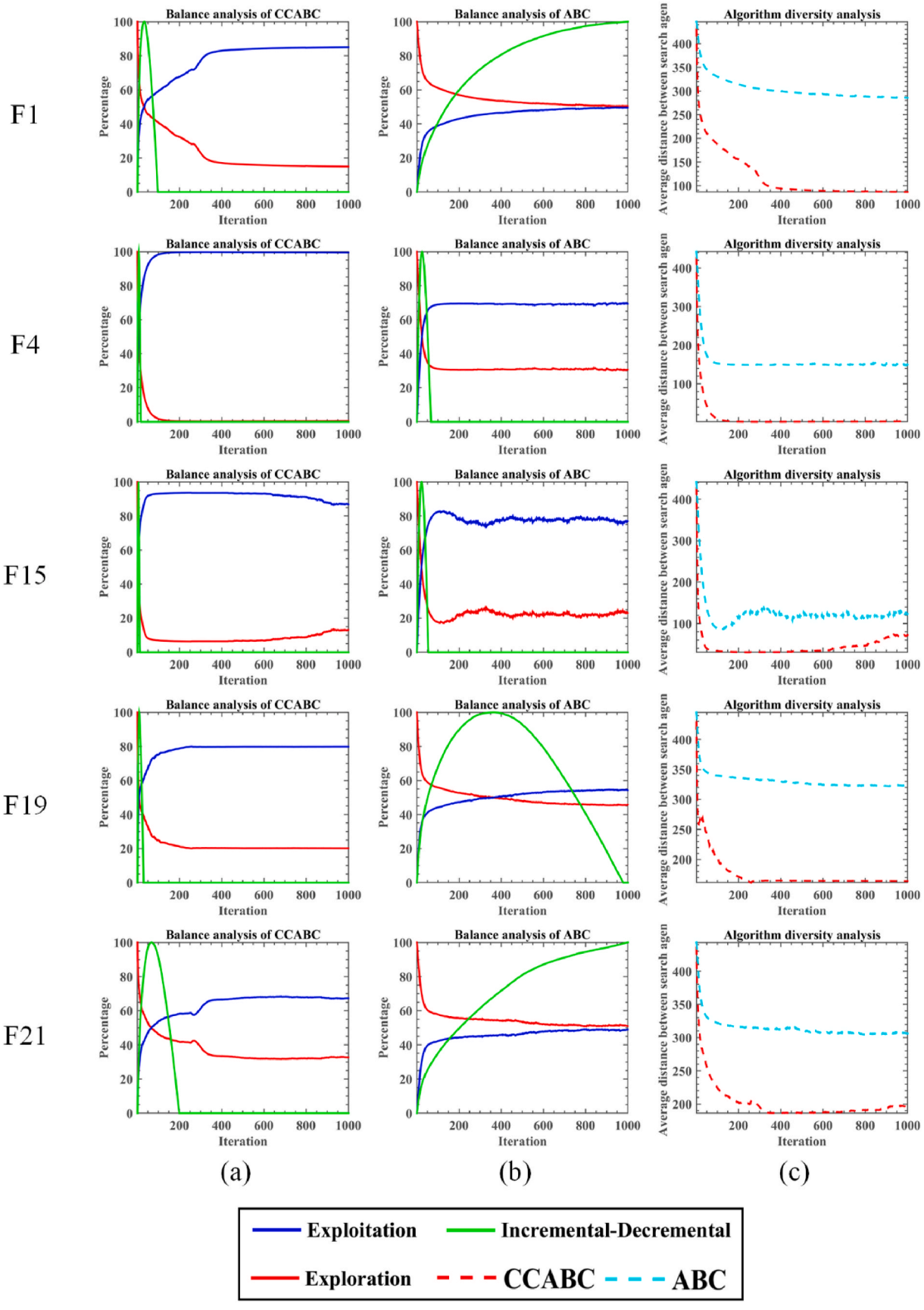

Fig. 9. (a) The balance analysis of CCABC, (b) The balance analysis of ABC, (c) The diversity analysis of CCABC and ABC.

Table 5
Comparison of CCABC and ABC variants with Wilcoxon test and Friedman test.

Fun	Item	CCABC	DEMABC	GAABC	ISABC	NNMABC
F1	AVG	**2.747E+06**	1.300E+08	8.951E+07	1.278E+08	9.722E+07
	STD	**1.006E+06**	2.519E+06	1.413E+07	4.222E+07	1.715E+08
F2	AVG	**2.626E+03**	3.244E+08	1.082E+10	2.869E+10	5.952E+09
	STD	**2.820E+03**	3.711E+03	1.126E+09	8.820E+09	1.334E+10
F3	AVG	**6.641E+02**	3.433E+04	2.815E+04	5.127E+04	2.837E+04
	STD	4.618E+02	**3.069E+02**	1.598E+04	1.383E+04	4.106E+04
F4	AVG	4.860E+02	**4.071E+02**	1.580E+03	1.268E+03	2.142E+03
	STD	2.527E+01	**1.688E+01**	1.733E+02	1.912E+02	4.632E+03
F5	AVG	5.202E+02	**5.200E+02**	5.206E+02	5.210E+02	5.203E+02
	STD	4.176E-02	**2.075E-03**	3.925E-02	5.065E-02	2.440E-01
F6	AVG	**6.095E+02**	6.319E+02	6.250E+02	6.417E+02	6.285E+02
	STD	2.425E+00	2.498E+00	**1.209E+00**	1.411E+00	4.762E+00
F7	AVG	**7.000E+02**	7.325E+02	7.789E+02	1.102E+03	7.786E+02
	STD	**6.377E-05**	3.918E-02	9.983E+00	8.340E+01	1.655E+02
F8	AVG	**8.000E+02**	9.676E+02	9.442E+02	1.296E+03	9.108E+02
	STD	**7.263E-14**	2.253E+01	9.153E+00	2.909E+01	7.433E+01
F9	AVG	**9.498E+02**	1.185E+03	1.099E+03	1.494E+03	1.154E+03
	STD	**7.814E+00**	1.269E+01	1.223E+01	4.721E+01	7.630E+01
F10	AVG	**1.001E+03**	3.491E+03	4.251E+03	7.701E+03	4.090E+03
	STD	**8.370E-01**	2.844E+02	1.926E+02	3.865E+02	1.479E+03
F11	AVG	**2.796E+03**	5.353E+03	6.105E+03	8.748E+03	5.534E+03
	STD	**2.077E+02**	3.246E+02	3.169E+02	3.448E+02	1.002E+03
F12	AVG	1.200E+03	**1.200E+03**	1.201E+03	1.203E+03	1.201E+03
	STD	**3.469E-02**	5.825E-02	9.906E-02	3.699E-01	3.826E-01
F13	AVG	**1.300E+03**	1.301E+03	1.303E+03	1.311E+03	1.302E+03
	STD	2.932E-02	**1.609E-02**	1.479E-01	1.118E+00	2.278E+00
F14	AVG	**1.400E+03**	1.400E+03	1.436E+03	1.685E+03	1.421E+03
	STD	1.793E-02	**9.209E-03**	3.715E+00	3.466E+01	5.774E+01
F15	AVG	**1.503E+03**	1.514E+03	2.461E+03	6.743E+03	5.995E+05
	STD	**4.909E-01**	2.558E+00	2.992E+02	2.940E+03	1.835E+06
F16	AVG	**1.609E+03**	1.613E+03	1.611E+03	1.614E+03	1.613E+03
	STD	3.938E-01	4.817E-01	2.274E-01	**1.693E-01**	4.591E-01
F17	AVG	**6.249E+05**	1.885E+06	4.612E+06	8.973E+06	4.446E+06
	STD	**3.220E+05**	7.342E+05	1.368E+06	2.772E+06	1.163E+07
F18	AVG	2.559E+03	**2.108E+03**	7.078E+07	8.338E+07	1.125E+08
	STD	9.569E+02	**4.348E+02**	2.149E+07	3.711E+07	4.591E+08
F19	AVG	**1.905E+03**	1.913E+03	1.977E+03	2.034E+03	1.991E+03
	STD	9.290E-01	**7.154E-01**	1.722E+01	3.424E+01	1.427E+02
F20	AVG	7.138E+03	2.227E+04	**5.849E+03**	1.596E+04	5.796E+04
	STD	2.144E+03	1.684E+03	**1.480E+03**	4.704E+03	2.870E+05
F21	AVG	**1.064E+05**	2.746E+05	1.129E+06	6.199E+06	1.455E+06
	STD	5.625E+04	**3.241E+04**	3.775E+05	3.034E+06	3.336E+06
F22	AVG	**2.380E+03**	1.297E+04	2.829E+03	2.803E+03	2.837E+03
	STD	**7.395E+01**	9.172E+01	1.118E+02	1.107E+02	1.909E+02
F23	AVG	**2.615E+03**	2.632E+03	2.668E+03	2.789E+03	2.707E+03
	STD	**1.665E-03**	9.021E-03	1.137E+01	5.372E+01	2.050E+02
F24	AVG	**2.600E+03**	2.642E+03	2.625E+03	2.912E+03	2.698E+03
	STD	**1.291E-02**	3.204E+00	7.217E+00	2.492E+01	8.169E+01
F25	AVG	**2.700E+03**	2.718E+03	2.710E+03	2.788E+03	2.722E+03
	STD	**0.000E+00**	1.652E+00	3.137E+00	2.264E+01	1.739E+01
F26	AVG	**2.700E+03**	2.800E+03	2.702E+03	2.704E+03	2.713E+03
	STD	1.105E-01	**5.848E-02**	4.243E-01	4.914E-01	2.869E+01
F27	AVG	**3.064E+03**	3.258E+03	3.176E+03	3.746E+03	3.702E+03
	STD	4.019E+01	1.920E+02	**1.317E+01**	1.921E+02	2.751E+02
F28	AVG	**3.649E+03**	9.875E+03	4.259E+03	4.783E+03	5.087E+03
	STD	**3.105E+01**	4.773E+02	5.202E+01	1.587E+02	8.883E+02
F29	AVG	4.438E+03	**4.109E+03**	1.181E+06	2.132E+06	4.451E+06
	STD	4.508E+02	**2.233E+02**	4.541E+05	9.942E+05	1.409E+07
F30	AVG	**5.808E+03**	3.535E+04	6.266E+04	5.016E+04	2.390E+04
	STD	**8.399E+02**	2.860E+03	1.530E+04	1.235E+04	3.092E+04

Table 6
Comparison results of CCABC with its variants and Wilcoxon ranking.

Item	CCABC	DEMABC	GAABC	ISABC	NNMABC
+/−/ =	~	25/4/1	29/1/0	30/0/0	29/0/1
Mean	1.20	2.73	3.00	4.47	3.60
rank	1	2	3	5	4

other algorithms, Mean indicates the level of overall mean, and Rank denotes the ranking result of the overall mean. Fig. 6 represents a further analysis of the comparative results of the benchmark functions using the Freidman test. The Wilcoxon signed-rank test and Freidman test analysis show that CCABC has the first performance in optimizing both benchmark functions.

In addition, Fig. 7 shows the convergence curves of CCABC and other similar algorithms on different functions. The convergence curves shown show that CCABC obtains better quality solutions than the other algorithms when optimizing the benchmark functions F6, F11, and F16. However, CCABC converges slightly slower than the other algorithms in the first stage. In optimizing high-quality solutions for F3, F9, F11, and F16, the algorithm has obvious inflection points for jumping out of the local optimum. In optimizing F19 and F25, it can be seen that CCABC

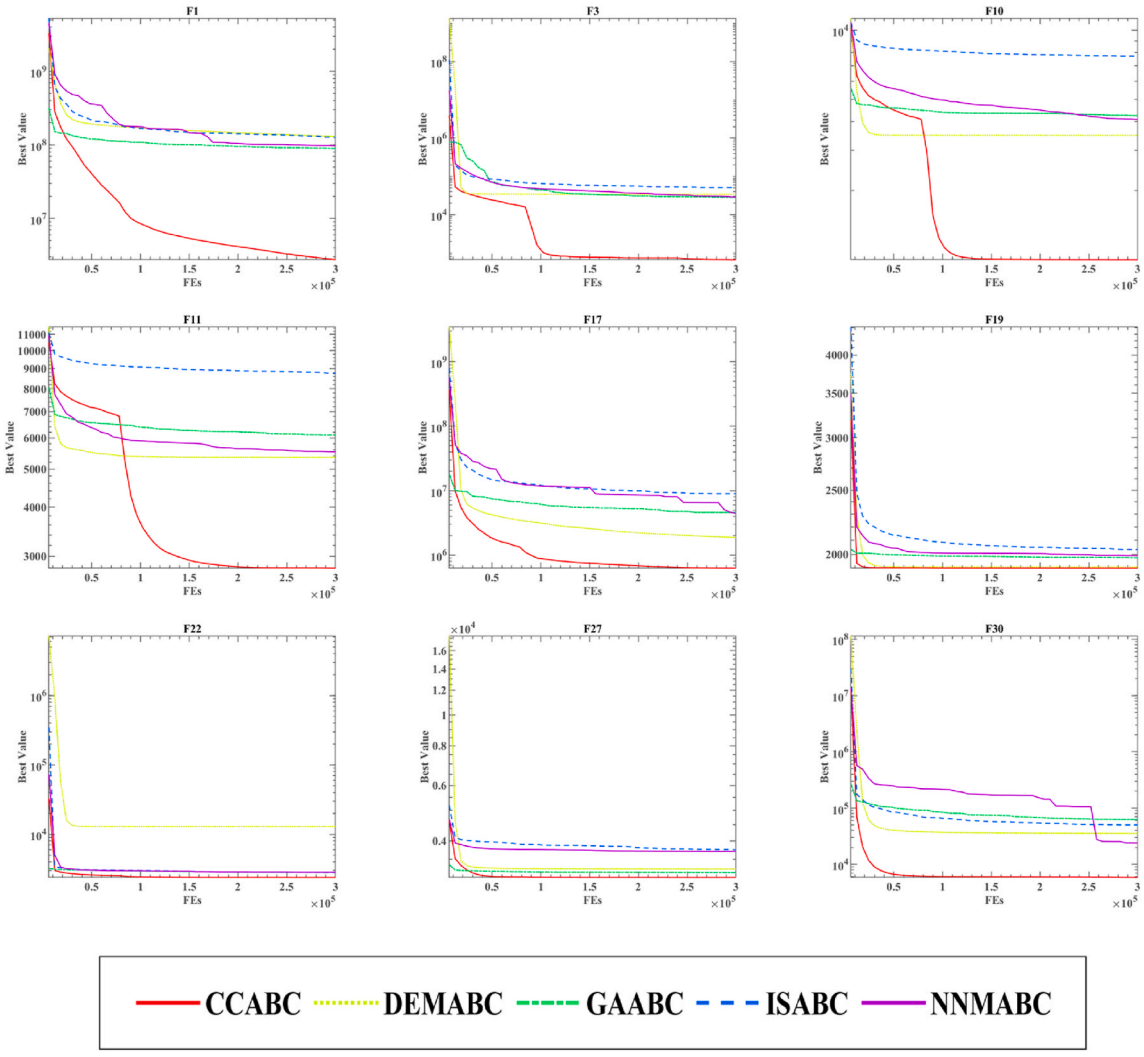

Fig. 10. Convergence curves of CCABC and ABC variants.

Table 7
Performance indicators of the multilevel image segmentation methods.

Evaluation Metrics	Core Formula	Description
Peak Signal to Noise Ratio (PSNR)	$PSNR = 20 \cdot \log_{10}\left(\frac{255}{RMSE}\right)$	Image quality evaluation technique based on the error between corresponding pixel points before and after image processing.
Structural Similarity Index (SSIM)	$SSIM = \frac{(2\mu_I\mu_{Seg} + c_1)(2\sigma_{I,Seg} + c_2)}{(\mu_I{}^2 + \mu_{Seg}{}^2 + c_1)(\sigma_I{}^2 + \sigma_{Seg}{}^2 + c_2)}$	Image evaluation metrics to evaluate the similarity between images from three perspectives.
Feature Similarity Index (FSIM)	$FSIM = \frac{\sum_{I\in\Omega} S_L(X) PC_m(X)}{\sum_{I\in\Omega} PC_m(X)}$	A variant of the SSIM technique that uses feature similarity for image quality evaluation.

obtains high-quality solutions and converges faster than other algorithms. Through the above analysis of the benchmark function results, CCABC can jump out of local optimum solutions, have a solid ability to obtain high-quality solutions and fast convergence speed. Therefore, CCABC is a superior method for optimizing the benchmark function and a very good SIOA.

5.2.2. *Analysis of CCABC in the iterative process*

The proposed CCABC algorithm mainly introduces the horizontal search mechanism and the vertical search mechanism into ABC. Therefore, this section focuses on the performance of CCABC and ABC in the process of optimizing benchmark functions.

Fig. 8 shows the results of the qualitative inspection of 23 benchmark functions by CCABC and ABC. The graph in the first column (a) exposes the 3D location distribution of the CCABC search history. The graph in the second column (b) discloses the two-dimensional location distribution of CCABC search history. The graph in the third column (c) discloses the trajectories of CCABC individuals in the first dimension. The graph in the fourth column (d) reveals the average fitness of CCABC, and the graph in the fifth column (e) reveals the convergence curves of CCABC and ABC. Fig. 8 (a) and (b) record the positions and distribution of individuals searching or developing in each iteration. It can be seen that most of the individual search positions are near the optimal solution, and a small number of positions are scattered in the space. This means that after the individuals in the population have searched most of the space, CCABC can still find the location of the optimal solution during the convergence process. In Fig. 8 (c), we can see that the values of the first dimension in the individuals are more volatile and random in the

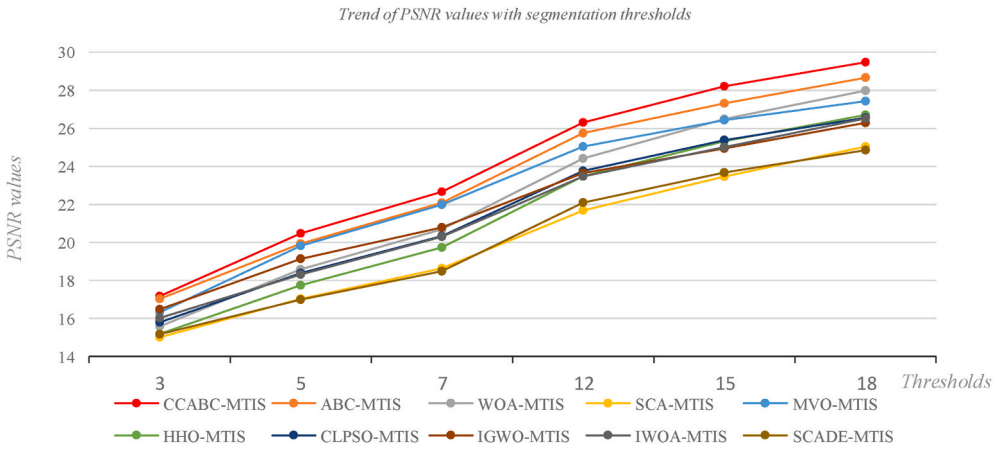

Fig. 11. The PSNR values of CCABC and other similar segmentation models.

early stage and more smoothly rational in the later stage, which indicates that CCABC has good randomness in the early stage to traverse the space as much as possible, while it does not change much in the later stage of the algorithm and favors exploitation. Fig. 8 (d) shows the average fitness curve, from which it can be seen that the fitness range is wide, and the curve decreases rapidly with the increase of the number of iterations, indicating that CCABC has good convergence characteristics. In addition, it is obvious in the figure that there is a move to expand the search range in the middle of the algorithm to jump out of the local optimum, especially F8 successfully jumps out of the position of the previous local optimum solution. Fig. 8 (e) shows that CCABC is able to find higher-quality solutions faster than ABC.

The balance and diversity of CCABC and ABC were analyzed on 30 functions of CEC2014, and the performance of CCABC was further investigated.

Fig. 9 (a) and (b) show the equilibrium analysis of CCABC and ABC, and Fig. 9 (c) shows the diversity analysis of CCABC and ABC. We added increment-decrement curves in Fig. 9 (a) and (b). When the value of the mining result is greater than or equal to the mining result, the curve increases. Otherwise, it decreases. When it has a negative value, it is set to zero. Thus, its high value represents extensive search activity, and its low value represents strong exploitation activity. In addition, the duration of the high or low value in the graph reflects the sustained effect of search or exploitation in the search for excellence. The increment-decrement curve is maximized when the search effect is at the same level as the exploitation effect. In Fig. 9 (c), the x-axis represents the number of iterations, and the y-axis represents the diversity. We can see that the population diversity is extensive at the beginning due to random initialization and gradually decreases with the number of iterations. Of course, we also know through the above that the algorithm does not just perform one extensive search, so the diversity of the population fluctuates throughout the search process, especially when many individuals do not find the optimal solution during the exploitation process. Individuals regenerate completely new solutions, such as F15 and F21 in Fig. 9 (c).

In the metaheuristic algorithm, the search process and the exploitation process affect each other and can influence the final result of the optimal search, so it is necessary to consider the balance between these two. In Fig. 9 (a) and (b), by observing the incremental-decremental curves, it is evident that the search and exploitation results of CCABC reach superiority significantly earlier than ABC, which indicates that CCABC is able to find a better solution faster in the search phase and can be developed quickly. In addition, it can be seen by the separate search and exploitation curves that CCABC search and exploitation effects are significantly stronger than ABC.

5.2.3. Comparative analysis of CCABC and ABC variants

In this section, CCABC is compared with four variants of the ABC algorithm based on 30 benchmark functions, including DEMABC [120], GAABC [121], ISABC [122] and NNMABC [123]. The experimental results of CCABC compared with the variants of the ABC algorithm are shown in Table 5, where AVG denotes the mean value of the algorithm after 50 independent runs and STD denotes the variance of the algorithm. By looking at the mean and variance, we can initially see that CCABC has the smallest mean and variance in most of the benchmark function tests. Further, In Table 6, this paper further analyzes the benchmark function optimization effect between CCABC and a variant of the ABC algorithm using the Wilcoxon signed-rank test. can be seen that CCABC is ranked No. 1 and there is a statistically significant difference between them.

In addition, Fig. 10 shows the convergence curves of CCABC and ABC algorithm variants on different functions. The convergence curves show that CCABC obtains better solution quality than the other algorithms when optimizing the benchmark functions F22 and F27. Still, CCABC converges slightly slower than the other algorithms in the initial stage. In optimizing F3, F10, and F11, both the high-quality solutions and the algorithm have obvious inflection points for jumping out of the local optimum. By optimizing F1, F17, F19, and F30, it can be seen that CCABC obtains high-quality solutions and converges faster than the other algorithms. Through the above analysis of the benchmark function results, CCABC also has the same large advantage over the other variant algorithms.

5.3. CCABC for multi-threshold image segmentation

This paper compares MTIS experiments for CCABC-MTIS, ABC-MTIS, WOA-MTIS, SCA-MTIS, MVO-MTIS, CLPSO-MTIS, IGWO-MTIS, IWOA-MTIS, and SCADE-MTIS using images A, B, C, D, E, F, G, and H.

5.3.1. Performance evaluation parameters

In this section, to accurately evaluate the quality of the segmentation results of each algorithm, we use PSNR, SSIM, and FSIM as the evaluation criteria. The definitions and descriptions of the three evaluation metrics are listed in Table 7, respectively.

When we use PSNR to evaluate the results of image segmentation, *RMSE* is the root mean square error of each pixel, defined as Eq. (14), where $M \times N$ denotes the size of the image, I_{ij} denotes the pixel gray value of the original image, and finally, Seg_{ij} denotes the gray value of the pixel in the segmented image.

$$RMSE = \sqrt{\frac{\sum_{i=0}^{M-1}\sum_{j=0}^{N-1}\left(I_{ij} - Seg_{ij}\right)^2}{M \times N}} \tag{14}$$

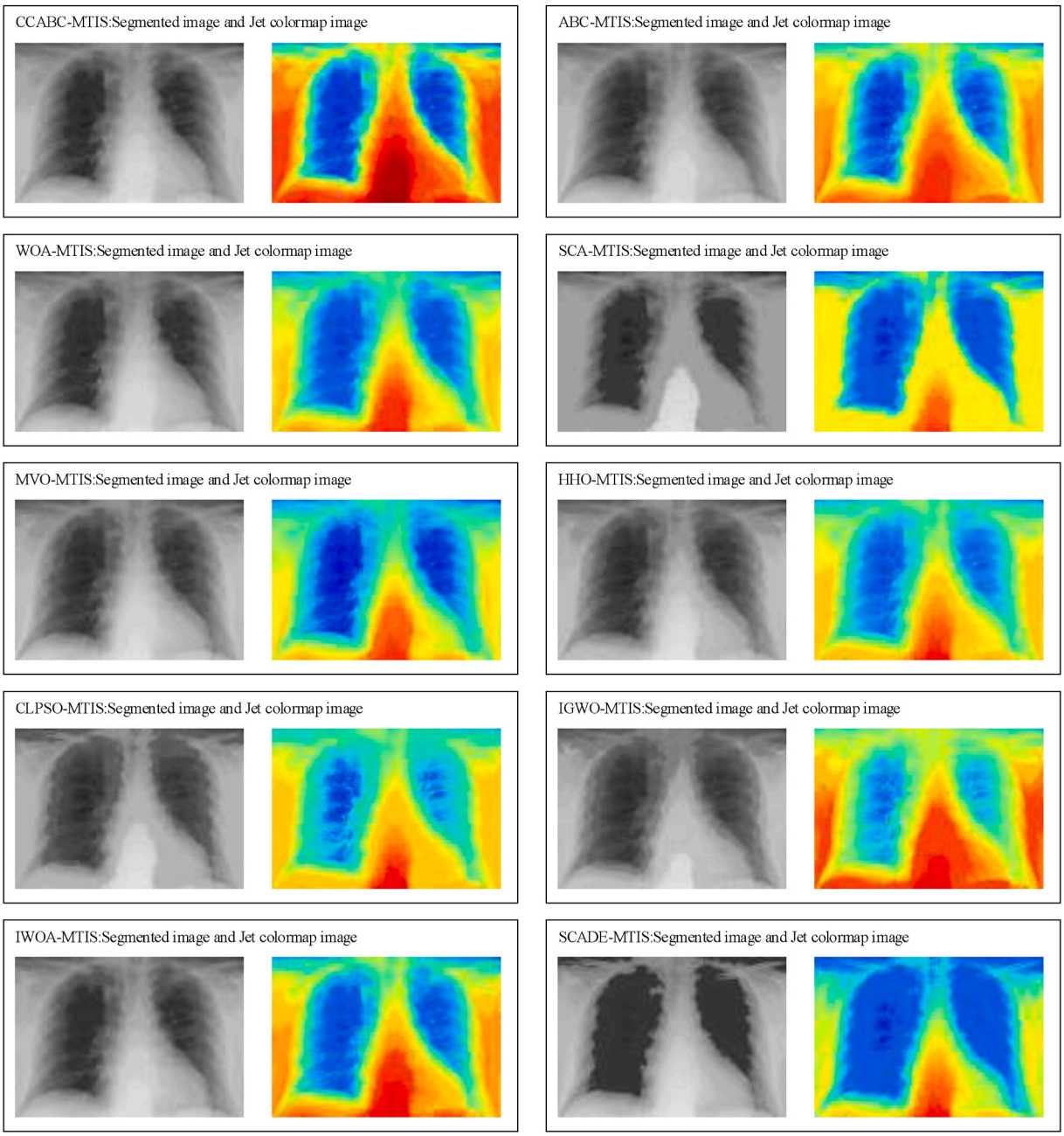

Fig. 12. The segmented results of H obtained by each algorithm at threshold value 18.

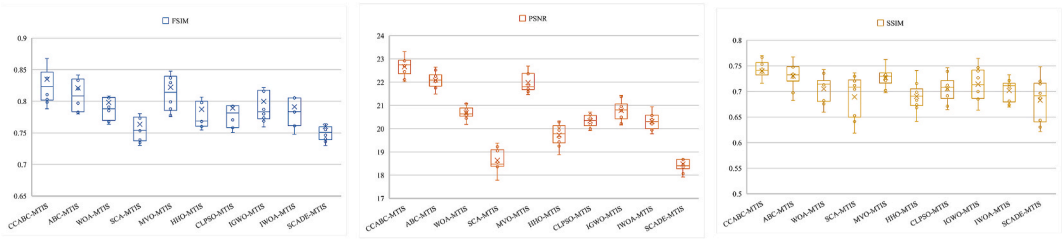

Fig. 13. FSIM, PSNR and SSIM evaluation results for each algorithm at a low threshold level of 7.

Simultaneously, the mean, variance, and Wilcoxon signed-rank test were used to further analyze the FSIM, PSNR, and SSIM evaluation results.

5.3.2. *Experimental result analyses*

Fig. 11 represents the performance of PSNR values of CCABC and other similar segmentation models at different threshold levels. In Fig. 4, the PSNR values are not high when the same type of models perform

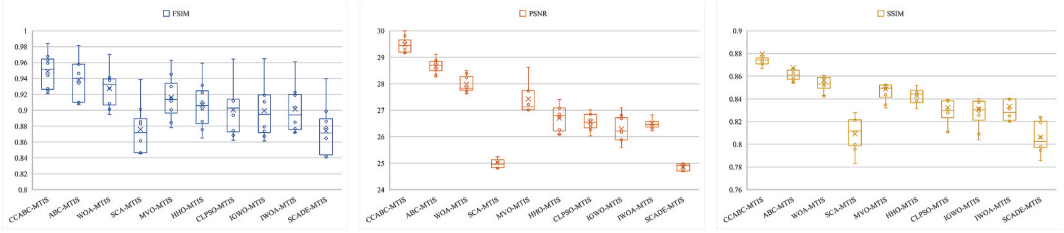

Fig. 14. FSIM, PSNR and SSIM evaluation results for each algorithm at a high threshold level of 18.

Table 8
The FSIM comparison results of CCABC-MTIS and other methods.

Thresholds		CCABC-MTIS	ABC-MTIS	WOA-MTIS	SCA-MTIS	MVO-MTIS	HHO-MTIS	CLPSO-MTIS	IGWO-MTIS	IWOA-MTIS	SCADE-MTIS
3	+/−/ =	~	1/0/7	6/0/2	8/0/0	3/0/5	8/0/0	8/0/0	2/1/5	5/0/3	4/0/4
	Mean	1.5	3	7.375	6.125	3.875	9.25	8.125	3.625	6.875	5.25
	Rank	1	2	8	6	4	10	9	3	7	5
5	+/−/ =	~	4/0/4	5/0/3	7/0/1	6/0/2	8/0/0	8/0/0	5/0/3	6/0/2	8/0/0
	Mean	1.125	3	5.5	8.625	3	7.875	6.5	3.5	6.875	9
	Rank	1	2	5	9	2	8	6	4	7	10
7	+/−/ =	~	3/0/5	8/0/0	8/0/0	3/0/5	8/0/0	5/1/2	5/2/1	5/1/2	7/1/0
	Mean	1.875	3.75	5.5	8.625	3.5	6.375	6.375	4.75	5.375	8.875
	Rank	1	3	6	9	2	7	7	4	5	10
12	+/−/ =	~	4/0/4	8/0/0	8/0/0	7/0/1	8/0/0	8/0/0	8/0/0	8/0/0	8/0/0
	Mean	1	2	4.125	9.625	3	6.125	6.25	6.75	6.75	9.375
	Rank	1	2	4	10	3	5	6	7	7	9
15	+/−/ =	~	6/0/2	8/0/0	8/0/0	8/0/0	8/0/0	8/0/0	8/0/0	8/0/0	8/0/0
	Mean	1	2	3.625	9.625	3.375	5.625	6.125	7.125	7.125	9.375
	Rank	1	2	4	10	3	5	6	7	7	9
18	+/−/ =	~	6/0/2	8/0/0	8/0/0	8/0/0	8/0/0	8/0/0	8/0/0	8/0/0	8/0/0
	Mean	1	2	3.125	9.375	4.375	5.75	6.625	6.75	6.375	9.625
	Rank	1	2	3	9	4	5	7	8	6	10

Table 9
The PSNR comparison results of CCABC-MTIS and other methods.

Thresholds		CCABC-MTIS	ABC-MTIS	WOA-MTIS	SCA-MTIS	MVO-MTIS	HHO-MTIS	CLPSO-MTIS	IGWO-MTIS	IWOA-MTIS	SCADE-MTIS
3	+/−/ =	~	1/1/6	8/0/0	8/0/0	5/0/3	8/0/0	6/0/2	5/0/3	5/0/3	8/0/0
	Mean	1.5	2	6.875	8.625	4.875	8.125	5.5	3.625	5.625	8.25
	Rank	1	2	7	10	4	8	5	3	6	9
5	+/−/ =	~	3/0/5	7/0/1	8/0/0	5/0/3	8/0/0	8/0/0	7/0/1	8/0/0	8/0/0
	Mean	1.125	2.125	5.625	9.625	2.75	7.875	5.75	4.25	6.5	9.375
	Rank	1	2	5	10	3	8	6	4	7	9
7	+/−/ =	~	4/0/4	8/0/0	8/0/0	4/0/4	8/0/0	8/0/0	7/0/1	8/0/0	8/0/0
	Mean	1	2.25	5.125	9.125	2.75	7.75	6.125	4.875	6.25	9.75
	Rank	1	2	5	9	3	8	6	4	7	10
12	+/−/ =	~	4/0/4	8/0/0	8/0/0	8/0/0	8/0/0	8/0/0	8/0/0	8/0/0	8/0/0
	Mean	1	2	4.25	9.625	3	6.5	6	6.625	6.625	9.375
	Rank	1	2	4	10	3	6	5	7	7	9
15	+/−/ =	~	6/0/2	8/0/0	8/0/0	8/0/0	8/0/0	8/0/0	8/0/0	8/0/0	8/0/0
	Mean	1	2.125	3.375	9.75	3.5	6.125	6	6.875	7	9.25
	Rank	1	2	3	10	4	6	5	7	8	9
18	+/−/ =	~	7/0/1	8/0/0	8/0/0	8/0/0	8/0/0	8/0/0	8/0/0	8/0/0	8/0/0
	Mean	1	2	3.125	9.25	4.125	6	6.375	7.125	6.25	9.75
	Rank	1	2	3	9	4	5	7	8	6	10

image segmentation at low threshold levels, which indicates that the segmented image is severely distorted compared to the original image and the noise level of the image is high. This indicates that the noise level and distortion degree of the images segmented by CCABC is the least, and they are most close to the details of the original image.

The PSNR evaluation criterion analyzes the difference of images before and after segmentation from the perspective of mathematical analysis. At the same time, FSIM and SSIM are evaluation criteria for image quality based on the human visual system (HVS). The general trend is that the higher the segmentation threshold level is, the more obvious the segmentation effect is. Each algorithm model's image segmentation results at the threshold level of 18 are selected as the samples for HVS analysis. The segmentation results under other threshold levels are shown in Tables A3-A5. Therefore, Fig. 12 shows image segmentation results by all algorithms for image H when the threshold level is 18. In Fig. 12, it can be seen from the perspective of HVS that after CCABC segmentation, the image is more consistent and uniform in the regions of the same feature, satisfying the internal consistency; the difference is more significant in the regions adjacent to different features; and the boundaries of the regions are simple and not rough, indicating that the spatial location is equally accurately located. Meanwhile, in Table A4 and Table A5, the FSIM values and SSIM values of CCABC at the threshold level of 18 are higher than those of other models, which indicates that the CCABC segmented image has the highest structural similarity and feature similarity with the original image, which is fully consistent with the results of HVS analysis. In addition, Fig. 13 and

Table 10
The SSIM comparison results of CCABC-MTIS and other methods.

Thresholds		CCABC-MTIS	ABC-MTIS	WOA-MTIS	SCA-MTIS	MVO-MTIS	HHO-MTIS	CLPSO-MTIS	IGWO-MTIS	IWOA-MTIS	SCADE-MTIS
3	+/−/ =	~	3/0/5	8/0/0	4/0/4	4/0/4	8/0/0	8/0/0	3/2/3	8/0/0	3/0/5
	Mean	1.375	2.5	8.875	4.625	5.375	9.625	7.25	3.25	7.5	4.625
	Rank	1	2	9	4	6	10	7	3	8	4
5	+/−/ =	~	2/0/6	6/0/2	7/0/1	5/0/3	7/0/1	7/0/1	2/1/5	7/0/1	6/0/2
	Mean	1.375	2.875	7.5	6.375	4.5	9.125	6.375	3.125	7.125	6.625
	Rank	1	2	9	5	4	10	5	3	8	7
7	+/−/ =	~	1/0/7	8/0/0	8/0/0	3/0/5	8/0/0	6/1/1	6/2/0	6/1/1	6/1/1
	Mean	2	3.25	5.25	7.375	3.5	7.5	5.875	5.375	6.75	8.125
	Rank	1	2	4	8	3	9	6	5	7	10
12	+/−/ =	~	4/0/4	7/0/1	8/0/0	4/0/4	8/0/0	8/0/0	8/0/0	8/0/0	8/0/0
	Mean	1	2.125	4.5	9.625	3	6	6.375	6.375	7	9
	Rank	1	2	4	10	3	5	6	6	8	9
15	+/−/ =	~	6/0/2	6/0/2	8/0/0	7/0/1	7/0/1	8/0/0	8/0/0	8/0/0	8/0/0
	Mean	1	2.5	3.125	9.5	3.375	5.75	6.25	7.25	6.75	9.5
	Rank	1	2	3	9	4	5	6	8	7	9
18	+/−/ =	~	7/0/1	8/0/0	8/0/0	8/0/0	8/0/0	8/0/0	8/0/0	8/0/0	8/0/0
	Mean	1	2	3.25	9.25	4	5.5	6.875	6.875	6.5	9.75
	Rank	1	2	3	9	4	5	7	7	6	10

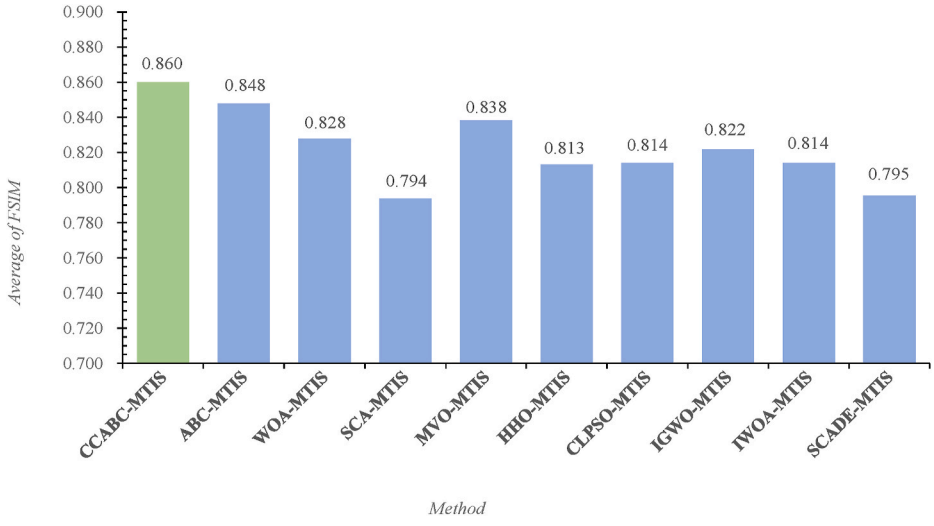

Fig. 15. The average of FSIM for all threshold levels.

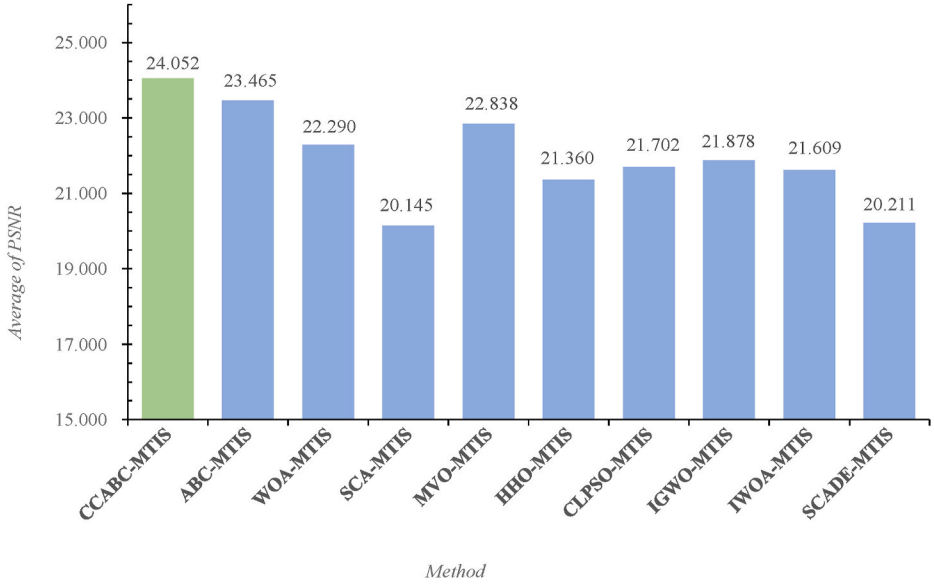

Fig. 16. The average of PSNR for all threshold levels.

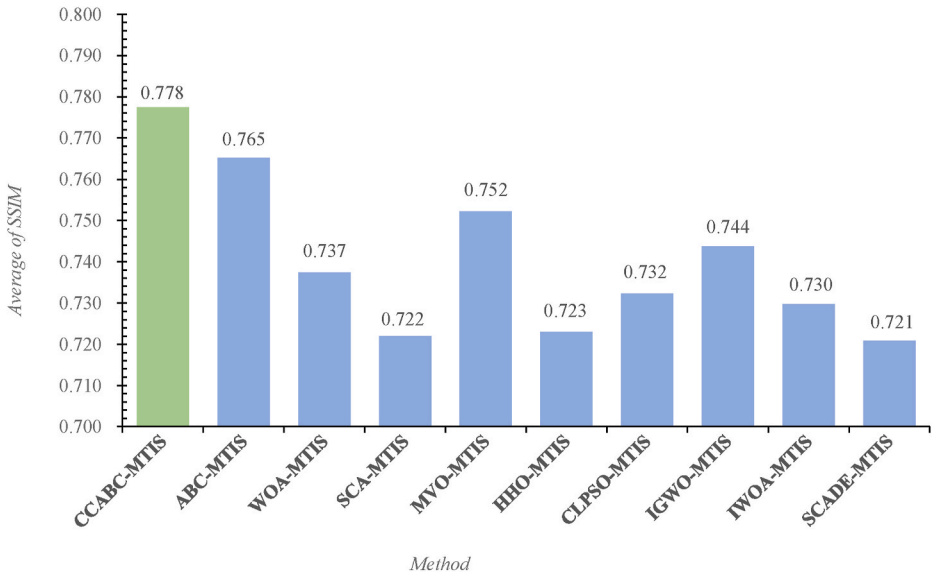

Fig. 17. The average of SSIM for all threshold levels.

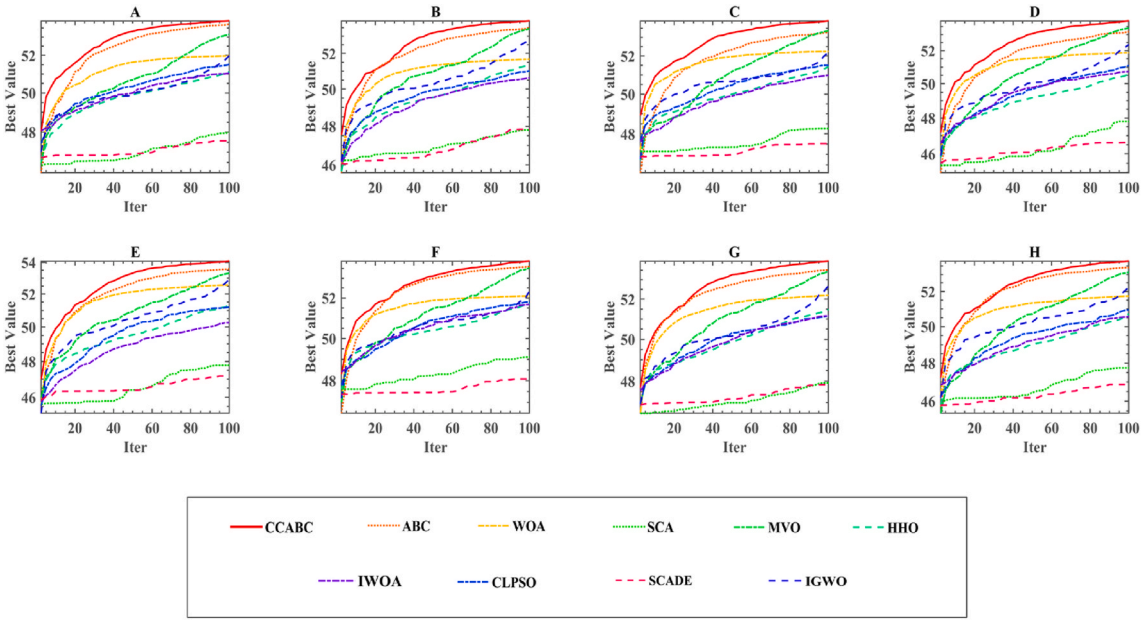

Fig. 18. The convergence curves of all methods at threshold level 7.

Fig. 14 show the box plots of CCABC-MTIS at a low threshold level of 7 and a high threshold level of 18. It can be seen that CCABC-MTIS has the best mean and variance under the three metrics of FSIM, PSNR, and SSIM, and the detailed data can be viewed in the Appendix Tables A3-A5.

Tables 8–10 represent the further analysis of the evaluation results using the Wilcoxon signed-rank test, where Mean indicates the overall mean and Rank indicates the ranking based on the overall mean. From the Wilcoxon signed-rank test analysis of the evaluation results for FSIM, PSNR, and SSIM, the overall average ranking of FSIM, PSNR, and SSIM at all threshold levels was the first. In addition, Figures B1-B3 represent the detailed evaluation results for each algorithm in the FSIM, PSNR, and SSIM evaluation metrics, respectively, where the horizontal axis indicates the name of each algorithm and the vertical axis indicates the threshold value of each segmentation. Figs. 15–17 show the average evaluation results of FSIM, PSNR, and SSIM evaluation metrics for different algorithms, respectively, focusing more on the overall performance of the algorithms. It can be seen in Figures B1-B3 and Figs. 15–17 that CCABC-MTIS has the largest average evaluation results for FSIM, PSNR, and SSIM at the same threshold levels and the same average evaluation results are the largest at all threshold levels. Therefore, the analysis of the evaluation results of FSIM, PSNR, and SSIM can prove the high superiority of the MTIS method based on CCABC.

Table A.6 represents the optimal solution found by each algorithm at each segmentation threshold level, i.e., the optimal KE. we can see that in terms of the optimal KE, most of the values found using CCABC are greater than those of the other algorithms. Moreover, the advantage of CCABC in finding specific segmentation thresholds becomes more and more evident as the number of segmentation thresholds increases starting from 7 threshold-level. Figures B4-B11represent the thresholds found by all algorithms on images A-H when the image segmentation level is all 7. The experimental results visually show that the segmentation thresholds vary significantly from one algorithm to another. Figs. 18–19 show the convergence curves of CCABC and similar

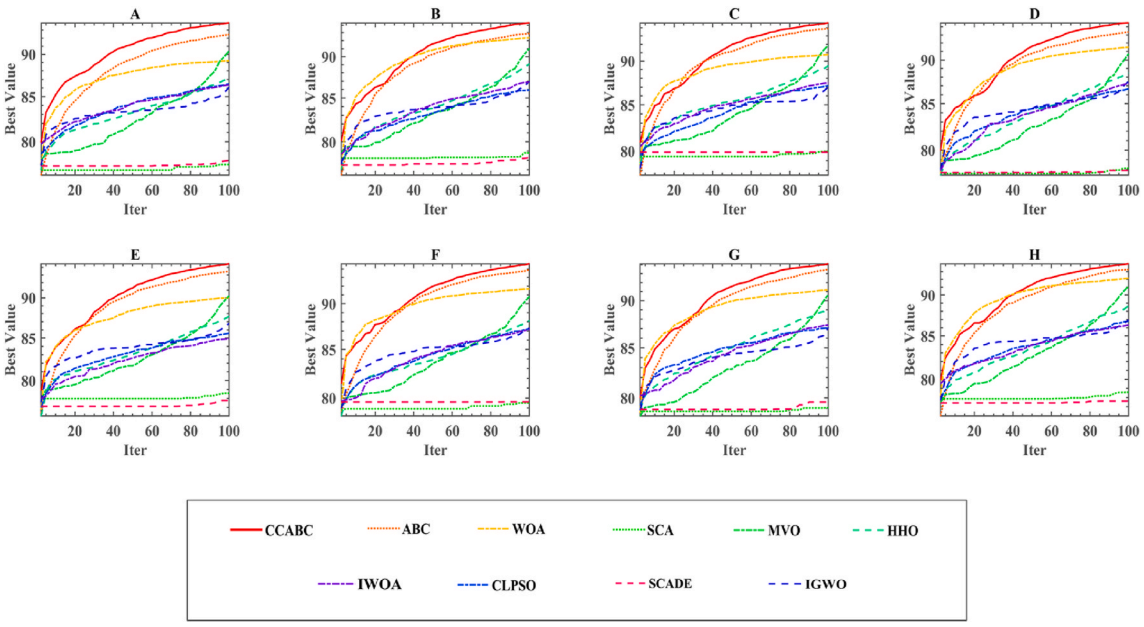

Fig. 19. The convergence curves of all methods at threshold level 18.

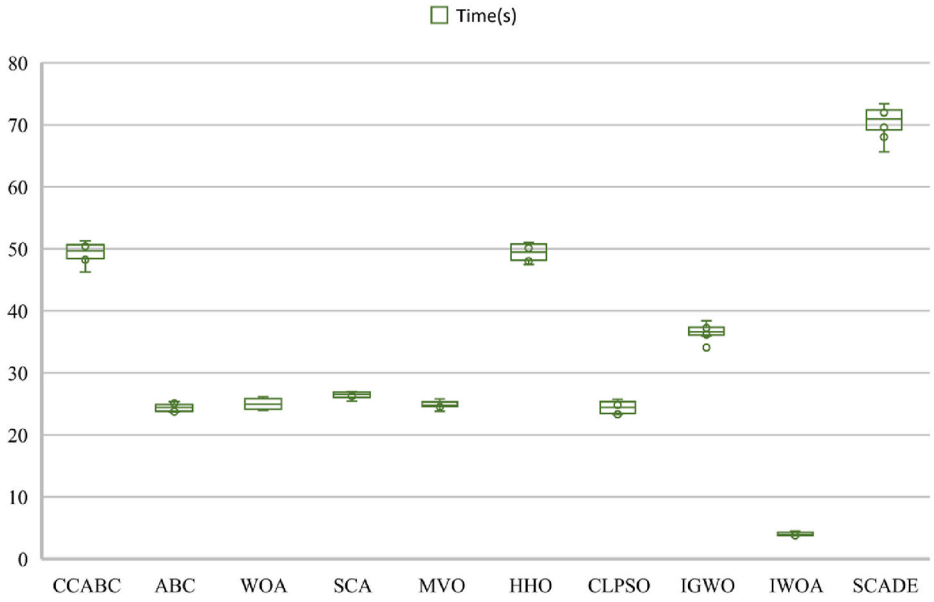

Fig. 20. The box plot of the optimization search time.

algorithms at low and high threshold levels, respectively, where 7 represents the low threshold level, and 8 represents the high threshold level. It can be seen that CCABC converges faster than other similar algorithms and has a better solving ability.

Fig. 20 represents the box plot of the optimization search time for CCABC and other algorithms. The theoretical algorithm complexity of CCABC has been analyzed in Section 3. Here, the actual time cost of CCABC is analyzed at the 18 threshold-level, which is the most difficult to optimize. The detailed time cost table for CCABC and other algorithms can be found in Table A7. It can be seen that the time spent in the process of segmenting 8 images is relatively constant for all the algorithms. CCABC does not have an advantage over other algorithms in terms of time complexity, but it is within a manageable range. Other algorithms such as HHO, IGWO, and SCADE also have high time complexity but have a considerable advantage over CCABC in terms of optimal search results. In conclusion, the CCABC algorithm has higher performance while the algorithm's complexity is still within a reasonable range.

Therefore, based on the optimal KE, specific threshold, convergence curve, segmentation results, and the analysis of the evaluation results from FSIM, PSNR, and SSIM, the improved MTIS based on CCABC can obtain better segmentation results, and it is a very excellent segmentation method. Owing to its strong search ability, the proposed CCABC can be applied to tackle other optimization problems such as video coding optimization [124]. Due to significant role of AI in medicine, we will apply the proposed CCABC to handle other datasets [125,126]. CCABC can also be explored to applied to the problems including information retrieval services [127–129], location-based services [130,131], image dehazing [132], kayak cycle phase segmentation [133], and human motion capture [134].

6. Conclusions and future works

To achieve high-quality segmentation of COVID-19 X-ray images, this paper proposes a very effective meta-heuristic algorithm CCABC and an improved MTIS method based on CCABC. CCABC is an improved algorithm based on ABC. In this paper, we introduce HCS and VCS into ABC as a way to improve the search ability and the ability to jump out of local optimum so that CCABC can obtain higher quality solutions. We first conducted comparative experiments using 30 benchmark functions. The comparison experiments above show that CCABC has a broader search performance than ABC. The ability to obtain high-quality solutions is better than ABC. in addition, based on the analysis and comparison of CCABC and its similar algorithms, it can be seen that CCABC also has a better overall ability to jump out of the local optimum trap and obtain higher quality solutions than its peers. Therefore, CCABC is a carefully validated excellent SIOA. Subsequently, we conducted MTIS experiments with CCABC and other similar algorithms and evaluated the segmentation results using FSIM, PSNR, and SSIM. In the preliminary evaluation results, CCABC was shown to have excellent FSIM, PSNR, and SSIM. The evaluation results were further analyzed using the Wilcoxon signed-rank test, and the results also showed that the overall ranking of CCABC was first in the comparison experiments. In addition, by evaluating FSIM, PSNR, and SSIM, we can see that the advantage of CCABC-based MTIS segmentation becomes more obvious as the threshold level increases. Finally, our observation and analysis of KE, specific thresholds, and segmentation results confirm that the specific thresholds found by CCABC are the most reasonable in the comparison experiments, and the segmentation results of CCABC are not only the best for segmenting images as a whole but also the most complete in terms of the details retained. Therefore, the improved MTIS method using CCABC is very excellent. However, the CPU computation for CCABC in MTIS will take longer due to HCS and VCS, resulting in CCABC being more complex than ABC. Still, with the rapid exploitation of parallel computing and high-performance computing techniques, this problem will be solved soon.

We will further apply CCABC to more advanced segmentation methods in future work. In addition, in helping COVID-19 diagnosis, we will not be limited to improving image segmentation techniques. Still, we can combine CCABC with fuzzy k-nearest neighbor or support vector machine to build assisted diagnosis models. Finally, CCABC can be applied to medical diagnosis, structural and artificial neural network optimization. We will consider further improving the performance of CCABC in different fields.

Declaration of competing interest

The authors declare that there is no conflict of interests regarding the publication of article.

Acknowledgments

This research is supported by the Natural Science Foundation of Zhejiang Province (LZ22F020005), National Natural Science Foundation of China (62076185, U1809209, 81873949), Medical Innovation Discipline of Zhejiang Province (Critical Care Medicine, Y2015), Wenzhou Science and Technology Bureau (2018ZG016, Y20210097), Wenzhou Key Technology Breakthrough Program on Prevention and Treatment for COVID-19 Epidemic (ZG2020012), University-Industry Collaborative Education Program. Minitry of Education. PRC. (202002236013). It is also supported by the Joint fund of Science & Technology Department of Liaoning Province and State Key Laboratory of Robotics, China (2020-KF-22-08), the “Thirteenth Five-Year” Science and Technology Project of Jilin Provincial Department of Education (JJKH20200829KJ), Science and Technology Research Project of Jilin Provincial Education Department (JJKH20210888KJ), Changchun Normal University Ph.D. Research Startup Funding Project (BS [2020]), the 5G Network-based Platform for Precision Emergency Medical Care in Regional Hospital Clusters. MIIT.PRC (2020NO.78)

Appendix A

Table A.1
Parametric setups for compared algorithms

Algorithm	Parameters
CCABC	$limit = 300$
ABC	$limit = 300$
SCA	$A = 2$
MFO	$b = 1; t = [-1, 1]; a \in [-1, -2]$
PSO	$c1 = 2; c2 = 2; vMax = 6$
SSA	$c_1 \in [2, 0]; c_2 \in [0, 1]; c_3 \in [0, 1]$
HHO	$Rabbit\ Energy = [2, 0]$
WOA	$a_1 = [2, 0]; a_2 = [-2, -1]; b = 1$
MVO	$existence\ probability \in [0.2, 1]$; $travelling\ distance\ rate \in [0.6, 1]$
NCHHO	$c = [2, 0]$; $Sine\ chaotic\ map = [1, 0]$; $Inertia\ factor = 0.5$
CBA	$Qmin = 0; Qmax = 2$;
SCADE	$c_{min} = 0.2; c_{max} = 0.8; p_{CR} = 0.8$
IGWO	$r_1 = r_2 = rand(0, 1)$; $C = 2 \times r_2$; $\beta = \omega = 10$
ACWOA	$a_1 = [2, 0]; a_2 = [-2, -1]; b = 1$
ASCA_PSO	$M = 4; N = 9; c_1 = 2; c_2 = 2; a = 2$
IWOA	$b = 1$; crossover $= 0.1$
CLPSO	$w = [0.2, 0.9]; c = 1.496$

Table A.2
Comparison of CCABC and excellent algorithms

Fun	Item	CCABC	ABC	SCA	MFO	PSO	SSA	HHO	NCHHO	CBA	SCADE	IGWO	ACWOA	ASCA_PSO
F1	AVG	2.549E+06	4.781E+06	2.356E+08	1.204E+08	8.458E+06	**1.603E+06**	1.148E+07	8.071E+07	4.157E+06	4.285E+08	1.702E+07	1.411E+08	1.990E+07
	STD	1.322E+06	1.663E+06	6.182E+07	1.593E+08	2.371E+06	**7.045E+05**	5.370E+06	3.904E+07	1.325E+06	8.941E+07	6.380E+06	6.109E+07	1.411E+07
F2	AVG	3.109E+03	**4.717E+02**	1.676E+10	1.249E+10	1.484E+08	1.255E+04	1.209E+07	4.555E+08	1.211E+04	2.869E+10	2.689E+06	7.398E+09	9.085E+08
	STD	3.958E+03	**2.710E+02**	2.837E+09	6.456E+09	1.355E+07	1.117E+04	2.446E+06	1.791E+08	9.911E+03	3.314E+09	1.403E+06	4.040E+09	1.373E+09
F3	AVG	**7.400E+02**	1.177E+03	3.915E+04	8.357E+04	9.339E+02	1.380E+03	5.714E+03	3.843E+04	8.941E+03	5.427E+04	6.516E+03	5.081E+04	1.965E+04
	STD	5.540E+02	7.907E+02	6.311E+03	4.300E+04	**1.259E+02**	5.914E+02	2.904E+03	1.111E+04	2.014E+04	6.108E+03	2.692E+03	8.613E+03	6.483E+03
F4	AVG	4.810E+02	**4.285E+02**	1.382E+03	1.679E+03	4.589E+02	4.874E+02	5.372E+02	7.679E+02	4.947E+02	2.429E+03	5.258E+02	1.189E+03	5.510E+02
	STD	**2.304E+01**	3.002E+01	2.527E+02	1.627E+03	3.264E+01	3.883E+01	5.030E+01	1.280E+02	2.474E+01	4.808E+02	2.952E+01	3.056E+02	8.358E+01
F5	AVG	5.202E+02	5.202E+02	5.209E+02	5.203E+02	5.209E+02	**5.201E+02**	5.203E+02	5.201E+02	5.202E+02	5.210E+02	5.205E+02	5.208E+02	5.209E+02
	STD	**3.139E-02**	3.912E-02	4.995E-02	1.766E-01	4.815E-02	1.125E-01	1.858E-01	1.629E-01	1.956E-01	5.880E-02	1.274E-01	1.746E-01	5.507E-02
F6	AVG	**6.090E+02**	6.144E+02	6.343E+02	6.234E+02	6.226E+02	6.186E+02	6.300E+02	6.362E+02	6.411E+02	6.342E+02	6.190E+02	6.337E+02	6.244E+02
	STD	2.810E+00	**1.266E+00**	2.454E+00	3.838E+00	3.008E+00	3.599E+00	3.790E+00	2.838E+00	2.888E+00	2.437E+00	2.734E+00	2.633E+00	3.302E+00
F7	AVG	7.000E+02	**7.000E+02**	8.351E+02	8.006E+02	7.023E+02	7.000E+02	7.011E+02	7.086E+02	7.000E+02	8.991E+02	7.010E+02	7.417E+02	7.090E+02
	STD	1.117E-03	**5.875E-05**	2.961E+01	5.971E+01	1.452E-01	1.360E-02	1.854E-02	2.629E+00	1.596E-02	4.047E+01	4.786E-02	2.765E+01	1.411E+01
F8	AVG	**8.000E+02**	8.000E+02	1.042E+03	9.373E+02	9.702E+02	9.075E+02	8.979E+02	9.488E+02	1.006E+03	1.068E+03	8.841E+02	9.985E+02	9.614E+02
	STD	7.443E-14	**7.079E-14**	2.077E+01	3.989E+01	2.071E+01	2.936E+01	1.379E+01	1.714E+01	4.561E+01	1.622E+01	1.666E+01	2.212E+01	2.821E+01
F9	AVG	**9.509E+02**	9.844E+02	1.174E+03	1.134E+03	1.113E+03	1.016E+03	1.090E+03	1.090E+03	1.163E+03	1.209E+03	1.017E+03	1.130E+03	1.115E+03
	STD	**7.988E+00**	1.202E+01	1.856E+01	4.526E+01	2.610E+01	2.668E+01	2.584E+01	2.131E+01	4.792E+01	1.700E+01	2.150E+01	2.201E+01	3.624E+01
F10	AVG	1.001E+03	**1.000E+03**	6.948E+03	4.740E+03	5.153E+03	4.523E+03	2.907E+03	4.144E+03	5.480E+03	7.404E+03	3.349E+03	4.790E+03	5.200E+03
	STD	8.596E-01	**4.147E-01**	5.963E+02	8.279E+02	6.593E+02	6.986E+02	7.619E+02	6.562E+02	7.099E+02	3.431E+02	5.906E+02	7.784E+02	6.876E+02
F11	AVG	**2.823E+03**	3.057E+03	8.035E+03	5.337E+03	5.786E+03	4.508E+03	5.200E+03	5.296E+03	5.804E+03	8.195E+03	4.246E+03	6.255E+03	6.104E+03
	STD	2.741E+02	**2.268E+02**	3.455E+02	6.466E+02	6.240E+02	6.328E+02	6.348E+02	8.228E+02	6.811E+02	2.324E+02	6.910E+02	7.831E+02	8.491E+02
F12	AVG	1.200E+03	**1.200E+03**	1.203E+03	1.200E+03	1.202E+03	1.200E+03	1.202E+03	1.201E+03	1.201E+03	1.203E+03	1.201E+03	1.202E+03	1.202E+03
	STD	3.354E-02	**2.847E-02**	3.114E-01	2.425E-01	2.539E-01	1.615E-01	4.135E-01	3.600E-01	5.093E-01	3.144E-01	2.888E-01	5.526E-01	3.001E-01
F13	AVG	1.300E+03	**1.300E+03**	1.303E+03	1.302E+03	1.300E+03	1.301E+03	1.301E+03	1.301E+03	1.300E+03	1.304E+03	1.301E+03	1.302E+03	1.301E+03
	STD	**2.524E-02**	2.814E-02	3.926E-01	1.239E+00	1.030E-01	1.074E-01	1.225E-01	1.189E-01	1.119E-01	3.672E-01	9.749E-02	9.903E-01	1.210E-01
F14	AVG	1.400E+03	**1.400E+03**	1.444E+03	1.429E+03	1.400E+03	1.400E+03	1.400E+03	1.400E+03	1.400E+03	1.485E+03	1.400E+03	1.419E+03	1.402E+03
	STD	1.635E-02	**1.562E-02**	7.957E+00	1.807E+01	1.395E-01	2.017E-01	1.812E-01	9.965E-01	2.037E-01	1.539E+01	2.595E-01	1.386E+01	3.885E+00
F15	AVG	**1.503E+03**	1.508E+03	4.655E+03	2.496E+05	1.517E+03	1.508E+03	1.538E+03	1.633E+03	1.561E+03	2.098E+04	1.516E+03	2.027E+03	1.533E+03
	STD	**3.574E-01**	1.313E+00	3.127E+03	4.739E+05	1.420E+00	2.713E+00	7.643E+00	6.485E+01	1.726E+01	8.879E+03	4.663E+00	5.856E+02	7.262E+01
F16	AVG	**1.609E+03**	1.610E+03	1.613E+03	1.613E+03	1.612E+03	1.611E+03	1.612E+03	1.612E+03	1.613E+03	1.613E+03	1.612E+03	1.612E+03	1.612E+03
	STD	3.610E-01	3.833E-01	2.662E-01	4.503E-01	4.621E-01	5.978E-01	4.322E-01	2.945E-01	3.253E-01	**2.242E-01**	5.250E-01	5.805E-01	3.611E-01
F17	AVG	5.907E+05	2.671E+06	5.751E+06	5.047E+06	2.841E+05	**1.102E+05**	1.513E+06	6.381E+06	2.257E+05	1.427E+07	8.295E+05	1.555E+07	1.000E+06
	STD	3.171E+05	1.063E+06	2.772E+06	9.696E+06	1.338E+05	**8.442E+04**	1.095E+06	5.183E+06	1.355E+05	6.135E+06	5.526E+05	1.291E+07	1.008E+06
F18	AVG	**2.535E+03**	2.575E+03	1.558E+08	9.940E+07	2.058E+06	6.316E+03	8.810E+04	2.278E+05	8.883E+03	2.005E+08	2.596E+04	3.647E+07	3.712E+06
	STD	8.064E+02	**6.382E+02**	7.610E+07	2.680E+08	6.108E+05	4.689E+03	4.556E+04	7.803E+05	8.043E+03	1.179E+08	4.153E+04	3.279E+07	1.035E+06
F19	AVG	**1.905E+03**	1.907E+03	1.994E+03	1.980E+03	1.917E+03	1.917E+03	1.939E+03	1.996E+03	1.936E+03	2.013E+03	1.921E+03	2.014E+03	1.929E+03
	STD	9.228E-01	**8.647E-01**	2.472E+01	6.085E+01	2.606E+00	1.378E+01	4.100E+01	3.622E+01	3.297E+01	1.532E+01	1.924E+01	3.303E+01	2.833E+01
F20	AVG	7.398E+03	9.914E+03	1.595E+04	8.282E+04	2.340E+03	**2.325E+03**	1.279E+04	3.260E+04	3.588E+03	2.537E+04	2.882E+03	3.243E+04	6.484E+03
	STD	2.350E+03	4.591E+03	3.746E+03	8.958E+04	**7.602E+01**	1.157E+02	6.903E+03	1.897E+04	2.765E+03	7.857E+03	5.840E+02	1.580E+04	3.370E+03
F21	AVG	1.103E+05	2.151E+05	1.384E+06	1.183E+06	1.089E+05	**5.748E+04**	4.783E+05	1.947E+06	9.921E+04	2.281E+06	3.375E+05	6.306E+06	3.035E+05
	STD	7.818E+04	1.238E+05	7.763E+05	3.994E+06	6.109E+04	**3.453E+04**	3.505E+05	2.253E+06	5.658E+04	1.115E+06	2.698E+05	4.528E+06	2.526E+05
F22	AVG	**2.358E+03**	2.456E+03	2.968E+03	3.072E+03	2.890E+03	2.571E+03	2.974E+03	3.047E+03	3.430E+03	3.106E+03	2.555E+03	3.072E+03	2.778E+03
	STD	**7.048E+01**	9.252E+01	1.515E+02	2.751E+02	2.096E+02	1.746E+02	2.679E+02	2.476E+02	3.086E+02	1.307E+02	1.789E+02	2.672E+02	2.030E+02
F23	AVG	2.615E+03	2.615E+03	2.671E+03	2.671E+03	2.616E+03	2.615E+03	**2.500E+03**	2.500E+03	2.616E+03	2.500E+03	2.621E+03	2.529E+03	2.625E+03
	STD	7.048E-04	2.969E-01	1.304E+01	4.500E+01	6.728E-01	2.940E-01	**0.000E+00**	0.000E+00	2.791E-01	0.000E+00	2.418E+00	7.319E+01	5.458E+00
F24	AVG	2.600E+03	2.626E+03	2.600E+03	2.676E+03	2.628E+03	2.642E+03	2.600E+03	**2.600E+03**	2.674E+03	2.600E+03	2.600E+03	2.600E+03	2.639E+03
	STD	1.187E-02	5.285E+00	4.817E-02	2.622E+01	6.498E+00	5.886E+00	8.035E-05	**0.000E+00**	2.734E+01	2.100E-06	5.202E-03	7.572E-06	7.985E+00
F25	AVG	**2.700E+03**	2.708E+03	2.726E+03	2.717E+03	2.712E+03	2.712E+03	2.700E+03	2.700E+03	2.731E+03	2.700E+03	2.711E+03	2.700E+03	2.713E+03
	STD	**0.000E+00**	1.275E+00	8.172E+00	7.918E+00	6.427E+00	4.948E+00	0.000E+00	0.000E+00	1.257E+01	0.000E+00	3.192E+00	0.000E+00	5.430E+00
F26	AVG	2.706E+03	**2.700E+03**	2.702E+03	2.704E+03	2.774E+03	2.701E+03	2.770E+03	2.770E+03	2.720E+03	2.704E+03	2.701E+03	2.756E+03	2.701E+03
	STD	2.391E+01	**8.979E-02**	5.949E-01	1.400E+01	4.434E+01	1.241E-01	4.610E+01	4.609E+01	7.474E+01	4.532E-01	1.347E-01	4.979E+01	1.649E-01
F27	AVG	3.052E+03	3.108E+03	3.477E+03	3.675E+03	3.422E+03	3.446E+03	**2.900E+03**	2.900E+03	4.000E+03	3.258E+03	3.110E+03	3.724E+03	3.474E+03
	STD	3.888E+01	2.712E+00	3.405E+02	1.663E+02	2.800E+02	1.671E+02	**0.000E+00**	0.000E+00	4.397E+02	2.414E+02	2.964E+00	3.506E+02	2.719E+02
F28	AVG	3.649E+03	3.781E+03	4.816E+03	3.941E+03	6.734E+03	3.827E+03	**3.000E+03**	3.000E+03	5.250E+03	5.152E+03	3.836E+03	4.190E+03	4.360E+03
	STD	4.012E+01	6.740E+01	2.975E+02	1.845E+02	9.907E+02	1.551E+02	**0.000E+00**	0.000E+00	6.650E+02	8.375E+02	1.664E+02	1.186E+03	3.542E+02
F29	AVG	4.356E+03	3.901E+03	1.283E+07	2.869E+06	5.466E+04	1.501E+06	3.855E+03	**3.100E+03**	5.311E+07	1.726E+07	1.227E+06	2.427E+07	4.448E+06
	STD	4.428E+02	9.831E+01	8.452E+06	3.473E+06	1.156E+05	4.116E+06	3.885E+03	**0.000E+00**	4.639E+07	9.219E+06	3.678E+06	1.997E+07	6.461E+06
F30	AVG	5.847E+03	5.351E+03	2.207E+05	4.386E+04	1.407E+04	1.106E+04	7.566E+03	**3.200E+03**	3.700E+04	4.814E+05	2.253E+04	3.407E+05	4.595E+04
	STD	8.035E+02	5.890E+02	6.279E+04	4.389E+04	6.473E+03	2.615E+03	6.581E+03	**0.000E+00**	8.760E+04	1.447E+05	8.708E+03	2.518E+05	5.549E+04

Table A.3
The PSNR comparison of CCABC-MTIS and other methods

Image	Thresholds	Item	CCABC-MTIS	ABC-MTIS	WOA-MTIS	SCA-MTIS	MVO-MTIS	HHO-MTIS	CLPSO-MTIS	IGWO-MTIS	IWOA-MTIS	SCADE-MTIS
A	3	AVG	**1.8643E+01**	1.8120E+01	1.5904E+01	1.7202E+01	1.7936E+01	1.5461E+01	1.6341E+01	1.7971E+01	1.6999E+01	1.6234E+01
		STD	**7.0670E-01**	9.7337E-01	2.6926E+00	1.9191E+00	1.1901E+00	3.1182E+00	1.3091E+00	1.1591E+00	1.5180E+00	2.0423E+00
	5	AVG	**1.9988E+01**	1.9535E+01	1.8650E+01	1.7511E+01	1.9486E+01	1.8315E+01	1.8675E+01	1.9328E+01	1.8322E+01	1.7664E+01
		STD	**7.4482E-01**	1.1252E+00	2.2891E+00	2.3315E+00	1.1326E+00	2.4037E+00	1.6205E+00	1.9438E+00	2.4584E+00	2.4418E+00
	7	AVG	**2.2449E+01**	2.1753E+01	2.0444E+01	1.8363E+01	2.1711E+01	1.9431E+01	2.0710E+01	2.0780E+01	2.0624E+01	1.9368E+01
		STD	**9.0046E-01**	1.2605E+00	1.7927E+00	1.9870E+00	1.3571E+00	2.0504E+00	1.2672E+00	1.8845E+00	2.9772E+00	3.0777E+00

(*continued on next page*)

Table A.3 (*continued*)

Image	Thresholds	Item	CCABC-MTIS	ABC-MTIS	WOA-MTIS	SCA-MTIS	MVO-MTIS	HHO-MTIS	CLPSO-MTIS	IGWO-MTIS	IWOA-MTIS	SCADE-MTIS
	12	AVG	**2.6036E+01**	2.5399E+01	2.4204E+01	2.2744E+01	2.4336E+01	2.2780E+01	2.4010E+01	2.3901E+01	2.3489E+01	2.1822E+01
		STD	**9.1327E-01**	1.1898E+00	1.9842E+00	2.4624E+00	1.9106E+00	2.3437E+00	1.8964E+00	2.3732E+00	1.6984E+00	2.4352E+00
	15	AVG	**2.8156E+01**	2.7190E+01	2.6290E+01	2.3562E+01	2.5837E+01	2.5761E+01	2.5673E+01	2.4690E+01	2.4963E+01	2.3866E+01
		STD	**9.2686E-01**	1.0098E+00	2.1618E+00	2.8137E+00	2.2792E+00	2.3160E+00	1.8704E+00	1.8160E+00	2.1298E+00	2.3578E+00
	18	AVG	**2.9157E+01**	2.8891E+01	2.7719E+01	2.5095E+01	2.7011E+01	2.6734E+01	2.6862E+01	2.6687E+01	2.6829E+01	2.4976E+01
		STD	**8.9739E-01**	1.8413E+00	2.1494E+00	2.7725E+00	2.0453E+00	2.2734E+00	1.7370E+00	1.2249E+00	2.2587E+00	1.6579E+00
B	3	AVG	**1.7851E+01**	1.7376E+01	1.7004E+01	1.5624E+01	1.7178E+01	1.6554E+01	1.6185E+01	1.7474E+01	1.6665E+01	1.5657E+01
		STD	**5.4214E-01**	1.3027E+00	1.3536E+00	1.5492E+00	1.2766E+00	1.9579E+00	1.2589E+00	6.5627E-01	1.5524E+00	1.3473E+00
	5	AVG	**2.0870E+01**	2.0430E+01	1.9240E+01	1.7314E+01	2.0049E+01	1.8109E+01	1.8334E+01	1.9848E+01	1.9463E+01	1.7497E+01
		STD	**7.4832E-01**	9.7277E-01	1.8471E+00	1.7950E+00	1.6109E+00	2.7780E+00	1.6951E+00	1.2449E+00	1.3851E+00	1.8731E+00
	7	AVG	**2.2028E+01**	2.1493E+01	2.0181E+01	1.9047E+01	2.1462E+01	1.8886E+01	2.0181E+01	2.1383E+01	2.0396E+01	1.8691E+01
		STD	**1.1639E+00**	1.6551E+00	2.3375E+00	2.7506E+00	1.5481E+00	3.4491E+00	1.4185E+00	1.3283E+00	2.4092E+00	2.2775E+00
	12	AVG	**2.6469E+01**	2.5801E+01	2.4867E+01	2.1517E+01	2.5334E+01	2.2723E+01	2.4146E+01	2.3671E+01	2.3960E+01	2.2469E+01
		STD	**9.0550E-01**	1.3143E+00	1.9315E+00	2.2938E+00	1.4077E+00	2.3040E+00	1.9154E+00	2.5608E+00	1.7147E+00	2.7696E+00
	15	AVG	**2.7883E+01**	2.7600E+01	2.6968E+01	2.3299E+01	2.6562E+01	2.6069E+01	2.5338E+01	2.4454E+01	2.5174E+01	2.3856E+01
		STD	1.0501E+00	**8.0615E-01**	1.9517E+00	1.7337E+00	1.3085E+00	1.8848E+00	1.7726E+00	2.3969E+00	1.4579E+00	2.4426E+00
	18	AVG	**2.9168E+01**	2.8249E+01	2.7851E+01	2.4838E+01	2.7789E+01	2.6852E+01	2.6632E+01	2.6258E+01	2.6385E+01	2.4243E+01
		STD	**8.0687E-01**	1.5210E+00	2.3724E+00	2.1065E+00	1.4583E+00	1.7640E+00	1.3334E+00	2.1026E+00	1.6734E+00	2.8028E+00
C	3	AVG	1.6839E+01	**1.7059E+01**	1.3864E+01	1.5129E+01	1.4911E+01	1.4182E+01	1.5272E+01	1.5932E+01	1.4531E+01	1.5456E+01
		STD	1.3592E+00	**1.2361E+00**	1.9805E+00	1.9329E+00	2.0098E+00	2.7902E+00	1.9883E+00	2.3649E+00	2.2732E+00	1.9935E+00
	5	AVG	**2.1218E+01**	2.0018E+01	1.7891E+01	1.7049E+01	1.9797E+01	1.7127E+01	1.8020E+01	1.9524E+01	1.7398E+01	1.7055E+01
		STD	**1.1123E+00**	1.5965E+00	2.5494E+00	2.5204E+00	1.5753E+00	2.5092E+00	2.3310E+00	1.6443E+00	2.6699E+00	2.6079E+00
	7	AVG	**2.2705E+01**	2.2033E+01	2.1065E+01	1.8385E+01	2.1862E+01	1.9254E+01	1.9924E+01	2.0957E+01	2.0206E+01	1.8356E+01
		STD	**8.0632E-01**	1.3281E+00	1.7090E+00	2.1726E+00	1.3938E+00	1.9136E+00	2.1878E+00	1.6911E+00	1.9805E+00	2.5803E+00
	12	AVG	**2.6783E+01**	2.5765E+01	2.4486E+01	2.1077E+01	2.4982E+01	2.4159E+01	2.3866E+01	2.4259E+01	2.3303E+01	2.1778E+01
		STD	**1.0338E+00**	1.4685E+00	2.5691E+00	2.0947E+00	2.0521E+00	2.4447E+00	2.1111E+00	1.6407E+00	2.5423E+00	2.2733E+00
	15	AVG	**2.8555E+01**	2.7608E+01	2.6653E+01	2.3070E+01	2.6888E+01	2.4778E+01	2.5874E+01	2.4965E+01	2.5359E+01	2.3078E+01
		STD	1.3637E+00	**1.2446E+00**	1.7381E+00	2.5561E+00	1.7231E+00	2.6014E+00	1.4169E+00	1.8546E+00	2.5812E+00	3.1397E+00
	18	AVG	**2.9997E+01**	2.9112E+01	2.8234E+01	2.5667E+01	2.8617E+01	2.7400E+01	2.6455E+01	2.6174E+01	2.6973E+01	2.5503E+01
		STD	**1.0098E+00**	1.0997E+00	1.8259E+00	2.1655E+00	1.6688E+00	1.7169E+00	1.7833E+00	1.9058E+00	1.7339E+00	1.8551E+00
D	3	AVG	1.5450E+01	1.5510E+01	1.4923E+01	1.3491E+01	1.5209E+01	1.4801E+01	**1.5709E+01**	1.5249E+01	1.5084E+01	1.3479E+01
		STD	**6.3283E-01**	9.4591E-01	8.9649E-01	1.9495E+00	8.0522E-01	1.4882E+00	1.3980E+00	7.1293E-01	1.1073E+00	1.9861E+00
	5	AVG	1.9365E+01	**1.9461E+01**	1.8451E+01	1.6016E+01	1.9026E+01	1.7655E+01	1.8404E+01	1.8604E+01	1.8194E+01	1.6345E+01
		STD	**8.0082E-01**	1.5436E+00	1.0920E+00	2.4024E+00	9.7489E-01	1.5412E+00	1.5700E+00	1.5876E+00	1.3677E+00	2.2033E+00
	7	AVG	**2.2923E+01**	2.2648E+01	2.1086E+01	1.7779E+01	2.2426E+01	1.9943E+01	2.0459E+01	2.0215E+01	1.9942E+01	1.8670E+01
		STD	**1.0957E+00**	1.1049E+00	1.9433E+00	2.9425E+00	1.3802E+00	2.3041E+00	1.4998E+00	1.8588E+00	1.8327E+00	1.7464E+00
	12	AVG	**2.6489E+01**	2.5904E+01	2.4496E+01	2.1855E+01	2.4819E+01	2.3463E+01	2.3073E+01	2.3284E+01	2.3615E+01	2.1743E+01
		STD	**7.5214E-01**	1.2327E+00	1.6173E+00	1.5665E+00	1.6412E+00	1.5348E+00	1.4955E+00	2.0332E+00	1.3851E+00	1.9949E+00
	15	AVG	**2.8102E+01**	2.7274E+01	2.6367E+01	2.3138E+01	2.5978E+01	2.4916E+01	2.4879E+01	2.5016E+01	2.4653E+01	2.3719E+01
		STD	**7.8461E-01**	1.0612E+00	1.7388E+00	2.5508E+00	2.0753E+00	1.6196E+00	1.4156E+00	1.3206E+00	1.8662E+00	2.1548E+00
	18	AVG	**2.9201E+01**	2.8322E+01	2.7802E+01	2.5240E+01	2.7012E+01	2.6087E+01	2.6253E+01	2.5587E+01	2.6480E+01	2.4674E+01
		STD	**9.8706E-01**	9.9550E-01	1.7668E+00	2.0425E+00	1.7345E+00	2.3587E+00	1.3259E+00	2.2685E+00	1.5289E+00	2.0450E+00
E	3	AVG	**1.7535E+01**	1.7214E+01	1.6004E+01	1.4998E+01	1.6749E+01	1.5218E+01	1.6320E+01	1.6803E+01	1.6474E+01	1.6053E+01
		STD	7.7020E-01	1.6363E+00	2.1315E+00	1.8718E+00	1.1862E+00	2.0723E+00	1.3633E+00	**6.7415E-01**	1.3984E+00	1.4255E+00
	5	AVG	**2.1098E+01**	2.0112E+01	1.8820E+01	1.7352E+01	1.9986E+01	1.7525E+01	1.8255E+01	1.9460E+01	1.9120E+01	1.6701E+01
		STD	**6.6127E-01**	1.4538E+00	2.7772E+00	2.0882E+00	1.7685E+00	2.1426E+00	2.3419E+00	1.4631E+00	1.8951E+00	3.1170E+00
	7	AVG	**2.2110E+01**	2.1856E+01	2.0590E+01	1.9223E+01	2.1594E+01	2.0289E+01	2.0611E+01	2.0836E+01	1.9777E+01	1.8455E+01
		STD	**9.4508E-01**	1.0316E+00	1.7439E+00	1.8427E+00	1.0911E+00	3.1825E+00	1.6581E+00	1.6860E+00	2.1538E+00	3.0887E+00
	12	AVG	**2.6266E+01**	2.5664E+01	2.4035E+01	2.1015E+01	2.5434E+01	2.2904E+01	2.3878E+01	2.3517E+01	2.2988E+01	2.1981E+01
		STD	**9.8603E-01**	1.5383E+00	2.9006E+00	2.9169E+00	1.4039E+00	2.2695E+00	1.7835E+00	1.6597E+00	1.8180E+00	2.4837E+00
	15	AVG	**2.8446E+01**	2.7844E+01	2.6104E+01	2.3414E+01	2.6468E+01	2.5176E+01	2.5424E+01	2.5632E+01	2.5002E+01	2.3073E+01
		STD	**8.6255E-01**	1.0790E+00	2.3954E+00	1.7529E+00	1.6368E+00	2.3684E+00	1.7379E+00	1.6878E+00	1.9597E+00	2.1603E+00
	18	AVG	**2.9595E+01**	2.8606E+01	2.7767E+01	2.4881E+01	2.7028E+01	2.6094E+01	2.6030E+01	2.5883E+01	2.6456E+01	2.4715E+01
		STD	**1.0715E+00**	1.4114E+00	1.6880E+00	1.9503E+00	1.9769E+00	2.5611E+00	2.1052E+00	1.6578E+00	2.2058E+00	2.4212E+00
F	3	AVG	**1.8186E+01**	1.8152E+01	1.6500E+01	1.5819E+01	1.7747E+01	1.5982E+01	1.6364E+01	1.7965E+01	1.6349E+01	1.5809E+01
		STD	4.0036E-01	6.6658E-01	2.0391E+00	1.3241E+00	1.1799E+00	2.1177E+00	1.5811E+00	**3.8165E-01**	1.7867E+00	1.6265E+00
	5	AVG	**2.1233E+01**	2.0814E+01	1.9127E+01	1.7608E+01	2.0669E+01	1.8145E+01	1.8588E+01	1.9884E+01	1.8009E+01	1.7222E+01
		STD	**1.0968E+00**	1.2206E+00	2.3437E+00	1.9010E+00	1.0999E+00	2.8123E+00	1.7414E+00	1.6534E+00	2.4169E+00	2.4254E+00
	7	AVG	**2.3020E+01**	2.2132E+01	2.0687E+01	1.8566E+01	2.1756E+01	2.0082E+01	2.0559E+01	2.1437E+01	2.0945E+01	1.8349E+01
		STD	**7.6179E-01**	9.4401E-01	2.5747E+00	2.1490E+00	1.7709E+00	2.1989E+00	1.7635E+00	1.9342E+00	1.9148E+00	2.6285E+00
	12	AVG	**2.5926E+01**	2.5461E+01	2.3693E+01	2.0859E+01	2.4837E+01	2.4125E+01	2.3727E+01	2.3299E+01	2.3397E+01	2.2873E+01
		STD	1.1659E+00	**1.1161E+00**	2.7404E+00	2.1968E+00	1.6623E+00	1.9159E+00	1.8497E+00	2.0756E+00	1.7766E+00	2.1413E+00
	15	AVG	**2.8104E+01**	2.6815E+01	2.6822E+01	2.3642E+01	2.6476E+01	2.5398E+01	2.5135E+01	2.4846E+01	2.5198E+01	2.4205E+01
		STD	**1.0128E+00**	1.3650E+00	1.5081E+00	2.2948E+00	1.6531E+00	2.3603E+00	1.6243E+00	2.0511E+00	2.2363E+00	2.6740E+00
	18	AVG	**2.9306E+01**	2.8549E+01	2.7618E+01	2.4797E+01	2.7220E+01	2.6260E+01	2.6363E+01	2.6808E+01	2.6460E+01	2.4971E+01
		STD	1.3358E+00	**1.0321E+00**	1.7046E+00	2.3775E+00	1.9502E+00	2.3400E+00	1.4331E+00	1.6421E+00	2.2746E+00	2.0292E+00
G	3	AVG	**1.6862E+01**	1.6007E+01	1.5596E+01	1.3954E+01	1.5307E+01	1.4654E+01	1.4491E+01	1.4485E+01	1.6595E+01	1.4484E+01
		STD	**1.7872E+00**	2.6668E+00	2.9150E+00	2.4101E+00	2.4416E+00	2.9303E+00	3.0047E+00	2.6995E+00	2.0260E+00	2.4240E+00
	5	AVG	**1.9578E+01**	1.9141E+01	1.8433E+01	1.6590E+01	1.9380E+01	1.7234E+01	1.8044E+01	1.7606E+01	1.7475E+01	1.6569E+01
		STD	1.8912E+00	**1.5174E+00**	2.2728E+00	2.8376E+00	1.7068E+00	2.6630E+00	2.0413E+00	2.3809E+00	2.3397E+00	2.8375E+00
	7	AVG	**2.3311E+01**	2.2258E+01	2.0567E+01	1.8387E+01	2.2363E+01	1.9628E+01	2.0263E+01	2.0159E+01	2.0015E+01	1.8064E+01
		STD	**1.1347E+00**	1.3204E+00	2.4568E+00	2.4281E+00	1.3418E+00	2.4595E+00	1.8870E+00	2.2722E+00	1.8821E+00	3.0270E+00
	12	AVG	**2.6331E+01**	2.6251E+01	2.4957E+01	2.2542E+01	2.5422E+01	2.3753E+01	2.3849E+01	2.3509E+01	2.3860E+01	2.2180E+01
		STD	1.0290E+00	**9.9881E-01**	1.6395E+00	2.0588E+00	1.9726E+00	2.3702E+00	1.8749E+00	1.8142E+00	2.0100E+00	2.0316E+00
	15	AVG	**2.7902E+01**	2.7212E+01	2.6700E+01	2.3545E+01	2.6832E+01	2.4967E+01	2.5476E+01	2.5281E+01	2.4996E+01	2.3929E+01
		STD	**1.0506E+00**	1.3899E+00	2.2517E+00	2.0652E+00	1.4085E+00	2.2916E+00	1.3563E+00	1.7856E+00	1.9299E+00	1.9541E+00

(*continued on next page*)

Table A.3 (*continued*)

Image	Thresholds	Item	CCABC-MTIS	ABC-MTIS	WOA-MTIS	SCA-MTIS	MVO-MTIS	HHO-MTIS	CLPSO-MTIS	IGWO-MTIS	IWOA-MTIS	SCADE-MTIS
	18	AVG	**2.9810E+01**	2.8786E+01	2.8501E+01	2.5033E+01	2.7026E+01	2.7082E+01	2.7018E+01	2.7093E+01	2.6326E+01	2.4861E+01
		STD	**7.2629E-01**	1.1518E+00	1.5325E+00	1.6655E+00	1.7135E+00	2.0717E+00	1.6410E+00	1.2611E+00	1.9993E+00	2.1156E+00
H	3	AVG	1.6064E+01	**1.6752E+01**	1.4890E+01	1.3886E+01	1.5489E+01	1.4545E+01	1.5680E+01	1.5925E+01	1.5498E+01	1.4181E+01
		STD	1.0813E+00	**8.5253E-01**	1.4440E+00	2.3479E+00	1.0258E+00	1.9197E+00	1.7858E+00	1.0004E+00	1.6719E+00	2.3045E+00
	5	AVG	**2.0451E+01**	1.9913E+01	1.8028E+01	1.6792E+01	2.0199E+01	1.7774E+01	1.8774E+01	1.8788E+01	1.8544E+01	1.6823E+01
		STD	1.0375E+00	1.1686E+00	1.9940E+00	1.9610E+00	**1.0013E+00**	2.1364E+00	1.3601E+00	2.0979E+00	1.5296E+00	2.0988E+00
	7	AVG	**2.2785E+01**	2.2523E+01	2.0833E+01	1.9380E+01	2.2690E+01	2.0324E+01	1.9991E+01	2.0497E+01	2.0568E+01	1.7918E+01
		STD	**1.0329E+00**	1.2764E+00	1.9141E+00	2.2402E+00	1.5296E+00	2.0348E+00	1.7251E+00	1.7327E+00	2.1779E+00	2.5229E+00
	12	AVG	**2.6143E+01**	2.5828E+01	2.4612E+01	2.1866E+01	2.5180E+01	2.4027E+01	2.3486E+01	2.3716E+01	2.3182E+01	2.1902E+01
		STD	1.3980E+00	**1.1579E+00**	2.0435E+00	2.5515E+00	1.7704E+00	1.8395E+00	1.5527E+00	1.6291E+00	2.5870E+00	2.2088E+00
	15	AVG	**2.8528E+01**	2.7038E+01	2.5988E+01	2.3990E+01	2.6437E+01	2.5566E+01	2.5260E+01	2.4614E+01	2.4767E+01	2.3655E+01
		STD	**8.9647E-01**	1.9624E+00	2.0135E+00	2.3525E+00	2.2377E+00	1.8259E+00	1.6937E+00	1.6629E+00	2.2013E+00	1.7723E+00
	18	AVG	**2.9583E+01**	2.8822E+01	2.8389E+01	2.4816E+01	2.7730E+01	2.7104E+01	2.6846E+01	2.5880E+01	2.6221E+01	2.4950E+01
		STD	**7.7488E-01**	1.1326E+00	1.1780E+00	2.0019E+00	1.5350E+00	2.2860E+00	1.5719E+00	1.6988E+00	1.9682E+00	2.1268E+00

Table A.4
The FSIM comparison of CCABC-MTIS and other methods

Image	Thresholds	Item	CCABC-MTIS	ABC-MTIS	WOA-MTIS	SCA-MTIS	MVO-MTIS	HHO-MTIS	CLPSO-MTIS	IGWO-MTIS	IWOA-MTIS	SCADE-MTIS
A	3	AVG	**8.5468E-01**	8.3995E-01	7.7179E-01	7.9197E-01	8.3061E-01	7.6209E-01	7.7215E-01	8.3848E-01	7.9309E-01	7.7930E-01
		STD	**2.2995E-02**	2.8749E-02	8.2054E-02	7.5628E-02	3.7543E-02	8.6860E-02	4.0718E-02	2.9791E-02	5.6441E-02	5.5476E-02
	5	AVG	**8.9228E-01**	8.7616E-01	8.4674E-01	8.0883E-01	8.7544E-01	8.3381E-01	8.5162E-01	8.6779E-01	8.3848E-01	8.2069E-01
		STD	**2.1878E-02**	3.4095E-02	7.5598E-02	7.3442E-02	3.4974E-02	7.1671E-02	5.5401E-02	5.1651E-02	7.1098E-02	7.0107E-02
	7	AVG	8.0291E-01	7.8274E-01	7.7058E-01	7.3010E-01	7.7585E-01	7.5455E-01	**8.9710E-01**	8.9249E-01	8.8097E-01	8.4941E-01
		STD	**2.2103E-02**	2.2693E-02	3.0454E-02	3.6014E-02	3.0843E-02	3.1191E-02	3.1731E-02	4.5387E-02	8.1517E-02	8.4456E-02
	12	AVG	**9.7268E-01**	9.6641E-01	9.3677E-01	9.1277E-01	9.4807E-01	9.1348E-01	9.3671E-01	9.2929E-01	9.2919E-01	8.9272E-01
		STD	**6.3993E-03**	1.0560E-02	3.8153E-02	4.9248E-02	2.8800E-02	4.9399E-02	3.3328E-02	4.6097E-02	3.4850E-02	5.2970E-02
	15	AVG	**9.8172E-01**	9.7580E-01	9.5977E-01	9.1815E-01	9.5510E-01	9.5150E-01	9.5230E-01	9.4338E-01	9.4324E-01	9.2853E-01
		STD	**5.4036E-03**	7.8615E-03	2.3887E-02	5.3622E-02	3.0963E-02	3.1739E-02	3.2338E-02	2.7857E-02	3.8626E-02	4.1612E-02
	18	AVG	**9.8385E-01**	9.8133E-01	9.7023E-01	9.3850E-01	9.6305E-01	9.5915E-01	9.6445E-01	9.6492E-01	9.6105E-01	9.3967E-01
		STD	**4.9314E-03**	9.5176E-03	1.8822E-02	5.0959E-02	2.4414E-02	2.5060E-02	1.8235E-02	1.5562E-02	3.1411E-02	2.9291E-02
B	3	AVG	**7.0762E-01**	7.0197E-01	7.0088E-01	6.9786E-01	7.0304E-01	6.9009E-01	6.7698E-01	7.0689E-01	6.9477E-01	6.9773E-01
		STD	**4.7342E-03**	1.2235E-02	2.3170E-02	1.8212E-02	2.1693E-02	2.7710E-02	2.6987E-02	5.9717E-03	2.2674E-02	2.3718E-02
	5	AVG	**7.4687E-01**	7.4324E-01	7.3200E-01	7.1266E-01	7.3837E-01	7.2637E-01	7.1799E-01	7.4619E-01	7.3883E-01	7.1211E-01
		STD	**1.9699E-02**	2.1747E-02	3.8935E-02	3.9764E-02	3.1805E-02	4.2866E-02	2.7609E-02	2.5823E-02	3.1546E-02	3.5053E-02
	7	AVG	**8.3642E-01**	8.2001E-01	7.9079E-01	7.5325E-01	8.2962E-01	7.6806E-01	7.5052E-01	7.7370E-01	7.6176E-01	7.3611E-01
		STD	3.3680E-02	4.8979E-02	5.8764E-02	5.9403E-02	3.7241E-02	7.2336E-02	3.2167E-02	**2.9396E-02**	3.9788E-02	3.7729E-02
	12	AVG	**8.8177E-01**	8.6596E-01	8.5288E-01	7.8951E-01	8.5937E-01	8.2095E-01	8.3372E-01	8.2860E-01	8.3020E-01	8.1148E-01
		STD	**2.0538E-02**	2.6074E-02	3.8411E-02	3.6263E-02	2.6942E-02	5.2650E-02	3.7511E-02	4.6028E-02	3.9022E-02	5.0649E-02
	15	AVG	**9.0746E-01**	8.9971E-01	8.9219E-01	8.2015E-01	8.8504E-01	8.7375E-01	8.6040E-01	8.4712E-01	8.5708E-01	8.3084E-01
		STD	**1.7426E-02**	1.8752E-02	3.6189E-02	3.2706E-02	2.7195E-02	3.7957E-02	2.8243E-02	3.9773E-02	2.3902E-02	4.8202E-02
	18	AVG	**9.2387E-01**	9.0969E-01	9.0833E-01	8.4665E-01	9.0060E-01	8.8586E-01	8.7422E-01	8.7351E-01	8.7682E-01	8.3985E-01
		STD	**1.3685E-02**	2.5306E-02	3.3659E-02	4.2853E-02	2.5400E-02	3.1694E-02	2.4898E-02	3.5905E-02	2.6784E-02	5.0510E-02
C	3	AVG	**7.4918E-01**	7.4832E-01	6.8010E-01	7.2984E-01	6.9398E-01	6.8493E-01	7.0254E-01	7.2758E-01	6.8209E-01	7.4338E-01
		STD	1.0291E-02	**9.0110E-03**	4.3131E-02	3.1729E-02	5.2098E-02	4.8873E-02	4.3452E-02	4.6259E-02	4.1244E-02	3.1877E-02

(*continued on next page*)

Table A.4 (*continued*)

Image	Thresholds	Item	CCABC-MTIS	ABC-MTIS	WOA-MTIS	SCA-MTIS	MVO-MTIS	HHO-MTIS	CLPSO-MTIS	IGWO-MTIS	IWOA-MTIS	SCADE-MTIS
	5	AVG	**8.2324E-01**	7.9616E-01	7.4316E-01	7.4399E-01	7.8325E-01	7.3812E-01	7.5295E-01	7.7701E-01	7.4161E-01	7.4201E-01
		STD	**3.0393E-02**	3.7379E-02	5.5581E-02	4.3842E-02	4.7295E-02	5.7191E-02	4.5586E-02	4.1600E-02	5.1503E-02	4.9257E-02
	7	AVG	8.1050E-01	7.9696E-01	7.8529E-01	7.5487E-01	7.9921E-01	7.6113E-01	7.9299E-01	**8.1600E-01**	8.0530E-01	7.6439E-01
		STD	**2.5741E-02**	3.4161E-02	3.7015E-02	3.1706E-02	3.6690E-02	4.2900E-02	4.4271E-02	3.8298E-02	4.5781E-02	4.9920E-02
	12	AVG	**9.3413E-01**	9.1611E-01	8.8952E-01	8.2102E-01	8.9799E-01	8.8284E-01	8.7082E-01	8.7826E-01	8.6858E-01	8.3606E-01
		STD	**1.9255E-02**	2.5595E-02	5.2418E-02	4.8398E-02	4.1811E-02	5.0645E-02	4.7517E-02	3.4664E-02	4.6595E-02	4.4710E-02
	15	AVG	**9.5525E-01**	9.4344E-01	9.2765E-01	8.5636E-01	9.2862E-01	8.8908E-01	9.0530E-01	8.8671E-01	8.9581E-01	8.5984E-01
		STD	1.7880E-02	**1.6090E-02**	2.9499E-02	5.1933E-02	2.8857E-02	4.8557E-02	2.9042E-02	3.2653E-02	5.0515E-02	5.8963E-02
	18	AVG	**9.6776E-01**	9.5834E-01	9.3889E-01	9.0090E-01	9.4543E-01	9.3137E-01	9.1169E-01	9.1062E-01	9.2247E-01	8.9874E-01
		STD	**1.0278E-02**	1.4356E-02	2.7938E-02	4.6133E-02	2.5212E-02	2.4973E-02	3.4228E-02	3.2313E-02	2.6278E-02	3.3609E-02
D	3	AVG	**6.9905E-01**	6.9890E-01	6.8366E-01	6.8970E-01	6.9646E-01	6.8294E-01	6.8443E-01	6.9636E-01	6.8940E-01	6.9124E-01
		STD	**7.5397E-03**	8.7657E-03	1.7203E-02	1.8923E-02	1.4793E-02	1.8268E-02	1.6967E-02	1.0032E-02	2.1494E-02	2.0463E-02
	5	AVG	**7.5803E-01**	7.5198E-01	7.3950E-01	7.0561E-01	7.4457E-01	7.2237E-01	7.2746E-01	7.3772E-01	7.2839E-01	7.1756E-01
		STD	**1.2281E-02**	1.5069E-02	2.7355E-02	2.8390E-02	2.3472E-02	2.9714E-02	2.7142E-02	2.3086E-02	2.8326E-02	2.2555E-02
	7	AVG	**7.8812E-01**	7.8375E-01	7.6375E-01	7.3872E-01	7.8780E-01	7.6002E-01	7.5814E-01	7.5926E-01	7.6105E-01	7.2990E-01
		STD	**2.1854E-02**	2.8128E-02	3.3304E-02	4.1774E-02	3.2832E-02	3.7451E-02	2.8597E-02	3.1203E-02	3.3062E-02	3.5579E-02
	12	AVG	**8.7691E-01**	8.6591E-01	8.3690E-01	7.8834E-01	8.4912E-01	8.2705E-01	8.1658E-01	8.2541E-01	8.2880E-01	7.8507E-01
		STD	**1.3301E-02**	2.0158E-02	3.5677E-02	2.9650E-02	2.8266E-02	2.9495E-02	2.8648E-02	3.0950E-02	2.5737E-02	3.5582E-02
	15	AVG	**9.0742E-01**	8.8966E-01	8.7391E-01	8.2130E-01	8.7423E-01	8.4870E-01	8.3695E-01	8.4828E-01	8.4549E-01	8.1810E-01
		STD	**1.5290E-02**	1.9365E-02	3.6847E-02	3.6344E-02	2.7565E-02	3.0335E-02	2.8930E-02	2.6260E-02	3.4888E-02	3.9566E-02
	18	AVG	**9.2059E-01**	9.0692E-01	9.0119E-01	8.4637E-01	8.8455E-01	8.7575E-01	8.6840E-01	8.6725E-01	8.7172E-01	8.4446E-01
		STD	**1.4566E-02**	1.9316E-02	2.5394E-02	3.8597E-02	3.0331E-02	4.1737E-02	2.8116E-02	2.8773E-02	2.3123E-02	3.2463E-02
E	3	AVG	7.2607E-01	7.2239E-01	7.1264E-01	7.1585E-01	7.2874E-01	7.0385E-01	7.0848E-01	**7.3522E-01**	7.1644E-01	7.2213E-01
		STD	**1.0429E-02**	1.4793E-02	3.0512E-02	2.4150E-02	2.2336E-02	2.9843E-02	2.7843E-02	1.3010E-02	2.5768E-02	2.5846E-02
	5	AVG	**7.4793E-01**	7.3662E-01	7.3868E-01	7.3649E-01	7.3784E-01	7.2330E-01	7.3599E-01	7.4265E-01	7.3619E-01	7.3426E-01
		STD	**1.5203E-02**	2.5995E-02	3.8811E-02	3.4873E-02	2.8978E-02	3.7249E-02	2.5543E-02	2.4524E-02	3.0210E-02	2.8786E-02
	7	AVG	**9.3602E-01**	9.2934E-01	8.9382E-01	8.4338E-01	9.2363E-01	8.8113E-01	7.5841E-01	7.6850E-01	7.4770E-01	7.4623E-01
		STD	**1.5325E-02**	1.8675E-02	3.7918E-02	6.1942E-02	2.4779E-02	7.5843E-02	3.1565E-02	3.2028E-02	3.7649E-02	3.5230E-02
	12	AVG	**8.6731E-01**	8.5609E-01	8.3316E-01	7.8328E-01	8.5520E-01	8.0601E-01	8.2498E-01	8.1952E-01	8.0930E-01	7.9817E-01
		STD	**2.4777E-02**	3.0928E-02	4.8785E-02	4.0060E-02	3.0944E-02	4.4885E-02	3.2036E-02	2.8921E-02	3.7341E-02	3.9598E-02
	15	AVG	**9.0739E-01**	8.9914E-01	8.6960E-01	8.2357E-01	8.7523E-01	8.4872E-01	8.4838E-01	8.5665E-01	8.4694E-01	8.1194E-01
		STD	**1.7945E-02**	1.8391E-02	4.5280E-02	3.1947E-02	2.8501E-02	4.3589E-02	3.5559E-02	2.4774E-02	4.0869E-02	3.3718E-02
	18	AVG	**9.2719E-01**	9.1031E-01	8.9481E-01	8.4536E-01	8.7824E-01	8.6492E-01	8.6206E-01	8.6120E-01	8.7201E-01	8.4201E-01
		STD	**1.5994E-02**	2.5550E-02	3.0774E-02	3.5061E-02	3.4225E-02	4.6677E-02	3.2497E-02	3.3371E-02	2.9166E-02	4.3255E-02
F	3	AVG	7.4019E-01	7.3982E-01	7.2153E-01	7.2285E-01	**7.4439E-01**	7.1479E-01	7.1206E-01	7.4428E-01	7.2005E-01	7.2435E-01
		STD	**1.4307E-02**	1.6409E-02	3.7862E-02	3.4433E-02	2.1765E-02	3.7925E-02	3.8421E-02	1.9436E-02	3.2831E-02	3.5599E-02
	5	AVG	**8.0498E-01**	7.8659E-01	7.6509E-01	7.5358E-01	7.9348E-01	7.6680E-01	7.5536E-01	7.8434E-01	7.3911E-01	7.5450E-01

(*continued on next page*)

Table A.4 (*continued*)

Image	Thresholds	Item	CCABC-MTIS	ABC-MTIS	WOA-MTIS	SCA-MTIS	MVO-MTIS	HHO-MTIS	CLPSO-MTIS	IGWO-MTIS	IWOA-MTIS	SCADE-MTIS
		STD	**1.5270E-02**	3.1484E-02	4.9569E-02	4.1445E-02	2.7888E-02	5.5245E-02	3.0154E-02	3.8224E-02	4.2260E-02	4.7529E-02
	7	AVG	7.9859E-01	7.8003E-01	7.6760E-01	7.3463E-01	7.7767E-01	7.6992E-01	7.9301E-01	**8.2162E-01**	8.0524E-01	7.5513E-01
		STD	**1.6560E-02**	2.3344E-02	4.7579E-02	3.8589E-02	3.6636E-02	3.1509E-02	4.4600E-02	4.1870E-02	4.2086E-02	5.3941E-02
	12	AVG	**9.2546E-01**	9.1661E-01	8.7472E-01	8.0762E-01	8.9998E-01	8.8300E-01	8.7083E-01	8.6035E-01	8.6265E-01	8.4955E-01
		STD	2.1394E-02	**2.1062E-02**	5.6984E-02	5.1468E-02	2.9982E-02	4.0026E-02	4.4619E-02	4.9585E-02	4.1093E-02	4.5384E-02
	15	AVG	**9.5519E-01**	9.3884E-01	9.2685E-01	8.6060E-01	9.2671E-01	8.9993E-01	8.9357E-01	8.9225E-01	8.9777E-01	8.7815E-01
		STD	**1.4693E-02**	2.2849E-02	2.5813E-02	5.2716E-02	2.6874E-02	4.4589E-02	3.3277E-02	4.1203E-02	3.8891E-02	5.0418E-02
	18	AVG	**9.6335E-01**	9.5778E-01	9.3738E-01	8.8268E-01	9.2988E-01	9.1011E-01	9.1370E-01	9.2061E-01	9.1897E-01	8.8608E-01
		STD	1.6883E-02	**1.4026E-02**	2.3988E-02	4.4351E-02	3.3887E-02	4.2606E-02	2.8721E-02	2.7264E-02	3.4064E-02	4.2638E-02
G	3	AVG	**7.0362E-01**	6.7958E-01	6.6877E-01	6.5019E-01	6.5182E-01	6.4902E-01	6.5345E-01	6.4686E-01	6.8264E-01	6.6080E-01
		STD	**3.3949E-02**	5.2080E-02	5.1970E-02	5.0319E-02	5.3157E-02	5.4666E-02	5.6702E-02	5.2774E-02	4.1218E-02	4.5348E-02
	5	AVG	7.6842E-01	7.5025E-01	7.4219E-01	7.0235E-01	**7.6929E-01**	7.1286E-01	7.2747E-01	7.2787E-01	7.1787E-01	7.0733E-01
		STD	5.3189E-02	4.5850E-02	5.6828E-02	5.5548E-02	**3.9872E-02**	6.5523E-02	5.2054E-02	5.8139E-02	6.0421E-02	5.7129E-02
	7	AVG	**8.6759E-01**	8.4131E-01	8.0822E-01	7.7324E-01	8.4747E-01	7.9769E-01	7.9222E-01	7.8705E-01	7.8308E-01	7.4050E-01
		STD	**2.5508E-02**	3.5679E-02	5.2846E-02	4.7022E-02	3.1526E-02	4.6355E-02	4.9290E-02	5.6576E-02	4.3080E-02	5.7932E-02
	12	AVG	**9.1367E-01**	9.1274E-01	8.8553E-01	8.3717E-01	8.9951E-01	8.7111E-01	8.6652E-01	8.6373E-01	8.6610E-01	8.2657E-01
		STD	1.9214E-02	**1.8769E-02**	3.5302E-02	4.5802E-02	3.4795E-02	4.4518E-02	3.4593E-02	4.0261E-02	3.9397E-02	4.8618E-02
	15	AVG	**9.3924E-01**	9.2501E-01	9.1570E-01	8.5671E-01	9.2004E-01	8.8915E-01	8.9212E-01	8.8493E-01	8.7763E-01	8.5867E-01
		STD	**1.7849E-02**	2.5669E-02	3.6155E-02	4.4257E-02	2.2109E-02	3.6477E-02	2.9600E-02	3.2790E-02	3.7050E-02	4.1728E-02
	18	AVG	**9.5929E-01**	9.4624E-01	9.4111E-01	8.8578E-01	9.1556E-01	9.2195E-01	9.1449E-01	9.1902E-01	9.0354E-01	8.7813E-01
		STD	**9.9453E-03**	1.6424E-02	2.3293E-02	3.1954E-02	3.0858E-02	3.3293E-02	2.9972E-02	2.2726E-02	3.9339E-02	4.3236E-02
H	3	AVG	**7.3949E-01**	7.3460E-01	7.1569E-01	7.2443E-01	7.2639E-01	7.0096E-01	7.1398E-01	7.3701E-01	6.9890E-01	7.2546E-01
		STD	1.1029E-02	**7.0985E-03**	3.4984E-02	2.0006E-02	2.6736E-02	3.7662E-02	3.0872E-02	1.2024E-02	2.6464E-02	2.6924E-02
	5	AVG	**7.8058E-01**	7.5713E-01	7.4077E-01	7.4044E-01	7.6268E-01	7.4099E-01	7.4436E-01	7.6675E-01	7.4992E-01	7.3259E-01
		STD	**1.5311E-02**	2.2671E-02	4.2183E-02	3.2638E-02	2.8584E-02	3.7656E-02	2.9560E-02	4.0270E-02	3.5453E-02	3.7130E-02
	7	AVG	**8.3915E-01**	8.3325E-01	8.0549E-01	7.8046E-01	8.3699E-01	8.0656E-01	7.7065E-01	7.7995E-01	7.8405E-01	7.5785E-01
		STD	3.0542E-02	3.6870E-02	5.0327E-02	4.4008E-02	3.5785E-02	4.9238E-02	3.8674E-02	**2.7566E-02**	3.5714E-02	4.2214E-02
	12	AVG	**8.9210E-01**	8.8391E-01	8.6040E-01	8.1167E-01	8.7006E-01	8.5134E-01	8.3232E-01	8.4110E-01	8.3658E-01	8.1501E-01
		STD	2.9484E-02	**2.6271E-02**	4.8274E-02	4.8526E-02	3.6637E-02	3.3669E-02	3.1897E-02	3.3334E-02	5.0866E-02	4.3248E-02
	15	AVG	**9.3375E-01**	9.0496E-01	8.9171E-01	8.4535E-01	9.0331E-01	8.7989E-01	8.7138E-01	8.5201E-01	8.6956E-01	8.3845E-01
		STD	**1.6047E-02**	3.4619E-02	3.5587E-02	4.1582E-02	3.8088E-02	3.3356E-02	3.2417E-02	3.4367E-02	3.4157E-02	3.4693E-02
	18	AVG	**9.4361E-01**	9.3409E-01	9.2745E-01	8.6150E-01	9.1150E-01	9.0164E-01	8.9376E-01	8.7903E-01	8.8486E-01	8.6466E-01
		STD	**1.3193E-02**	2.0144E-02	1.8949E-02	3.5252E-02	2.6068E-02	3.9409E-02	2.9890E-02	3.1780E-02	3.4659E-02	3.9789E-02

Table A.5
The SSIM comparison of CCABC-MTIS and other method

Image	Thresholds	Item	CCABC-MTIS	ABC-MTIS	WOA-MTIS	SCA-MTIS	MVO-MTIS	HHO-MTIS	CLPSO-MTIS	IGWO-MTIS	IWOA-MTIS	SCADE-MTIS
A	3	AVG	**5.7867E-01**	5.5611E-01	4.5178E-01	5.2176E-01	5.4187E-01	4.2878E-01	4.6210E-01	5.5321E-01	5.0033E-01	4.7826E-01
		STD	**3.4749E-02**	4.4301E-02	1.3523E-01	9.6392E-02	5.5737E-02	1.6190E-01	6.2335E-02	5.0743E-02	7.6505E-02	9.3886E-02
	5	AVG	**6.5091E-01**	6.2759E-01	5.9199E-01	5.4305E-01	6.2706E-01	5.8284E-01	5.9703E-01	6.2297E-01	5.8222E-01	5.6152E-01
		STD	**3.5489E-02**	5.5653E-02	1.0467E-01	1.1250E-01	5.4679E-02	1.1118E-01	7.7616E-02	8.5848E-02	1.1060E-01	1.0763E-01
	7	AVG	**7.6665E-01**	7.5194E-01	7.3549E-01	7.2962E-01	7.3640E-01	7.1564E-01	6.9127E-01	6.8676E-01	6.7386E-01	6.2159E-01
		STD	**3.1577E-02**	3.9363E-02	5.5082E-02	5.2393E-02	4.7928E-02	7.6972E-02	5.2918E-02	7.7829E-02	1.3854E-01	1.4166E-01
	12	AVG	**8.7013E-01**	8.5274E-01	8.0850E-01	7.5765E-01	8.1752E-01	7.6471E-01	7.9893E-01	7.9468E-01	7.8230E-01	7.2783E-01
		STD	**2.1840E-02**	3.1172E-02	6.3027E-02	8.2995E-02	6.1121E-02	7.9616E-02	6.4516E-02	7.9617E-02	6.4826E-02	8.6540E-02
	15	AVG	**9.1288E-01**	8.9282E-01	8.6477E-01	7.7337E-01	8.5349E-01	8.4372E-01	8.4488E-01	8.2000E-01	8.2820E-01	7.9405E-01
		STD	**1.6456E-02**	2.2019E-02	4.9172E-02	9.7777E-02	6.0576E-02	6.6929E-02	5.7657E-02	5.3190E-02	6.4885E-02	7.0974E-02
	18	AVG	**9.2644E-01**	9.1860E-01	8.9012E-01	8.2130E-01	8.7588E-01	8.6927E-01	8.7372E-01	8.7275E-01	8.6968E-01	8.2436E-01
		STD	**1.4421E-02**	2.9468E-02	4.9598E-02	9.2835E-02	5.1849E-02	5.1009E-02	4.2559E-02	2.9325E-02	6.1421E-02	5.2523E-02
B	3	AVG	6.9155E-01	6.7854E-01	6.5516E-01	6.8122E-01	6.6888E-01	6.2620E-01	6.3501E-01	**7.0067E-01**	6.5533E-01	6.7629E-01
		STD	1.5745E-02	2.9757E-02	8.1257E-02	3.0698E-02	8.1092E-02	1.0536E-01	5.6622E-02	**1.2913E-02**	7.9663E-02	5.3171E-02
	5	AVG	7.1919E-01	7.1526E-01	6.8429E-01	6.9214E-01	6.9503E-01	6.6320E-01	6.8763E-01	**7.3470E-01**	7.0760E-01	6.8530E-01
		STD	**1.6720E-02**	3.1598E-02	8.4303E-02	5.7804E-02	6.3101E-02	9.1024E-02	3.3063E-02	2.1279E-02	3.4851E-02	5.2850E-02
	7	AVG	6.9100E-01	6.8241E-01	6.5940E-01	6.4123E-01	6.9759E-01	6.4132E-01	7.1510E-01	**7.4634E-01**	7.2149E-01	7.1506E-01
		STD	**2.8314E-02**	4.0034E-02	4.7735E-02	6.0322E-02	3.9878E-02	6.9875E-02	4.3306E-02	3.3709E-02	5.5499E-02	4.4728E-02
	12	AVG	**8.1887E-01**	8.0368E-01	7.9470E-01	7.6567E-01	8.0156E-01	7.7295E-01	7.9706E-01	7.8716E-01	7.9477E-01	7.7749E-01
		STD	**2.0206E-02**	2.6781E-02	4.3917E-02	4.3610E-02	2.7432E-02	6.0547E-02	2.6426E-02	5.8463E-02	2.5627E-02	5.4655E-02
	15	AVG	**8.4670E-01**	8.3836E-01	8.4087E-01	7.8400E-01	8.3612E-01	8.3285E-01	8.1543E-01	8.0406E-01	8.1721E-01	8.0058E-01
		STD	2.3096E-02	**1.5500E-02**	3.1450E-02	3.0979E-02	2.2335E-02	3.1458E-02	2.1305E-02	3.7534E-02	1.8634E-02	3.7918E-02
	18	AVG	**8.7084E-01**	8.5390E-01	8.5149E-01	8.1282E-01	8.5195E-01	8.4366E-01	8.3059E-01	8.2911E-01	8.3127E-01	8.0626E-01
		STD	**1.3339E-02**	2.2638E-02	3.8370E-02	3.0975E-02	2.2424E-02	2.9410E-02	2.4790E-02	3.6184E-02	2.3800E-02	3.6946E-02
C	3	AVG	**6.5895E-01**	6.5186E-01	5.2981E-01	6.3290E-01	5.7177E-01	5.1504E-01	5.7735E-01	6.2122E-01	5.5437E-01	6.5789E-01
		STD	**1.8315E-02**	1.8531E-02	6.2768E-02	4.6320E-02	6.6199E-02	1.0168E-01	5.4183E-02	6.3635E-02	5.8637E-02	4.2036E-02
	5	AVG	**6.8228E-01**	6.6794E-01	6.1217E-01	6.3252E-01	6.5066E-01	6.0145E-01	6.3005E-01	6.4318E-01	6.1697E-01	6.2981E-01
		STD	**2.5839E-02**	3.6923E-02	5.4237E-02	5.3804E-02	4.1314E-02	6.6486E-02	5.3694E-02	3.6101E-02	5.4420E-02	5.6511E-02
	7	AVG	**7.3736E-01**	7.2807E-01	7.1295E-01	7.1179E-01	7.2149E-01	6.8271E-01	6.6464E-01	6.8524E-01	6.8131E-01	6.4371E-01
		STD	**2.0610E-02**	2.7892E-02	4.6423E-02	3.7153E-02	3.6773E-02	5.4161E-02	3.5462E-02	3.3693E-02	3.8923E-02	6.4276E-02
	12	AVG	**8.0474E-01**	7.8381E-01	7.7061E-01	7.1323E-01	7.7431E-01	7.6539E-01	7.5392E-01	7.5542E-01	7.5444E-01	7.2272E-01
		STD	**2.4158E-02**	3.3710E-02	5.1338E-02	4.2293E-02	4.1878E-02	4.6492E-02	3.8733E-02	3.8607E-02	4.1818E-02	4.5889E-02
	15	AVG	**8.4802E-01**	8.2498E-01	8.1965E-01	7.5144E-01	8.1919E-01	7.8068E-01	7.9722E-01	7.7722E-01	7.8675E-01	7.5819E-01
		STD	**2.4625E-02**	2.5623E-02	3.1346E-02	4.4933E-02	2.8859E-02	4.7470E-02	2.6886E-02	3.3143E-02	5.1240E-02	4.8899E-02
	18	AVG	**8.7539E-01**	8.5908E-01	8.4263E-01	7.9561E-01	8.5265E-01	8.3128E-01	8.1077E-01	8.0397E-01	8.2051E-01	7.9469E-01
		STD	**1.8056E-02**	1.9998E-02	3.2380E-02	4.8895E-02	3.0271E-02	3.4012E-02	3.3721E-02	3.7645E-02	3.4166E-02	3.3611E-02

(*continued on next page*)

Table A.5 (*continued*)

Image	Thresholds	Item	CCABC-MTIS	ABC-MTIS	WOA-MTIS	SCA-MTIS	MVO-MTIS	HHO-MTIS	CLPSO-MTIS	IGWO-MTIS	IWOA-MTIS	SCADE-MTIS
D	3	AVG	**6.9342E-01**	6.8722E-01	5.9648E-01	6.7718E-01	6.6693E-01	6.0128E-01	6.4094E-01	6.8515E-01	6.2200E-01	6.8163E-01
		STD	**1.4469E-02**	1.9810E-02	1.0433E-01	5.2629E-02	5.9601E-02	9.7835E-02	7.9040E-02	3.7610E-02	8.7250E-02	5.2638E-02
	5	AVG	**7.4704E-01**	7.2427E-01	7.0491E-01	7.0035E-01	6.9019E-01	6.8814E-01	6.9311E-01	7.2531E-01	7.0557E-01	7.0048E-01
		STD	**4.0430E-02**	5.5802E-02	7.7099E-02	5.3145E-02	6.9898E-02	7.8852E-02	6.5745E-02	6.1982E-02	7.4037E-02	6.9473E-02
	7	AVG	**7.7004E-01**	7.6727E-01	7.4290E-01	7.3619E-01	7.6257E-01	7.4103E-01	7.3909E-01	7.4008E-01	7.1314E-01	7.1999E-01
		STD	2.4665E-02	**2.2942E-02**	4.8488E-02	7.4768E-02	4.0885E-02	4.4109E-02	5.6097E-02	5.1804E-02	6.5950E-02	5.3120E-02
	12	AVG	**8.2944E-01**	8.1394E-01	8.0340E-01	7.8088E-01	8.0607E-01	8.0543E-01	7.8583E-01	7.8314E-01	7.8888E-01	7.5702E-01
		STD	**1.1865E-02**	2.5766E-02	2.9484E-02	3.2796E-02	3.6641E-02	3.2141E-02	3.2671E-02	4.6142E-02	3.8410E-02	5.2316E-02
	15	AVG	**8.5622E-01**	8.4428E-01	8.2970E-01	8.0365E-01	8.2369E-01	8.2083E-01	8.1359E-01	8.2290E-01	8.1502E-01	7.9548E-01
		STD	**1.4182E-02**	1.6310E-02	3.1121E-02	3.0892E-02	3.1192E-02	2.7134E-02	1.5778E-02	2.3226E-02	3.0802E-02	3.6688E-02
	18	AVG	**8.7306E-01**	8.6286E-01	8.5815E-01	8.2224E-01	8.4971E-01	8.4600E-01	8.3801E-01	8.3160E-01	8.3967E-01	8.1918E-01
		STD	**9.7655E-03**	1.4699E-02	2.3031E-02	2.8144E-02	2.1945E-02	2.7801E-02	2.1240E-02	4.0016E-02	1.9429E-02	3.6637E-02
E	3	AVG	7.2772E-01	7.1940E-01	6.6900E-01	7.1415E-01	7.2141E-01	6.4899E-01	6.8921E-01	**7.4548E-01**	6.9820E-01	7.0457E-01
		STD	2.2609E-02	2.6471E-02	8.9038E-02	4.1439E-02	6.8057E-02	9.9420E-02	5.4878E-02	**1.0295E-02**	6.2621E-02	5.0476E-02
	5	AVG	7.5281E-01	7.2824E-01	7.1620E-01	7.3614E-01	7.2849E-01	6.7801E-01	7.3344E-01	**7.5339E-01**	7.1895E-01	7.3503E-01
		STD	**1.4053E-02**	4.3215E-02	7.8587E-02	3.8477E-02	4.9121E-02	7.8835E-02	3.3751E-02	3.1503E-02	4.6569E-02	3.7415E-02
	7	AVG	7.4359E-01	7.3355E-01	6.8211E-01	6.1883E-01	7.2648E-01	6.7387E-01	7.4625E-01	**7.6442E-01**	7.3243E-01	7.4826E-01
		STD	3.7107E-02	4.2067E-02	7.2288E-02	8.0656E-02	4.4149E-02	1.2202E-01	3.4238E-02	**3.3003E-02**	4.6345E-02	4.2810E-02
	12	AVG	**8.2519E-01**	8.1299E-01	8.0344E-01	7.7894E-01	8.2380E-01	7.8829E-01	8.0049E-01	8.0375E-01	7.8778E-01	7.9290E-01
		STD	2.5525E-02	3.1038E-02	3.5507E-02	4.1579E-02	**2.1876E-02**	3.4467E-02	2.8427E-02	2.4261E-02	3.1940E-02	3.5365E-02
	15	AVG	**8.5908E-01**	8.5102E-01	8.3131E-01	8.1697E-01	8.3824E-01	8.2864E-01	8.2348E-01	8.2944E-01	8.2310E-01	8.0027E-01
		STD	**1.5262E-02**	1.7269E-02	3.3763E-02	2.2848E-02	2.3181E-02	2.9188E-02	2.6739E-02	2.0271E-02	3.3129E-02	2.6964E-02
	18	AVG	**8.7778E-01**	8.6699E-01	8.5460E-01	8.2783E-01	8.4915E-01	8.4482E-01	8.3944E-01	8.4003E-01	8.4026E-01	8.2352E-01
		STD	**1.3912E-02**	1.8916E-02	2.6529E-02	2.3443E-02	2.1912E-02	3.2536E-02	2.1193E-02	2.4260E-02	2.1046E-02	3.0446E-02
F	3	AVG	6.6749E-01	**6.7745E-01**	6.0256E-01	6.4542E-01	6.5054E-01	6.0616E-01	6.1324E-01	6.6546E-01	5.8334E-01	6.5515E-01
		STD	**2.0819E-02**	2.2285E-02	1.0797E-01	4.9127E-02	6.4971E-02	1.0141E-01	7.4201E-02	2.5306E-02	1.0626E-01	4.8475E-02
	5	AVG	6.9876E-01	**6.9881E-01**	6.6121E-01	6.9058E-01	6.9200E-01	6.6992E-01	6.5605E-01	6.9391E-01	6.5077E-01	6.9140E-01
		STD	4.4552E-02	3.9360E-02	8.1132E-02	**3.6807E-02**	4.4538E-02	9.7269E-02	6.7949E-02	5.9628E-02	6.2322E-02	5.5687E-02
	7	AVG	**7.5330E-01**	7.4758E-01	7.1638E-01	7.2007E-01	7.3636E-01	6.9866E-01	7.0347E-01	7.2662E-01	7.1414E-01	6.8725E-01
		STD	**2.3774E-02**	2.4194E-02	7.4088E-02	4.5955E-02	3.9660E-02	7.8721E-02	4.2906E-02	6.1500E-02	5.4273E-02	5.4880E-02
	12	AVG	**7.9236E-01**	7.8211E-01	7.5882E-01	6.9550E-01	7.7709E-01	7.6503E-01	7.4946E-01	7.4472E-01	7.4080E-01	7.3040E-01
		STD	2.8535E-02	**2.7107E-02**	4.7713E-02	5.0483E-02	3.8022E-02	3.9432E-02	4.2731E-02	4.4175E-02	4.0692E-02	4.5798E-02
	15	AVG	**8.4570E-01**	8.1937E-01	8.2036E-01	7.5407E-01	8.1541E-01	7.9653E-01	7.8789E-01	7.8739E-01	7.9050E-01	7.7538E-01
		STD	**2.0571E-02**	2.3016E-02	3.0452E-02	4.9698E-02	3.5101E-02	4.7812E-02	3.4750E-02	4.7174E-02	4.4526E-02	4.4769E-02
	18	AVG	**8.7086E-01**	8.5521E-01	8.4263E-01	7.8308E-01	8.3205E-01	8.1427E-01	8.1094E-01	8.2539E-01	8.1976E-01	7.8547E-01
		STD	2.3433E-02	**2.2513E-02**	2.9526E-02	4.2203E-02	3.6786E-02	4.5012E-02	3.0926E-02	3.3200E-02	3.6848E-02	3.8536E-02
G	3	AVG	**6.2769E-01**	5.9565E-01	5.3762E-01	5.8785E-01	5.4657E-01	5.2667E-01	5.4953E-01	5.4805E-01	5.7423E-01	5.9047E-01

(*continued on next page*)

Table A.5 (*continued*)

Image	Thresholds	Item	CCABC-MTIS	ABC-MTIS	WOA-MTIS	SCA-MTIS	MVO-MTIS	HHO-MTIS	CLPSO-MTIS	IGWO-MTIS	IWOA-MTIS	SCADE-MTIS
		STD	**4.7366E-02**	9.6445E-02	9.3854E-02	5.6528E-02	9.3700E-02	9.0182E-02	9.4927E-02	1.0005E-01	6.8674E-02	4.7509E-02
	5	AVG	**6.4749E-01**	6.3073E-01	6.1259E-01	5.9639E-01	6.3777E-01	5.9572E-01	6.1888E-01	5.9893E-01	5.9533E-01	5.9960E-01
		STD	4.8476E-02	**4.2783E-02**	5.7100E-02	7.3761E-02	4.2863E-02	5.7344E-02	4.3068E-02	5.6103E-02	5.1868E-02	6.1186E-02
	7	AVG	**7.1605E-01**	6.9741E-01	6.7577E-01	6.5275E-01	7.0189E-01	6.6829E-01	6.7123E-01	6.6342E-01	6.6983E-01	6.3043E-01
		STD	**2.0660E-02**	2.9425E-02	4.2691E-02	5.1104E-02	3.3597E-02	4.3774E-02	5.3146E-02	4.4917E-02	3.8250E-02	6.3421E-02
	12	AVG	**8.1109E-01**	8.1082E-01	7.9054E-01	7.5578E-01	8.0014E-01	7.8036E-01	7.7700E-01	7.7845E-01	7.7373E-01	7.4764E-01
		STD	**2.4778E-02**	2.6205E-02	3.8771E-02	3.8661E-02	4.3512E-02	4.5679E-02	3.2747E-02	3.9130E-02	3.3220E-02	4.3377E-02
	15	AVG	**8.4439E-01**	8.3204E-01	8.2775E-01	7.8874E-01	8.3284E-01	8.0892E-01	8.0934E-01	7.9905E-01	7.9934E-01	7.7851E-01
		STD	2.2939E-02	2.6082E-02	3.9338E-02	4.6260E-02	**2.1829E-02**	4.2783E-02	2.5095E-02	3.9251E-02	3.6522E-02	3.5919E-02
	18	AVG	**8.7535E-01**	8.6471E-01	8.6076E-01	8.1074E-01	8.3483E-01	8.5195E-01	8.2892E-01	8.3714E-01	8.2488E-01	7.9812E-01
		STD	**1.3531E-02**	1.8632E-02	2.7852E-02	3.4097E-02	3.2542E-02	3.0728E-02	3.1403E-02	2.8340E-02	3.5154E-02	4.1955E-02
H	3	AVG	**7.0748E-01**	7.0181E-01	6.3913E-01	6.7283E-01	6.7564E-01	6.0196E-01	6.5342E-01	6.9807E-01	6.2351E-01	6.7263E-01
		STD	6.8506E-03	**6.4824E-03**	7.0011E-02	4.5152E-02	5.7819E-02	9.5877E-02	6.7660E-02	2.8481E-02	6.8694E-02	4.6385E-02
	5	AVG	**7.2701E-01**	7.0928E-01	6.6840E-01	6.9311E-01	7.0238E-01	6.6809E-01	6.8521E-01	7.0505E-01	6.9788E-01	6.7934E-01
		STD	**1.9006E-02**	2.3938E-02	6.7690E-02	3.5509E-02	3.4820E-02	6.6288E-02	3.4686E-02	5.4041E-02	4.3846E-02	5.5992E-02
	7	AVG	**7.3949E-01**	7.3087E-01	7.1575E-01	7.0436E-01	7.3263E-01	7.0173E-01	7.1208E-01	6.9986E-01	7.0891E-01	6.9642E-01
		STD	**2.1166E-02**	4.3498E-02	4.8985E-02	6.8634E-02	4.5503E-02	6.7097E-02	3.6905E-02	5.0028E-02	5.1212E-02	7.6662E-02
	12	AVG	**8.0032E-01**	7.9548E-01	7.8678E-01	7.4498E-01	7.8529E-01	7.7784E-01	7.6552E-01	7.6575E-01	7.7258E-01	7.5170E-01
		STD	3.0021E-02	**2.6971E-02**	4.5365E-02	5.5872E-02	3.0346E-02	3.2109E-02	3.2330E-02	3.3265E-02	3.8439E-02	4.9779E-02
	15	AVG	**8.4481E-01**	8.2131E-01	8.1552E-01	7.8500E-01	8.2736E-01	8.0806E-01	8.0615E-01	7.8697E-01	8.0531E-01	7.7881E-01
		STD	**1.7584E-02**	3.6528E-02	3.3591E-02	3.4006E-02	3.4864E-02	3.0816E-02	3.1940E-02	3.0263E-02	3.5664E-02	3.1607E-02
	18	AVG	**8.6688E-01**	8.5804E-01	8.5153E-01	7.9973E-01	8.4355E-01	8.3854E-01	8.2766E-01	8.0903E-01	8.2149E-01	7.9885E-01
		STD	**1.2588E-02**	1.7556E-02	2.0853E-02	3.0470E-02	2.0605E-02	3.8630E-02	2.4826E-02	2.9432E-02	2.9783E-02	3.8342E-02

Table A.6
The fitness values obtained by each algorithm

Image	Thresholds	CCABC	ABC	WOA	SCA	MVO	HHO	CLPSO	IGWO	IWOA	SCADE
A	3	**3.2379E+01**	3.2376E+01	3.2374E+01	3.2106E+01	3.2307E+01	3.2095E+01	3.2186E+01	3.2320E+01	3.2224E+01	3.1915E+01
	5	**4.4008E+01**	4.3465E+01	4.3936E+01	4.1711E+01	4.3954E+01	4.2916E+01	4.2880E+01	4.3769E+01	4.2767E+01	4.2108E+01
	7	5.4160E+01	5.3907E+01	5.3931E+01	5.1683E+01	**5.4172E+01**	5.2873E+01	5.2317E+01	5.3372E+01	5.2203E+01	5.1460E+01
	12	**7.5545E+01**	7.5097E+01	7.3619E+01	6.8010E+01	7.4468E+01	7.3122E+01	7.1414E+01	7.2174E+01	7.2122E+01	6.8362E+01
	15	**8.6113E+01**	8.5329E+01	8.3955E+01	7.7028E+01	8.4731E+01	8.2795E+01	8.0892E+01	8.2368E+01	8.1514E+01	7.6332E+01
	18	**9.5105E+01**	9.4237E+01	9.3568E+01	8.2721E+01	9.2882E+01	9.2196E+01	8.8939E+01	9.0106E+01	9.2296E+01	8.4471E+01
B	3	**3.2538E+01**	3.2535E+01	3.2529E+01	3.2345E+01	3.2538E+01	3.2463E+01	3.2378E+01	3.2530E+01	3.2465E+01	3.2260E+01
	5	**4.4276E+01**	4.4185E+01	4.4218E+01	4.2951E+01	4.4248E+01	4.3656E+01	4.2812E+01	4.4189E+01	4.3705E+01	4.2613E+01
	7	**5.4697E+01**	5.4154E+01	5.4466E+01	5.1787E+01	5.4528E+01	5.3958E+01	5.2171E+01	5.4490E+01	5.3603E+01	5.0894E+01
	12	**7.6459E+01**	7.5242E+01	7.5695E+01	6.6875E+01	7.5603E+01	7.4968E+01	7.2782E+01	7.2920E+01	7.2568E+01	7.1026E+01
	15	8.6131E+01	**8.6476E+01**	8.6236E+01	7.8721E+01	8.4854E+01	8.4465E+01	8.2515E+01	8.2448E+01	8.2712E+01	7.6185E+01
	18	**9.5624E+01**	9.4743E+01	9.5175E+01	8.4360E+01	9.3465E+01	9.3696E+01	8.9776E+01	9.1127E+01	9.2242E+01	8.4546E+01
C	3	**3.2660E+01**	3.2338E+01	3.2660E+01	3.2076E+01	3.2645E+01	3.1773E+01	3.2225E+01	3.2605E+01	3.2515E+01	3.2294E+01
	5	4.4133E+01	4.3238E+01	**4.4209E+01**	4.2061E+01	4.3910E+01	4.3311E+01	4.3211E+01	4.3617E+01	4.3230E+01	4.2135E+01
	7	5.4419E+01	5.3781E+01	5.4106E+01	5.1670E+01	**5.4551E+01**	5.3083E+01	5.2801E+01	5.3256E+01	5.3131E+01	5.0267E+01
	12	**7.6030E+01**	7.5304E+01	7.4169E+01	6.9149E+01	7.5797E+01	7.3754E+01	7.2621E+01	7.3300E+01	7.3353E+01	6.7721E+01
	15	8.6163E+01	**8.6351E+01**	8.5866E+01	7.6255E+01	8.6014E+01	8.3312E+01	8.3137E+01	8.1822E+01	8.2389E+01	7.5951E+01
	18	**9.5809E+01**	9.5740E+01	9.4473E+01	8.4126E+01	9.4386E+01	9.2973E+01	9.0121E+01	9.0876E+01	9.1056E+01	8.4441E+01
D	3	**3.2006E+01**	3.2005E+01	3.2003E+01	3.1736E+01	3.2006E+01	3.1989E+01	3.1873E+01	3.1998E+01	3.1935E+01	3.1644E+01
	5	**4.4015E+01**	4.3714E+01	4.3954E+01	4.2013E+01	4.3964E+01	4.3792E+01	4.2909E+01	4.3643E+01	4.3150E+01	4.1993E+01

(*continued on next page*)

Table A.6 (*continued*)

Image	Thresholds	CCABC	ABC	WOA	SCA	MVO	HHO	CLPSO	IGWO	IWOA	SCADE
	7	**5.4418E+01**	5.3982E+01	5.4147E+01	5.1012E+01	5.4090E+01	5.3170E+01	5.2584E+01	5.3488E+01	5.2890E+01	4.9759E+01
	12	**7.5748E+01**	7.5329E+01	7.4947E+01	6.8591E+01	7.5046E+01	7.4738E+01	7.1183E+01	7.2953E+01	7.2310E+01	6.7728E+01
	15	8.6006E+01	**8.6240E+01**	8.6019E+01	7.7327E+01	8.5696E+01	8.4591E+01	8.2699E+01	8.2660E+01	8.4302E+01	7.7323E+01
	18	**9.6371E+01**	9.5265E+01	9.4804E+01	8.3787E+01	9.5096E+01	9.2151E+01	8.9580E+01	9.0601E+01	9.0986E+01	8.2188E+01
E	3	3.2615E+01	3.2608E+01	3.2611E+01	3.2510E+01	3.2615E+01	3.2526E+01	3.2426E+01	**3.2616E+01**	3.2580E+01	3.2415E+01
	5	4.4411E+01	4.4254E+01	4.4317E+01	4.2846E+01	**4.4416E+01**	4.3833E+01	4.3624E+01	4.4339E+01	4.4341E+01	4.2912E+01
	7	**5.4733E+01**	5.4725E+01	5.4597E+01	5.1726E+01	5.4626E+01	5.3719E+01	5.2860E+01	5.4080E+01	5.2822E+01	5.1952E+01
	12	**7.6277E+01**	7.5536E+01	7.5049E+01	6.8902E+01	7.5326E+01	7.3780E+01	7.2563E+01	7.5025E+01	7.3099E+01	6.9137E+01
	15	**8.7038E+01**	8.6387E+01	8.5926E+01	7.5918E+01	8.5473E+01	8.3965E+01	8.0900E+01	8.2646E+01	8.3296E+01	7.6781E+01
	18	**9.5977E+01**	9.5540E+01	9.4388E+01	8.6877E+01	9.4400E+01	9.4013E+01	8.8299E+01	8.9902E+01	8.8715E+01	8.3884E+01
F	3	3.2292E+01	3.2291E+01	3.2302E+01	3.1992E+01	**3.2303E+01**	3.2186E+01	3.2126E+01	3.2297E+01	3.2144E+01	3.2041E+01
	5	**4.4366E+01**	4.3862E+01	4.4177E+01	4.2387E+01	4.4323E+01	4.3789E+01	4.2792E+01	4.4192E+01	4.3563E+01	4.3169E+01
	7	**5.4445E+01**	5.4342E+01	5.4432E+01	5.1564E+01	5.4385E+01	5.3614E+01	5.2533E+01	5.3403E+01	5.2787E+01	5.2056E+01
	12	7.4912E+01	**7.5262E+01**	7.5038E+01	6.9224E+01	7.4865E+01	7.3735E+01	7.1417E+01	7.3573E+01	7.2610E+01	6.7913E+01
	15	**8.5865E+01**	8.5647E+01	8.5454E+01	7.7280E+01	8.4292E+01	8.3536E+01	8.1815E+01	8.1939E+01	8.2275E+01	7.6165E+01
	18	**9.5500E+01**	9.5274E+01	9.3557E+01	8.6031E+01	9.3884E+01	9.3265E+01	9.0765E+01	9.0046E+01	9.0515E+01	8.6786E+01
G	3	3.2790E+01	3.2562E+01	3.2788E+01	3.2345E+01	**3.2801E+01**	3.2589E+01	3.2727E+01	3.2772E+01	3.2406E+01	3.2146E+01
	5	4.4643E+01	**4.4645E+01**	4.4537E+01	4.2292E+01	4.4316E+01	4.4347E+01	4.3433E+01	4.3708E+01	4.4422E+01	4.2192E+01
	7	5.5058E+01	**5.5245E+01**	5.5091E+01	5.0557E+01	5.4890E+01	5.4307E+01	5.3841E+01	5.3389E+01	5.4121E+01	4.9984E+01
	12	**7.7011E+01**	7.5181E+01	7.5137E+01	6.8725E+01	7.5421E+01	7.4132E+01	7.2757E+01	7.2394E+01	7.4175E+01	6.7608E+01
	15	**8.7044E+01**	8.6391E+01	8.6892E+01	7.6652E+01	8.5814E+01	8.4090E+01	8.1642E+01	8.2771E+01	8.4775E+01	7.9031E+01
	18	**9.5989E+01**	9.5296E+01	9.4713E+01	8.5726E+01	9.3939E+01	9.3189E+01	8.9209E+01	8.9329E+01	9.1520E+01	8.4408E+01
H	3	**3.2382E+01**	3.2356E+01	3.2382E+01	3.2218E+01	3.2375E+01	3.2313E+01	3.2034E+01	3.2379E+01	3.2152E+01	3.2252E+01
	5	**4.4340E+01**	4.3981E+01	4.4247E+01	4.2712E+01	4.4334E+01	4.3697E+01	4.3012E+01	4.4147E+01	4.3721E+01	4.1737E+01
	7	5.4687E+01	5.4595E+01	5.4221E+01	4.9820E+01	**5.4696E+01**	5.3163E+01	5.2680E+01	5.3599E+01	5.3654E+01	4.9599E+01
	12	**7.5766E+01**	7.5623E+01	7.4364E+01	6.8579E+01	7.5194E+01	7.3299E+01	7.1889E+01	7.3417E+01	7.4093E+01	6.8809E+01
	15	**8.6553E+01**	8.5602E+01	8.5448E+01	7.6990E+01	8.5793E+01	8.4478E+01	8.1322E+01	8.2316E+01	8.2101E+01	7.6192E+01
	18	9.5320E+01	**9.6354E+01**	9.5919E+01	8.3236E+01	9.4552E+01	9.3899E+01	8.9438E+01	8.9907E+01	9.1793E+01	8.3200E+01

Table A.7
Time cost of CCABC and other algorithms (Unit: sec)

Image	CCABC	ABC	WOA	SCA	MVO	HHO	CLPSO	IGWO	IWOA	SCADE
A	48.86	24.36	24.20	26.23	24.53	48.23	23.50	35.94	3.76	72.54
B	48.23	23.68	24.04	26.53	24.61	48.02	23.32	36.75	3.70	71.98
C	48.48	23.84	24.32	26.49	24.60	48.80	24.08	36.16	3.79	73.36
D	50.42	24.51	25.56	26.88	24.93	51.05	24.82	36.48	4.01	72.30
E	50.85	25.08	26.09	26.88	25.79	50.12	25.32	37.26	4.26	69.95
F	50.58	25.37	25.77	25.44	25.21	50.96	25.41	37.65	4.44	68.04
G	51.31	24.81	26.12	26.96	25.60	50.72	25.76	38.38	4.36	69.58
H	46.29	23.73	23.94	24.59	23.82	47.47	23.27	34.06	3.77	65.62

Appendix B

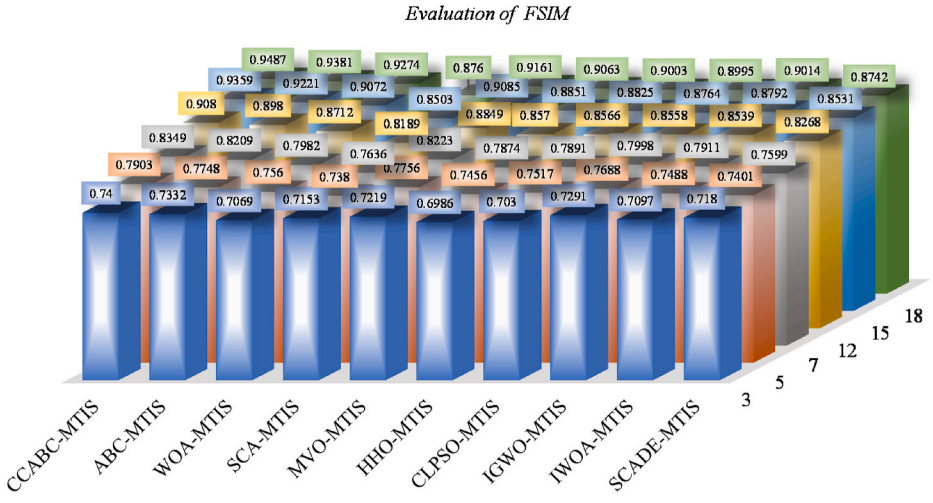

Fig. B.1. The average of FSIM at each threshold level

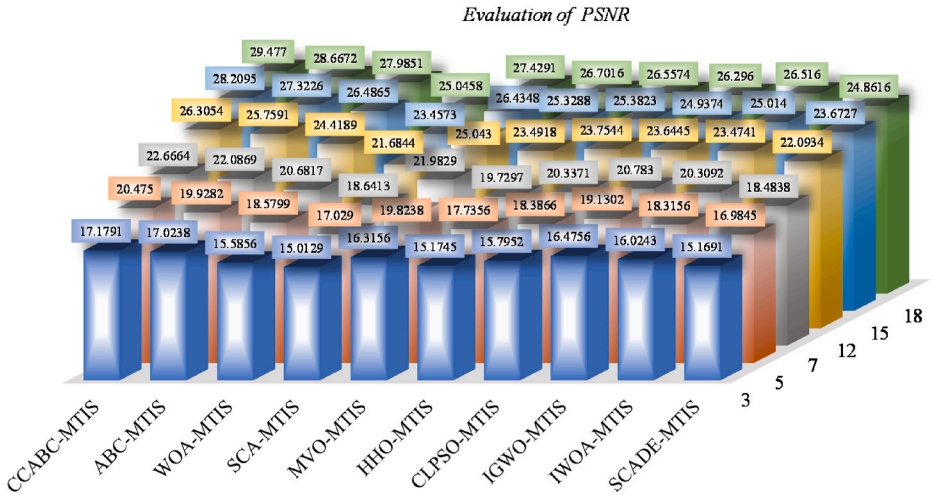

Fig. B.2. The average of PSNR at each threshold level

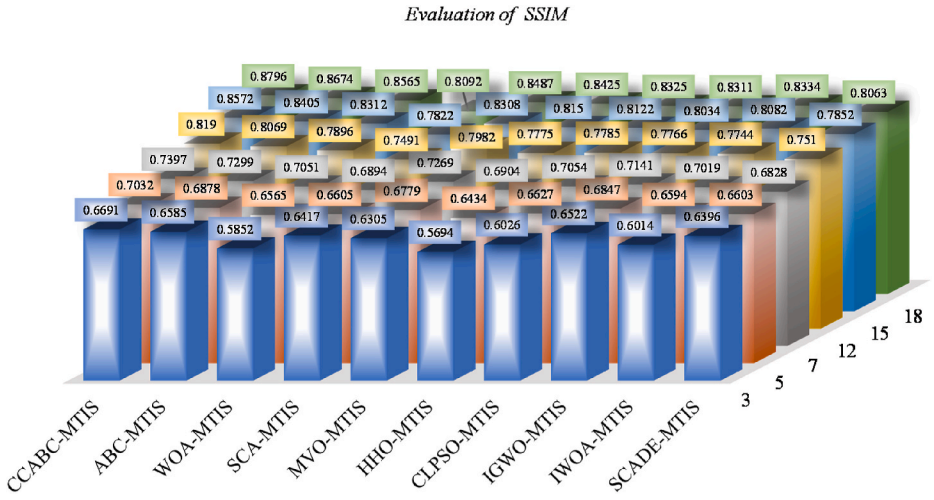

Fig. B.3. The average of SSIM at each threshold level

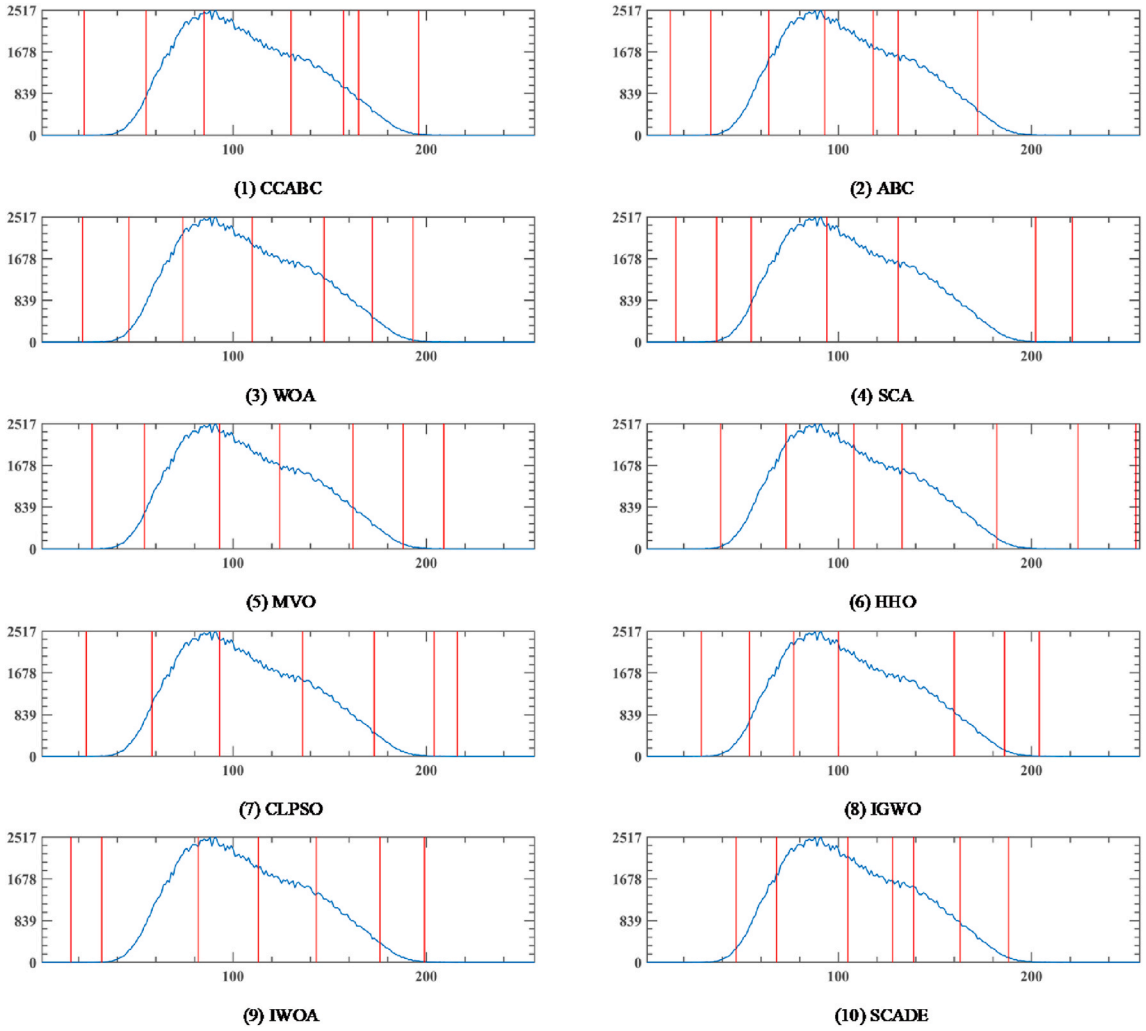

Fig. B.4. The threshold values of A obtained by each algorithm at level 7

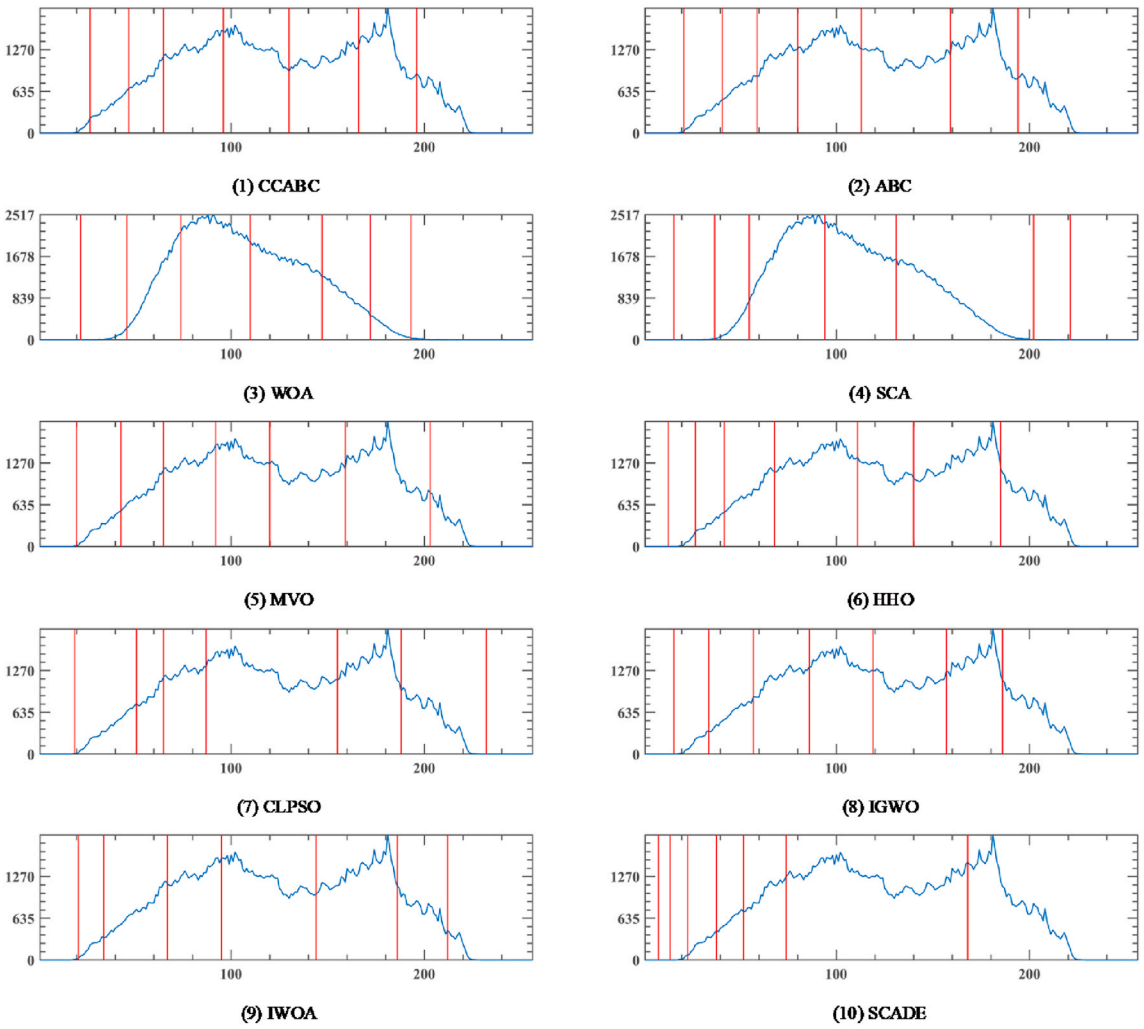

Fig. B.5. The threshold values of B obtained by each algorithm at level 7

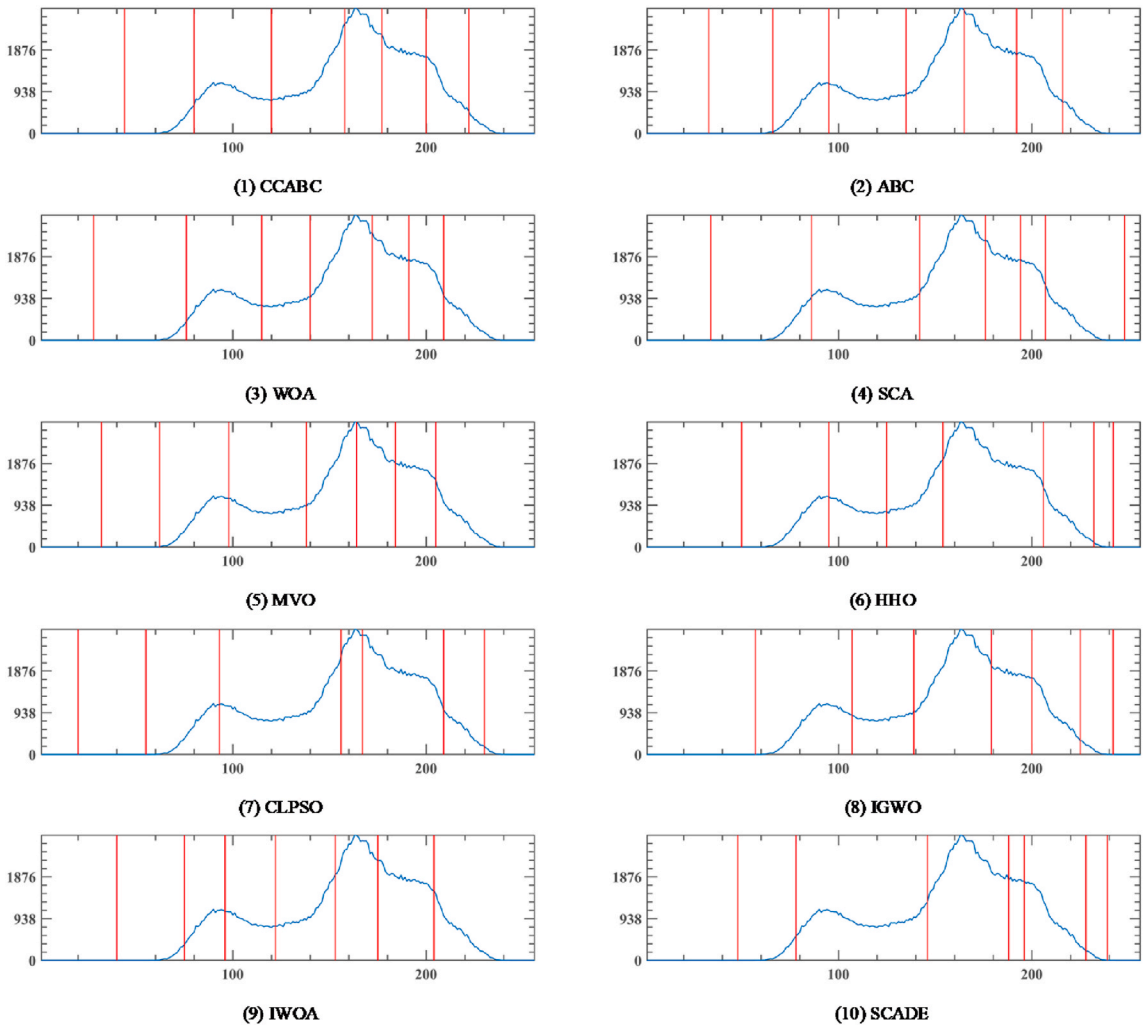

Fig. B.6. The threshold values of C obtained by each algorithm at level 7

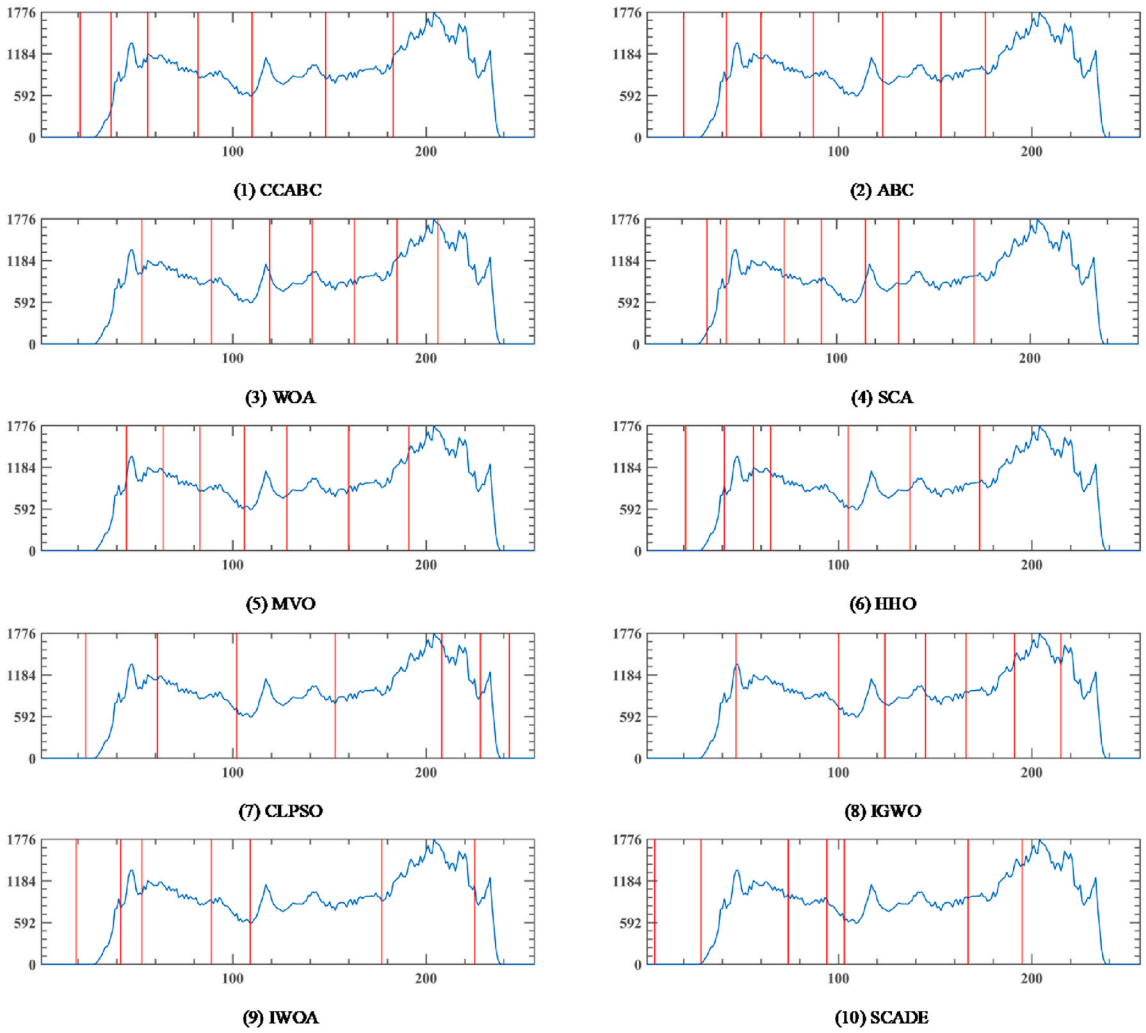

Fig. B.7. The threshold values of D obtained by each algorithm at level 7

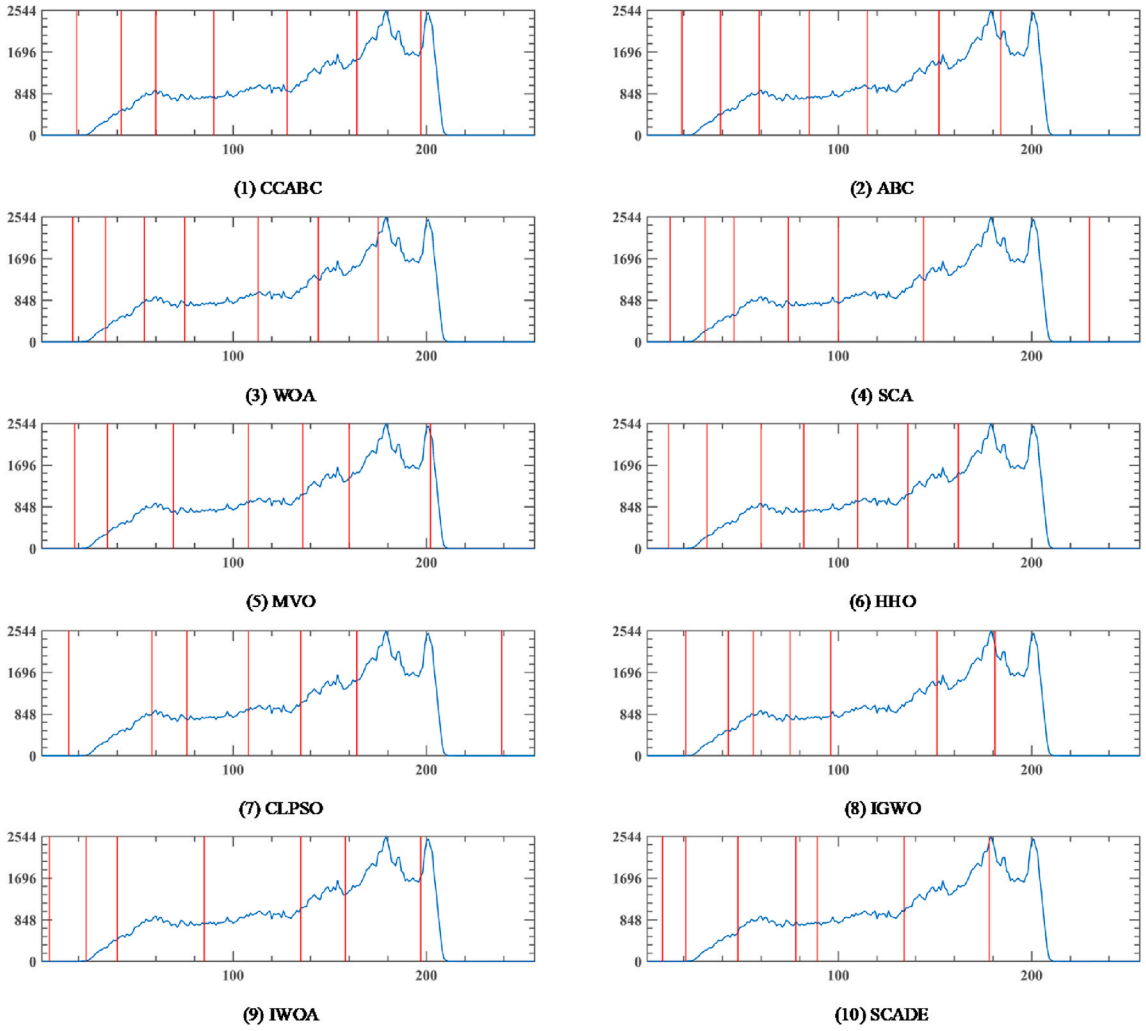

Fig. B.8. The threshold values of E obtained by each algorithm at level 7

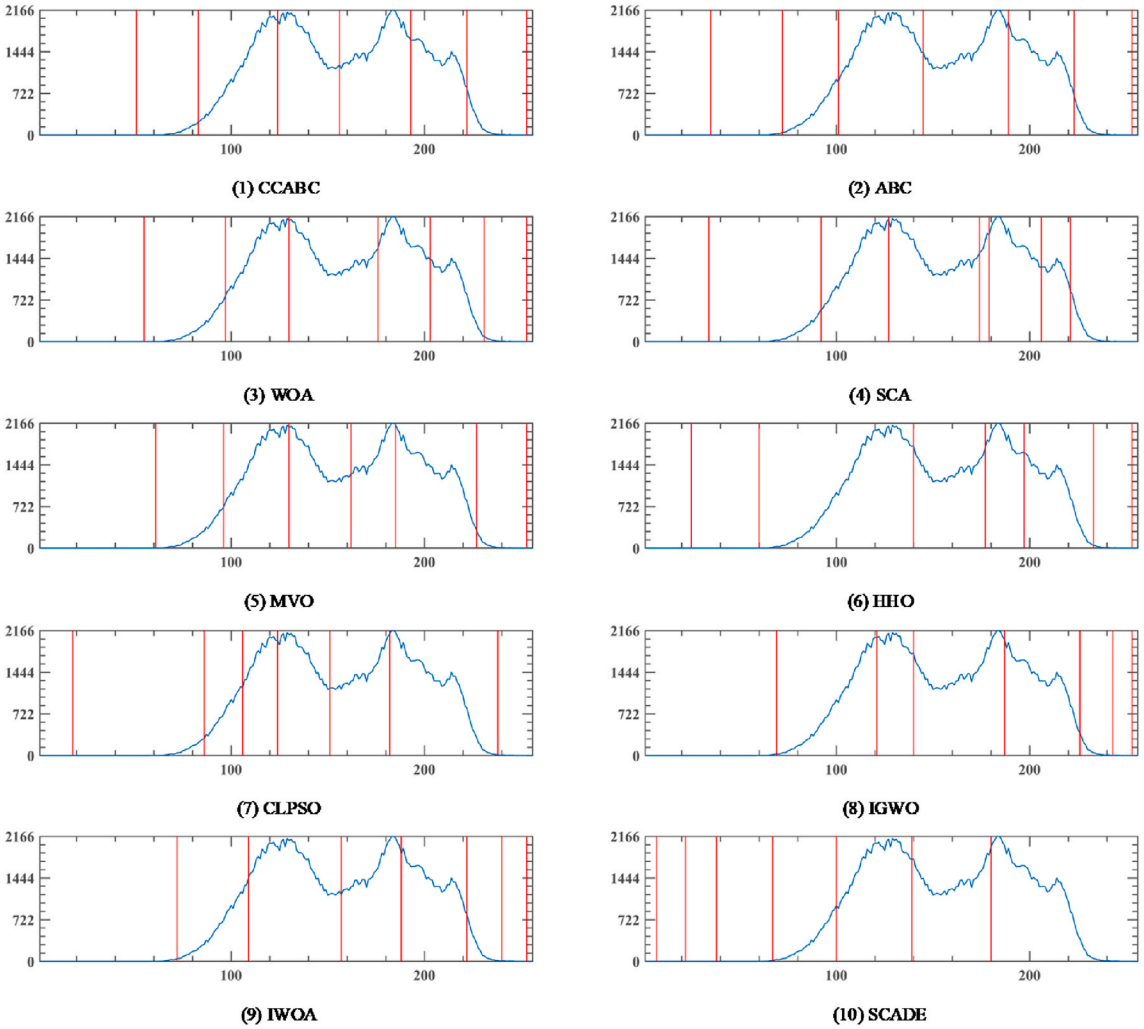

Fig. B.9. The threshold values of F obtained by each algorithm at level 7

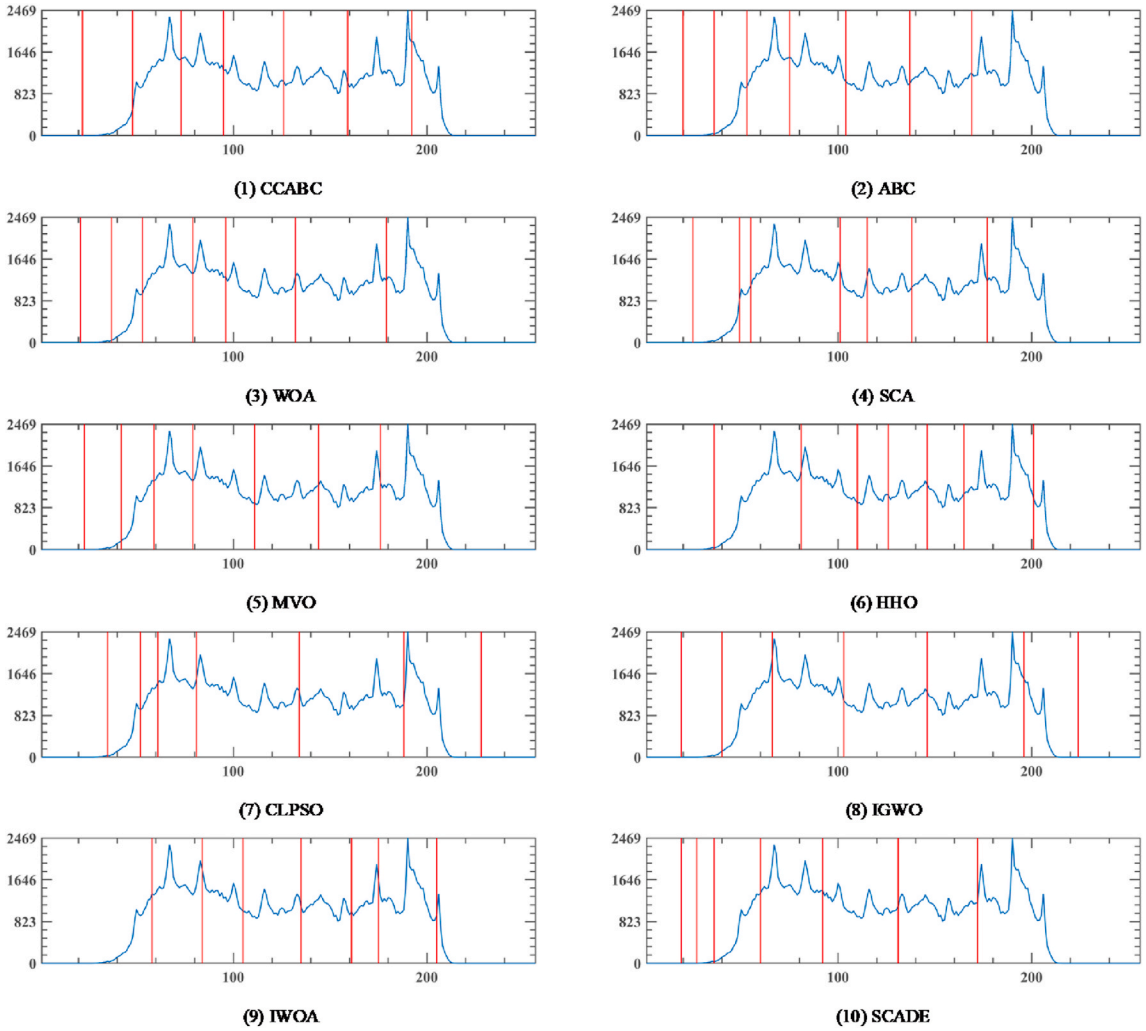

Fig. B.10. The threshold values of G obtained by each algorithm at level 7

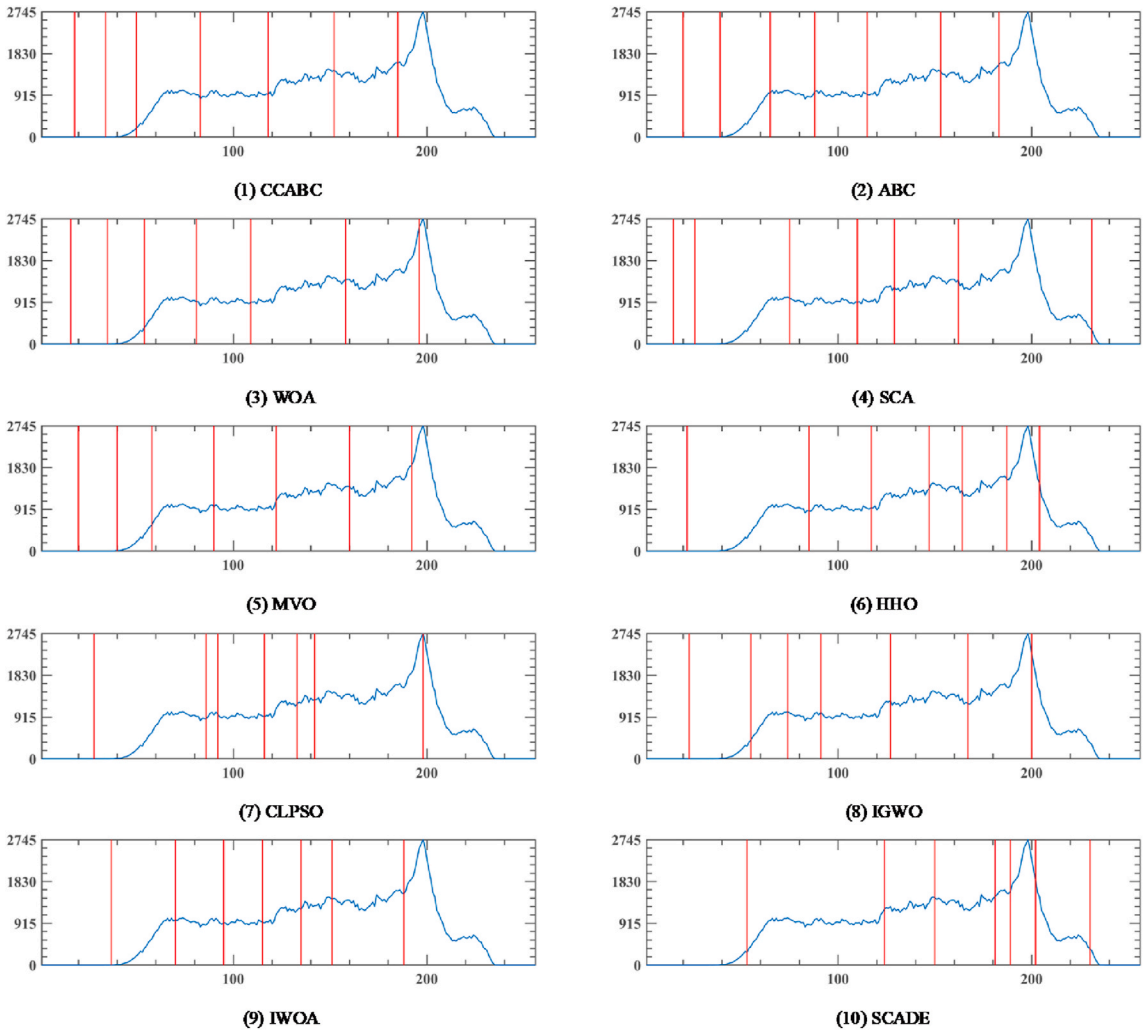

Fig. B.11. The threshold values of H obtained by each algorithm at level 7

References

[1] W. Zhou, Y. Lv, J. Lei, L. Yu, Global and local-contrast guides content-aware fusion for RGB-D saliency prediction, IEEE Transactions on Systems, Man, and Cybernetics: Systems 51 (2021) 3641–3649.

[2] S. Zhao, P. Wang, A.A. Heidari, H. Chen, H. Turabieh, M. Mafarja, C. Li, Multilevel threshold image segmentation with diffusion association slime mould algorithm and Renyi's entropy for chronic obstructive pulmonary disease, Comput. Biol. Med. 134 (2021), 104427.

[3] L. Liu, D. Zhao, F. Yu, A.A. Heidari, J. Ru, H. Chen, M. Mafarja, H. Turabieh, Z. Pan, Performance optimization of differential evolution with slime mould algorithm for multilevel breast cancer image segmentation, Comput. Biol. Med. 138 (2021), 104910.

[4] S. Zhao, P. Wang, A.A. Heidari, H. Chen, W. He, S. Xu, Performance optimization of salp swarm algorithm for multi-threshold image segmentation: comprehensive study of breast cancer microscopy, Comput. Biol. Med. 139 (2021), 105015.

[5] C. Chen, X. Wang, A.A. Heidari, H. Yu, H. Chen, Multi-threshold image segmentation of maize diseases based on elite comprehensive particle swarm optimization and Otsu, Front. Plant Sci. 12 (2021).

[6] M. Abd Elaziz, D. Oliva, A.A. Ewees, S.W. Xiong, Multi-level thresholding-based grey scale image segmentation using multi-objective multi-verse optimizer, Expert Syst. Appl. 125 (2019) 112–129.

[7] J.Q. Gao, B.B. Wang, Z.Y. Wang, Y.F. Wang, F.Z. Kong, A wavelet transform-based image segmentation method, Optik (2020) 208.

[8] Y.F. Liang, L. Sun, W. Ser, F. Lin, E.Y. Tay, E.Y. Gan, T.G. Thng, Z.P. Lin, Hybrid threshold optimization between global image and local regions in image segmentation for melasma severity assessment, Multidimens. Syst. Signal Process. 28 (2017) 977–994.

[9] Q. Zheng, Y.H. Wu, Y. Fan, I. Alzheimer's dis neuroimaging, integrating semi-supervised and supervised learning methods for label fusion in multi-atlas based image segmentation, Front. Neuroinf. 12 (2018).

[10] X.H. Zhao, Y.C. Jiang, W.Q. Wang, SAR image segmentation based on analysing similarity with clutter spatial patterns, Electron. Lett. (2016) 52.

[11] L.C. Chen, G. Papandreou, I. Kokkinos, K. Murphy, A.L. Yuille, DeepLab: semantic image segmentation with deep convolutional nets, atrous convolution, and fully connected CRFs, IEEE Trans. Pattern Anal. Mach. Intell. 40 (2018) 834–848.

[12] L. Huang, B.X. Yao, P.D. Chen, A.P. Ren, Y. Xia, Superpixel segmentation method of high resolution remote sensing images based on hierarchical clustering, J. Infrared Millim. Waves 39 (2020) 263–272.

[13] H. Peng, J. Wang, M.J. Perez-Jimenez, Optimal multi-level thresholding with membrane computing, Digit. Signal Process. 37 (2015) 53–64.

[14] D. Zhao, L. Liu, F. Yu, A.A. Heidari, H. Chen, Chaotic random spare ant colony optimization for multi-threshold image segmentation of 2D Kapur entropy, Knowl. Base Syst. 216 (2020), 106510.

[15] Z.C. Zhang, J.Q. Yin, Bee foraging algorithm based multi-level thresholding for image segmentation, Ieee Access 8 (2020) 16269–16280.

[16] Z.K. Xing, H.M. Jia, An improved thermal exchange optimization based GLCM for multi-level image segmentation, Multimed. Tool. Appl. 79 (2020) 12007–12040.

[17] B. Wu, J.X. Zhou, X.Y. Ji, Y.J. Yin, X. Shen, An ameliorated teaching-learning-based optimization algorithm based study of image segmentation for multilevel thresholding using Kapur's entropy and Otsu's between class variance, Inf. Sci. 533 (2020) 72–107.

[18] A.A. Ewees, M. Abd Elaziz, M.A.A. Al-Qaness, H.A. Khalil, S. Kim, Improved artificial bee colony using sine-cosine algorithm for multi-level thresholding image segmentation, Ieee Access 8 (2020) 26304–26315.

[19] H.S.N. Alwerfali, M.A.A. Al-qaness, M. Abd Elaziz, A.A. Ewees, D. Oliva, S.F. Lu, Multi-level image thresholding based on modified spherical search optimizer and fuzzy entropy, Entropy 22 (2020).

[20] M. Abd Elaziz, A.A. Heidari, H. Fujita, H. Moayedi, A competitive chain-based Harris Hawks Optimizer for global optimization and multi-level image thresholding problems, Appl. Soft Comput. 95 (2020).

[21] Z.-H. Zhan, Z.-J. Wang, H. Jin, J. Zhang, Adaptive distributed differential evolution, IEEE Trans. Cybern. 50 (2019) 4633–4647.

[22] X.-F. Liu, Z.-H. Zhan, Y. Lin, W.-N. Chen, Y.-J. Gong, T.-L. Gu, H.-Q. Yuan, J. Zhang, Historical and heuristic-based adaptive differential evolution, IEEE Transactions on Systems, Man, and Cybernetics: Systems 49 (2018) 2623–2635.

[23] G. Sun, C. Li, L. Deng, An adaptive regeneration framework based on search space adjustment for differential evolution, Neural Comput. Appl. (2021) 1–17.

[24] F. Yin, X. Xue, C. Zhang, K. Zhang, J. Han, B. Liu, J. Wang, J. Yao, Multifidelity genetic transfer: an efficient framework for production optimization, SPE J. (2021) 1–22.

[25] S. Song, P. Wang, A.A. Heidari, M. Wang, X. Zhao, H. Chen, W. He, S. Xu, Dimension decided Harris hawks optimization with Gaussian mutation: balance analysis and diversity patterns, Knowl. Base Syst. (2020), 106425, https://doi.org/10.1016/j.knosys.2020.106425.

[26] X. Wang, H. Chen, A.A. Heidari, X. Zhang, J. Xu, Y. Xu, H. Huang, Multi-population following behavior-driven fruit fly optimization: a Markov chain convergence proof and comprehensive analysis, Knowl. Base Syst. 210 (2020), 106437.

[27] H. Moayedi, A. Mosavi, Synthesizing multi-layer perceptron network with ant lion biogeography-based dragonfly algorithm evolutionary strategy invasive weed and league champion optimization hybrid algorithms in predicting heating load in residential buildings, Sustainability 13 (2021) 3198.

[28] H. Moayedi, A. Mosavi, Suggesting a stochastic fractal search paradigm in combination with artificial neural network for early prediction of cooling load in residential buildings, Energies 14 (2021) 1649.

[29] H. Moayedi, A. Mosavi, An innovative metaheuristic strategy for solar energy management through a neural networks framework, Energies 14 (2021) 1196.

[30] H. Moayedi, A. Mosavi, Electrical power prediction through a combination of multilayer perceptron with water cycle ant lion and satin bowerbird searching optimizers, Sustainability 13 (2021) 2336.

[31] A. Seifi, M. Ehteram, V.P. Singh, A. Mosavi, Modeling and uncertainty analysis of groundwater level using six evolutionary optimization algorithms hybridized with ANFIS, SVM, and ANN, Sustainability, 12, 2020, p. 4023.

[32] Y. Zhang, R. Liu, X. Wang, H. Chen, C. Li, Boosted binary Harris hawks optimizer and feature selection, Eng. Comput. (2020) 1–30.

[33] J. Hu, H. Chen, A.A. Heidari, M. Wang, X. Zhang, Y. Chen, Z. Pan, Orthogonal learning covariance matrix for defects of grey wolf optimizer: insights, balance, diversity, and feature selection, Knowl. Base Syst. 213 (2021), 106684.

[34] X. Zhang, Y. Xu, C. Yu, A.A. Heidari, S. Li, H. Chen, C. Li, Gaussian mutational chaotic fruit fly-built optimization and feature selection, Expert Syst. Appl. 141 (2020), 112976.

[35] Q. Li, H. Chen, H. Huang, X. Zhao, Z. Cai, C. Tong, W. Liu, X. Tian, An enhanced grey wolf optimization based feature selection wrapped kernel extreme learning machine for medical diagnosis, Comput. Math. Methods Med. (2017), 2017.

[36] T. Liu, L. Hu, C. Ma, Z.-Y. Wang, H.-L. Chen, A fast approach for detection of erythemato-squamous diseases based on extreme learning machine with maximum relevance minimum redundancy feature selection, Int. J. Syst. Sci. 46 (2015) 919–931.

[37] M. Chen, G. Zeng, K. Lu, J. Weng, A two-layer nonlinear combination method for short-term wind speed prediction based on ELM, ENN, and LSTM, IEEE Internet Things J. 6 (2019) 6997–7010.

[38] H. Yu, W. Li, C. Chen, J. Liang, W. Gui, M. Wang, H. Chen, Dynamic Gaussian bare-bones fruit fly optimizers with abandonment mechanism: method and analysis, Eng. Comput. (2020) 1–29.

[39] B. Nautiyal, R. Prakash, V. Vimal, G. Liang, H. Chen, Improved Salp Swarm Algorithm with mutation schemes for solving global optimization and engineering problems, Eng. Comput. (2021) 1–23.

[40] D. Zhao, L. Liu, F. Yu, A.A. Heidari, M. Wang, G. Liang, K. Muhammad, H. Chen, Chaotic random spare ant colony optimization for multi-threshold image segmentation of 2D Kapur entropy, Knowl. Base Syst. (2020), 106510, https://doi.org/10.1016/j.knosys.2020.106510.

[41] K. Ahmed, R. Babers, A. Darwish, A.E. Hassanien, Swarm-based Analysis for Community Detection in Complex Networks, Big Data Analytics, CRC Press, 2018, pp. 213–230.

[42] K. Ahmed, A.E. Hassanien, E. Ezzat, An efficient approach for community detection in complex social networks based on elephant swarm optimization algorithm, in: Handbook of Research on Machine Learning Innovations and Trends, vol. 2, 2017.

[43] K. Ahmed, A. Hassanien, E. Ezzat, P.W. Tsai, An adaptive approach for community detection based on chicken swarm optimization algorithm, Genet. Evol. Comput. 536 (2016) 281–288.

[44] K. Ahmed, A.I. Hafez, A.E. Hassanien, A Discrete Krill Herd Optimization Algorithm for Community Detection, 11th International Computer Engineering Conference (ICENCO) 2015, IEEE, 2016.

[45] K. Ahmed, A.E. Hassanien, E. Ezzat, S. Bhattacharyya, Swarming Behaviors of Chicken for Predicting Posts on Facebook Branding Pages, International Conference on Advanced Machine Learning Technologies and Applications, 2018.

[46] G.-q. Zeng, Y.-z. Lu, W.-J. Mao, Modified extremal optimization for the hard maximum satisfiability problem, J. Zhejiang Univ. - Sci. C 12 (2011) 589–596.

[47] G. Zeng, Y. Lu, Y. Dai, Z. Wu, W. Mao, Z. Zhang, C.J. Zheng, Backbone guided extremal optimization for the hard maximum satisfiability problem, Int. J. Innov. Comput. Inf. Contr. 8 (2012) 8355–8366.

[48] K. Ahmed, A.A. Ewees, A.E. Hassanien, Prediction and management system for forest fires based on hybrid flower pollination optimization algorithm and adaptive neuro-fuzzy inference system, in: 2017 Eighth International Conference on Intelligent Computing and Information Systems (ICICIS), IEEE, 2017, pp. 299–304.

[49] K. Ahmed, A.A. Ewees, M. Abd El Aziz, A.E. Hassanien, T. Gaber, P.-W. Tsai, J.-S. Pan, A hybrid krill-ANFIS model for wind speed forecasting, in: International Conference on Advanced Intelligent Systems and Informatics, Springer, 2016, pp. 365–372.

[50] L. Hu, H. Li, Z. Cai, F. Lin, G. Hong, H. Chen, Z. Lu, A new machine-learning method to prognosticate paraquat poisoned patients by combining coagulation, liver, and kidney indices, PLoS One 12 (2017), e0186427.

[51] C. Li, L. Hou, B.Y. Sharma, H. Li, C. Chen, Y. Li, X. Zhao, H. Huang, Z. Cai, H. Chen, Developing a new intelligent system for the diagnosis of tuberculous pleural effusion, Comput. Methods Progr. Biomed. 153 (2018) 211–225.

[52] X. Zhao, X. Zhang, Z. Cai, X. Tian, X. Wang, Y. Huang, H. Chen, L. Hu, Chaos enhanced grey wolf optimization wrapped ELM for diagnosis of paraquat-poisoned patients, Comput. Biol. Chem. 78 (2019) 481–490.

[53] H. Huang, S. Zhou, J. Jiang, H. Chen, Y. Li, C. Li, A new fruit fly optimization algorithm enhanced support vector machine for diagnosis of breast cancer based on high-level features, BMC Bioinf. 20 (2019) 1–14.

[54] S.H. Basha, A. Tharwat, K. Ahmed, A.E. Hassanien, A Predictive Model for Seminal Quality Using Neutrosophic Rule-Based Classification System, International Conference on Advanced Intelligent Systems and Informatics, Springer, 2018, pp. 495–504.

[55] C. Zhao, S. Zhong, Q. Zhong, K. Shi, Synchronization of Markovian complex networks with input mode delay and Markovian directed communication via distributed dynamic event-triggered control, Nonlinear Anal.: Hybrid Syst. 36 (2020), 100883.

[56] Y. Zhang, R. Liu, A.A. Heidari, X. Wang, Y. Chen, M. Wang, H. Chen, Towards Augmented Kernel Extreme Learning Models for Bankruptcy Prediction: Algorithmic Behavior and Comprehensive Analysis, Neurocomputing, 2020, https://doi.org/10.1016/j.neucom.2020.1010.1038.

[57] C. Yu, M. Chen, K. Cheng, X. Zhao, C. Ma, F. Kuang, H. Chen, SGOA: annealing-behaved grasshopper optimizer for global tasks, Eng. Comput. (2021), https://doi.org/10.1007/s00366-00020-01234-00361.

[58] Z. Cai, J. Gu, J. Luo, Q. Zhang, H. Chen, Z. Pan, Y. Li, C. Li, Evolving an optimal kernel extreme learning machine by using an enhanced grey wolf optimization strategy, Expert Syst. Appl. 138 (2019), 112814.

[59] L. Shen, H. Chen, Z. Yu, W. Kang, B. Zhang, H. Li, B. Yang, D. Liu, Evolving support vector machines using fruit fly optimization for medical data classification, Knowl. Base Syst. 96 (2016) 61–75.

[60] M. Wang, H. Chen, B. Yang, X. Zhao, L. Hu, Z. Cai, H. Huang, C. Tong, Toward an optimal kernel extreme learning machine using a chaotic moth-flame optimization strategy with applications in medical diagnoses, Neurocomputing 267 (2017) 69–84.

[61] M. Wang, H. Chen, Chaotic multi-swarm whale optimizer boosted support vector machine for medical diagnosis, Appl. Soft Comput. 88 (2020), 105946.

[62] G.-Q. Zeng, K.-D. Lu, Y.-X. Dai, Z.-J. Zhang, M.-R. Chen, C.-W. Zheng, D. Wu, W.-W.J.N. Peng, Binary-coded extremal optimization for the design of PID controllers, Neurocomputing 138 (2014) 180–188.

[63] G.-Q. Zeng, J. Chen, Y.-X. Dai, L.-M. Li, C.-W. Zheng, M.-R.J.N. Chen, Design of fractional order PID controller for automatic regulator voltage system based on multi-objective extremal optimization, Neurocomputing 160 (2015) 173–184.

[64] G.-Q. Zeng, X.-Q. Xie, M.-R. Chen, J. Weng, Adaptive population extremal optimization-based PID neural network for multivariable nonlinear control systems, Swarm Evol. Comput. 44 (2019) 320–334.

[65] W. Deng, H. Liu, J. Xu, H. Zhao, Y.J. Song, Measurement, an Improved Quantum-Inspired Differential Evolution Algorithm for Deep Belief Network, IEEE Transactions on Instrumentation & Measurement, 2020, https://doi.org/10.1109/TIM.2020.2983233.

[66] H. Zhao, H. Liu, J. Xu, W.J. Deng, Measurement, Performance Prediction Using High-Order Differential Mathematical Morphology Gradient Spectrum Entropy and Extreme Learning Machine, IEEE Transactions on Instrumentation & Measurement, 2019, https://doi.org/10.1109/TIM.2019.2948414.

[67] X.-F. Liu, Z.-H. Zhan, J. Zhang, Resource-aware distributed differential evolution for training expensive neural-network-based controller in power electronic circuit, IEEE Transact. Neural Networks Learn. Syst. (2021), https://doi.org/10.1109/TNNLS.2021.3075205.

[68] Z.-H. Zhan, X.-F. Liu, H. Zhang, Z. Yu, J. Weng, Y. Li, T. Gu, J. Zhang, Cloudde: A heterogeneous differential evolution algorithm and its distributed cloud version, IEEE Trans. Parallel Distr. Syst. 28 (2016) 704–716.

[69] X. Zhao, D. Li, B. Yang, C. Ma, Y. Zhu, H. Chen, Feature selection based on improved ant colony optimization for online detection of foreign fiber in cotton, Appl. Soft Comput. 24 (2014) 585–596.

[70] X. Zhao, D. Li, B. Yang, H. Chen, X. Yang, C. Yu, S. Liu, A two-stage feature selection method with its application, Comput. Electr. Eng. 47 (2015) 114–125.

[71] Y. Wei, H. Lv, M. Chen, M. Wang, A.A. Heidari, H. Chen, C. Li, Predicting entrepreneurial intention of students: an extreme learning machine with Gaussian barebone Harris hawks optimizer, IEEE Access 8 (2020) 76841–76855.

[72] W. Zhu, C. Ma, X. Zhao, M. Wang, A.A. Heidari, H. Chen, C. Li, Evaluation of sino foreign cooperative education project using orthogonal sine cosine optimized kernel extreme learning machine, IEEE Access 8 (2020) 61107–61123.

[73] A. Lin, Q. Wu, A.A. Heidari, Y. Xu, H. Chen, W. Geng, C. Li, Predicting intentions of students for master programs using a chaos-induced sine cosine-based fuzzy K-Nearest neighbor classifier, Ieee Access 7 (2019) 67235–67248.

[74] J. Tu, A. Lin, H. Chen, Y. Li, C. Li, Predict the entrepreneurial intention of fresh graduate students based on an adaptive support vector machine framework, Math. Probl Eng. (2019) 1–16, 2019.
[75] Y. Wei, N. Ni, D. Liu, H. Chen, M. Wang, Q. Li, X. Cui, H. Ye, An improved grey wolf optimization strategy enhanced SVM and its application in predicting the second major, Math. Probl Eng. (2017) 1–12, 2017.
[76] J. Kennedy, Particle swarm optimization, Proc. of 1995 IEEE Int 4 (2011) 1942–1948.
[77] G.-G. Wang, Moth search algorithm: a bio-inspired metaheuristic algorithm for global optimization problems, Memet. Comput. 10 (2018) 151–164.
[78] Y. Feng, S. Deb, G.-G. Wang, A.H. Alavi, Monarch butterfly optimization: a comprehensive review, Expert Syst. Appl. 168 (2021), 114418.
[79] Y. Yang, H. Chen, A.A. Heidari, A.H. Gandomi, Hunger games search: visions, conception, implementation, deep analysis, perspectives, and towards performance shifts, Expert Syst. Appl. (2021), 114864.
[80] A.A. Heidari, S. Mirjalili, H. Faris, I. Aljarah, M. Mafarja, H. Chen, Harris hawks optimization: algorithm and applications, Future Gen. Comput. Syst. Int. J. Esci. 97 (2019) 849–872.
[81] S. Li, H. Chen, M. Wang, A.A. Heidari, S. Mirjalili, Slime mould algorithm: a new method for stochastic optimization, Future Generat. Comput. Syst. 111 (2020) 300–323.
[82] I. Ahmadianfar, A. Asghar Heidari, A.H. Gandomi, X. Chu, H. Chen, RUN beyond the metaphor: an efficient optimization algorithm based on Runge Kutta method, Expert Syst. Appl. (2021), 115079.
[83] J. Tu, H. Chen, M. Wang, A.H. Gandomi, The colony predation algorithm, JBE 18 (2021) 674–710.
[84] D. Karaboga, B. Basturk, A powerful and efficient algorithm for numerical function optimization: artificial bee colony (ABC) algorithm, J. Global Optim. 39 (2007) 459–471.
[85] W.Q. Zou, Q.K. Pan, T. Meng, L. Gao, Y.L. Wang, An effective discrete artificial bee colony algorithm for multi-AGVs dispatching problem in a matrix manufacturing workshop, Expert Syst. Appl. (2020) 161.
[86] K. Zhou, Y.Z. Wen, W.Y. Wu, Z.Y. Ni, T.G. Jin, X.J. Long, Cloud service optimization method based on dynamic artificial ant-bee colony algorithm in agricultural equipment manufacturing, Math. Probl. Eng. (2020), 2020.
[87] C.J. Zhao, H.D. Zhao, G.Z. Wang, H. Chen, Improvement SVM classification performance of hyperspectral image using chaotic sequences in artificial bee colony, Ieee Access 8 (2020) 73947–73956.
[88] G. Lin, H.P. Xu, X. Chen, J. Guan, An effective binary artificial bee colony algorithm for maximum set k-covering problem, Expert Syst. Appl. (2020) 161.
[89] Z.H. Ding, K.S. Fu, W. Deng, J. Li, Z.R. Lu, A modified Artificial Bee Colony algorithm for structural damage identification under varying temperature based on a novel objective function, Appl. Math. Model. 88 (2020) 122–141.
[90] X.H. Chu, S.X. Li, D. Gao, W. Zhao, J.S. Cui, L.Y. Huang, A binary superior tracking artificial bee colony with dynamic Cauchy mutation for feature selection, Complexity (2020), 2020.
[91] X. Chen, X. Wei, G.X. Yang, W.L. Du, Fireworks explosion based artificial bee colony for numerical optimization, Knowl. Base Syst. (2020) 188.
[92] F. Boudardara, B. Gorkemli, Solving artificial ant problem using two artificial bee colony programming versions, Appl. Intell. 50 (2020) 3695–3717.
[93] Y.G. Yue, L. Cao, Z.Q. Luo, Hybrid artificial bee colony algorithm for improving the coverage and connectivity of wireless sensor networks, Wireless Pers. Commun. 108 (2019) 1719–1732.
[94] S. García, A. Fernández, J. Luengo, F. Herrera, Advanced nonparametric tests for multiple comparisons in the design of experiments in computational intelligence and data mining: experimental analysis of power, Inf. Sci. 180 (2010) 2044–2064.
[95] J. Derrac, S. García, D. Molina, F. Herrera, A practical tutorial on the use of nonparametric statistical tests as a methodology for comparing evolutionary and swarm intelligence algorithms, Swarm Evol. Comput. 1 (2011) 3–18.
[96] L. Zhang, L. Zhang, X. Mou, D. Zhang, FSIM: a feature similarity Index for image quality assessment, IEEE Trans. Image Process. 20 (2011) 2378–2386.
[97] Q. Huynh-Thu, M. Ghanbari, Scope of validity of PSNR in image/video quality assessment, Electron. Lett. 44 (2008) 800–801.
[98] W. Zhou, A.C. Bovik, H.R. Sheikh, E.P. Simoncelli, Image quality assessment: from error visibility to structural similarity, IEEE Trans. Image Process. 13 (2004) 600–612.
[99] A.S. Abutaleb, Automatic thresholding of gray-level pictures using two-dimensional entropy, Comput. Vis. Graph Image Process 47 (1989) 22–32.
[100] A. Buades, B. Coll, J. Morel, A non-local algorithm for image denoising, in: 2005 IEEE Computer Society Conference on Computer Vision and Pattern Recognition (CVPR'05), vol. 62, 2005, pp. 60–65.
[101] A.B. Meng, Y.C. Chen, H. Yin, S.Z. Chen, Crisscross optimization algorithm and its application, Knowl. Base Syst. 67 (2014) 218–229.
[102] R.S. Patwal, N. Narang, Crisscross PSO algorithm for multi-objective generation scheduling of pumped storage hydrothermal system incorporating solar units, Energy Convers. Manag. 169 (2018) 238–254.
[103] D. Zhao, L. Liu, F. Yu, A.A. Heidari, H. Chen, Ant colony optimization with horizontal and vertical crossover search: fundamental visions for multi-threshold image segmentation, Expert Syst. Appl. 167 (2020), 114122.
[104] R. Liu, X. Wang, H. Lu, Z. Wu, Q. Fan, S. Li, X. Jin, SCCGAN: style and characters inpainting based on CGAN, Mobile Network. Appl. 26 (2021) 3–12.
[105] L. Zhong, Z. Fang, F. Liu, B. Yuan, G. Zhang, J. Lu, Bridging the theoretical bound and deep algorithms for open set domain adaptation, IEEE Transact. Neural Networks Learn. Syst. (2021) 1–15.
[106] J. Chen, Q. Zou, J. Li, DeepM6ASeq-EL: prediction of human N6-methyladenosine (m6A) Sites with LSTM and ensemble learning, Front. Comput. Sci. 16 (2022) 1–7.
[107] Y. Zhang, X. Shi, H. Zhang, Y. Cao, V. Terzija, Review on deep learning applications in frequency analysis and control of modern power system, Int. J. Electr. Power Energy Syst. 136 (2022), 107744.
[108] T. Uyar Cankay, M. Besenek, What do we over-look during covid-19 pandemic? an adolescent stroke case presumed conversion disorder, Psychiatr. Danub. 32 (2020) 300–302.
[109] D. Salopek-Žiha, M. Hlavati, Z. Gvozdanović, M. Gašić, H. Placento, H. Jakić, D. Klapan, H. Šimić, Differences in distress and coping with the COVID-19 stressor in nurses and physicians, Psychiatr. Danub. 32 (2020) 287–293.
[110] K. Ćosić, S. Popović, M. Šarlija, I. Kesedžić, Impact of human disasters and COVID-19 pandemic on mental health: potential of digital psychiatry, Psychiatr. Danub. 32 (2020) 25–31.
[111] L. Liu, D. Zhao, F. Yu, A.A. Heidari, C. Li, J. Ouyang, H. Chen, M. Mafarja, H. Turabieh, J. Pan, Ant colony optimization with Cauchy and greedy Levy mutations for multilevel COVID 19 X-ray image segmentation, Comput. Biol. Med. 136 (2021), 104609.
[112] Q. Zhang, Z. Wang, A.A. Heidari, W. Gui, Q. Shao, H. Chen, A. Zaguia, H. Turabieh, M. Chen, Gaussian barebone salp swarm algorithm with stochastic fractal search for medical image segmentation: a COVID-19 case study, Comput. Biol. Med. 139 (2021), 104941.
[113] S. Mirjalili, J.S. Dong, A. Lewis, Nature-inspired Optimizers: Theories, Literature Reviews and Applications, Springer, 2019.
[114] A. Aad, B. Ass, D. Smc, E. Kzg, Nonlinear-based Chaotic Harris Hawks Optimizer: Algorithm and Internet of Vehicles Application, Applied Soft Computing, 2021.
[115] B.R. Adarsh, T. Raghunathan, T. Jayabarathi, X.-S. Yang, Economic dispatch using chaotic bat algorithm, Energy 96 (2016) 666–675.
[116] H. Nenavath, R.K. Jatoth, Hybridizing sine cosine algorithm with differential evolution for global optimization and object tracking, Appl. Soft Comput. 62 (2018) 1019–1043.
[117] M. Tubishat, M.A.M. Abushariah, N. Idris, I. Aljarah, Improved whale optimization algorithm for feature selection in Arabic sentiment analysis, Appl. Intell. 49 (2019) 1688–1707.
[118] M.A. Elhosseini, A.Y. Haikal, M. Badawy, N. Khashan, Biped robot stability based on an A–C parametric Whale Optimization Algorithm, J. Comput. Sci. 31 (2019) 17–32.
[119] M. Issa, A. Hassanien, D. Oliva, A. Helmi, I. Ziedan, A. Alzohairy, ASCA-PSO: Adaptive sine cosine optimization algorithm integrated with particle swarm for pairwise local sequence alignment, Expert Syst. Appl. 99 (2018) 56–70.
[120] W.F. Gao, S.Y. Liu, A modified artificial bee colony algorithm, Comput. Oper. Res. 39 (2012) 687–697.
[121] X. Zhong, S. Jiang, H. Song, ABCGA Algorithm for the Two Echelon Vehicle Routing Problem, ABCGA Algorithm for the Two Echelon Vehicle Routing Problem, 2017.
[122] K. Hanbay, M.F. Talu, Segmentation of SAR images using improved artificial bee colony algorithm and neutrosophic set, Appl. Soft Comput. 21 (2014) 433–443.
[123] D.M.H. Ilmawan, B. Warsito, S. Sugito, Penerapan Artificial Neural Network Dengan Optimasi Modified Artificial Bee Colony Untuk Meramalkan Harga Bitcoin Terhadap Rupiah, 2020.
[124] Y. Zhou, G. Xu, K. Tang, L. Tian, Y. Sun, Video coding optimization in AVS2, Inf. Process. Manag. 59 (2022), 102808.
[125] Q. Xu, Q. Guo, C.-X. Wang, S. Zhang, C.-B. Wen, T. Sun, W. Peng, J. Chen, W.-H. Li, Network differentiation: a computational method of pathogenesis diagnosis in traditional Chinese medicine based on systems science, Artif. Intell. Med. 118 (2021), 102134.
[126] M. Zhang, Y. Chen, W. Susilo, PPO-CPQ: A privacy-preserving optimization of clinical pathway query for e-healthcare systems, IEEE Internet Things J. 7 (2020) 10660–10672.
[127] Z. Wu, R. Li, J. Xie, Z. Zhou, J. Guo, X. Xu, A user sensitive subject protection approach for book search service, J. Assoc. Inf. Sci. Technol. 71 (2020) 183–195.
[128] Z. Wu, S. Shen, X. Lian, X. Su, E. Chen, A dummy-based user privacy protection approach for text information retrieval, Knowl. Base Syst. 195 (2020), 105679.
[129] Z. Wu, S. Shen, H. Zhou, H. Li, C. Lu, D. Zou, An effective approach for the protection of user commodity viewing privacy in e-commerce website, Knowl. Base Syst. 220 (2021), 106952.
[130] Z. Wu, G. Li, S. Shen, Z. Cui, X. Lian, G. Xu, Constructing dummy query sequences to protect location privacy and query privacy in location-based services, World Wide Web 24 (2021) 25–49.
[131] Z. Wu, R. Wang, Q. Li, X. Lian, G. Xu, A location privacy-preserving system based on query range cover-up for location-based services, IEEE Trans. Veh. Technol. (2020) 69.
[132] X. Zhang, T. Wang, J. Wang, G. Tang, L. Zhao, Pyramid channel-based feature attention network for image dehazing, Comput. Vis. Image Understand. 197 (2020), 103003.
[133] S. Qiu, Z. Hao, Z. Wang, L. Liu, J. Liu, H. Zhao, G. Fortino, Sensor combination selection strategy for kayak cycle phase segmentation based on body sensor networks, IEEE Internet Things J. (2021), https://doi.org/10.1109/JIOT.2021.3102856.
[134] S. Qiu, H. Zhao, N. Jiang, D. Wu, G. Song, H. Zhao, Z. Wang, Sensor network oriented human motion capture via wearable intelligent system, Int. J. Intell. Syst. 37 (2021) 1646–1673, https://doi.org/10.1002/int.22689.